Office of Groundwater Impact Assessment

Hydrogeological characterisation of faults in the Surat Basin

Assessing fault-induced connectivity between the Walloon Coal Measures and adjacent aquifers

December 2020

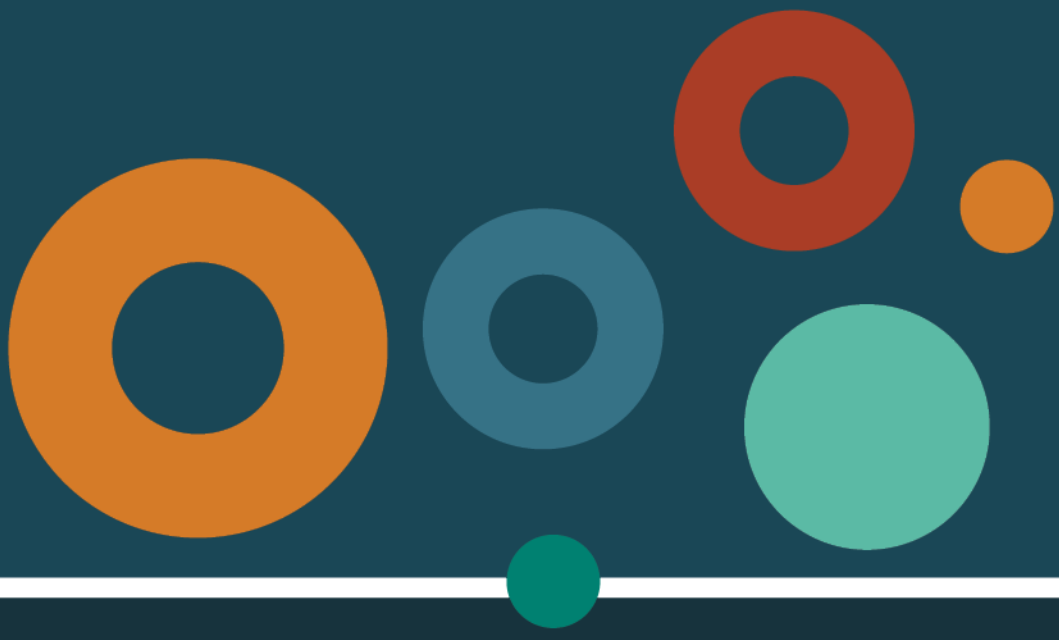

Queensland Government

Original version, authorised release in December 2020 by Sanjeev Pandey, Executive Director, Office of Groundwater Impact Assessment.

This publication has been compiled by the Office of Groundwater Impact Assessment, Department of Regional Development, Manufacturing and Water.

Bibliographic reference:

OGIA, 2020. *Hydrogeological characterisation of faults in the Surat Basin: assessing fault-induced connectivity between the Walloon Coal Measures and adjacent aquifers*. OGIA, Brisbane.

Interpreter statement:

The Queensland Government is committed to providing accessible services to Queenslanders from all culturally and linguistically diverse backgrounds. If you have difficulty in understanding this document, you can contact us within Australia on 13QGOV (13 74 68) and we will arrange an interpreter to effectively communicate the report to you.

Summary

The primary objective of this study is to assess the hydrogeological characteristics of faults in the Surat Basin, the key focus being on areas where fault-induced connectivity may allow the transmission of CSG-related depressurisation in the Walloon Coal Measures to surrounding aquifers – the Springbok Sandstone and the Hutton Sandstone.

This study explores both literature and multidisciplinary case studies to validate a framework for assessing fault hydrogeology in a connectivity context.

The two main mechanisms by which faults can act to increase aquifer connectivity are vertical transmission through fractures in the damage zone (vertical connectivity) and/or direct juxtaposition of permeable sections along the fault plane (horizontal connectivity).

Where thick intervening aquitards are present, vertical transmission is less likely, due to the healing properties of clays. In these instances, the primary risk of connectivity is through juxtaposition of permeable rocks (by offsetting the aquitard). Where no aquitard is present, vertical connectivity can occur where fractures are critically stressed (typically in shallower conditions).

The Hutton Sandstone is separated from the Walloon Coal Measures by the regionally ubiquitous Durabilla Formation aquitard; as such, the main risk of connectivity is through juxtaposition.

The Springbok Sandstone is less isolated from the Walloon Coal Measures and is separated by a thin upper non-coal zone, such that there is potential for faults to create both horizontal and vertical connectivity between these two formations.

Faults were mapped across the basin where seismic data were available and a fault juxtaposition and seal analysis were subsequently undertaken. Key findings include:

- two fault zones which have connectivity potential between the Walloon Coal Measures and Hutton Sandstone, namely the regionally significant Horrane and Hutton-Wallumbilla fault systems
- increased juxtaposition potential between the Walloon Coal Measures and Springbok Sandstone
- 16 faults which have geological characteristics similar to a site of known connectivity (Kenya East fault).

Fault orientation, with respect to principal horizontal stress, was assessed to identify faults which may facilitate vertical connectivity between the Walloon Coal Measures and near-surface features. At three sites, faults are oriented sub-parallel to current-day principal horizontal stresses and the formation depth is shallow. One of these is near a site of known fault influence (the Condamine River gas seeps) while the others do not have known surface features.

Table of contents

Table of Figures

1. Introduction

1.1 Background

The Office of Groundwater Impact Assessment (OGIA) is an independent entity established under Queensland legislation for the assessment and management of groundwater impacts from the extraction of associated water by petroleum and gas (P&G) and mining tenure holders (collectively referred to as resource tenure holders). OGIA is responsible for undertaking cumulative impact assessments and establishing management arrangements in areas where impacts from multiple tenure holders may overlap. Such areas are declared as 'cumulative management areas' (CMA). Currently, there is one CMA in Queensland that was established in 2011 in the Surat and southern Bowen basins. This CMA is referred to as the Surat CMA.

OGIA's assessment and management arrangements are set out in an Underground Water Impact Report (UWIR), which is revised every three years to provide for an adaptive reporting-monitoring-modelling cycle. The UWIR provides assessments of regional impacts on groundwater pressures and establishes integrated management arrangements, such as regional monitoring strategies. It also identifies individual responsibilities for implementing various aspects of the strategies. The UWIR is a statutory instrument and provides a basis for the ongoing management of groundwater impacts in line with the strategies outlined in the report. Responsible tenure holders have a statutory obligation to implement management arrangements identified in the UWIR.

The first UWIR for the Surat CMA was prepared by OGIA (then part of the Queensland Water Commission) in 2012 and was succeeded by the UWIR 2016 (OGIA, 2016e). More recently, these reports have been superseded by the UWIR 2019 (OGIA, 2019e).

A key component of the cumulative impact assessment that supports the UWIR is the conceptualisation and characterisation of faults in the Surat CMA. This informs the hydrogeological conceptualisation and is considered in assessing aquifer connectivity, analysing groundwater level trends and the construction of both geological and numerical models.

1.2 Previous OGIA assessments

Since 2011, OGIA has undertaken a number of research studies relating to various elements of groundwater conceptualisation, inter-aquifer connectivity, the hydrogeology of springs and groundwater flow modelling to support development of the UWIR 2012, UWIR 2016 and UWIR 2019. Findings of these studies are published in a number of technical reports which are available on OGIA's website and in the UWIR 2019 (OGIA, 2019e). The key reports are outlined in Appendix A.

1.3 Current assessment cycle and approach

Extensive knowledge continues to be built about the regional groundwater flow system through a number of ongoing research programs, including studies undertaken by OGIA, industry initiatives and other research organisations. Since the development of the UWIR 2016, a range of additional data sets have also become available, including geological and hydrogeological properties from additional CSG wells, groundwater monitoring data from a network of about 600 monitoring points established through the UWIR obligations, and a range of other monitoring data. OGIA utilised these additional data sets to develop an updated hydrogeological conceptualisation and regional groundwater flow model for the UWIR 2019.

In the first UWIR development cycle, OGIA's approach was to largely rely on pre-existing information and secondary interpretation of key data sets to build a regional conceptualisation, build a numerical groundwater flow model and undertake a predictive uncertainty analysis.

For the development of the second UWIR in 2016, the approach was to undertake primary data analysis, run hydrogeological investigations on aquifer connectivity and spring conceptualisation, and develop innovative modelling techniques and methods.

The overall approach for the UWIR 2019 was to build further on this work, with OGIA's research efforts focused on the following three areas:

- Improving regional-scale conceptualisation and modelling, e.g. revision of the geological model, analysis of regional trends in groundwater pressure, updating of the groundwater flow model, analysis of hydrochemistry and verification of baseflow-fed water courses.
- Sub-regional-scale hydrogeological assessments around CSG fields that have been in production for some time and where significant new monitoring data have now become available.
- Improving methods and tools for assessment, such as estimation of non-CSG water use, modelling techniques, uncertainties due to bore connectivity and geological faults, and spring monitoring.

1.4 Objectives

The primary objectives of this report are to summarise the current literature on the hydrogeological characterisation of faults in sedimentary basins and assess the likely hydraulic behaviour of faults in the Surat Basin. The focus is on faults that have the potential to transmit CSG depressurisation from the Walloon Coal Measures to adjacent aquifers in the Springbok Sandstone and the Hutton Sandstone.

It is intended that the findings of the current study will inform ongoing and future hydrogeological conceptualisation and impact assessment research projects undertaken by the Office of Groundwater Impact Assessment (OGIA). In particular, the study will attempt to identify areas where there is a relatively high potential for the transmission of CSG depressurisation impacts into adjacent aquifers via faults.

The analysis incorporates a multi-scale approach through analysis of data relating to all identified faults within the Surat CMA, and through a discussion of three 'case study' areas where more detailed information is available, in order to draw conclusions about the likely behaviour of key faults in these areas.

1.5 This report

This report summarises the results of work undertaken by OGIA since the UWIR 2016 (OGIA, 2016e) relating to the conceptualisation and characterisation of faults in the Surat Basin. Given OGIA's focus on assessing the impacts of CSG extraction within the basin, this report primarily focuses on all faults that affect either the upper or lower surface of the Walloon Coal Measures within areas of current or planned CSG extraction. Regional-scale fault systems that predominantly affect the underlying Bowen Basin sediments are discussed in a separate OGIA regional geology report (OGIA, 2019f).

The report is structured as follows:

- Chapter 2 presents a summary of concepts relevant to understanding faults and their likely hydrogeological behaviour, drawing on the available scientific literature.
- Chapter 3 presents a summary of the methods used to characterise faults.
- Chapter 4 presents the results and discussion of the work undertaken, including a summary of both the regional-scale data analysis and selected case studies.
- The main conclusions resulting from the study are presented in Chapter 5.

2. Relevant concepts

This chapter presents a summary of key concepts, processes and mechanisms relevant to fault geology and hydrogeology.

2.1 Fault architecture and geometry

Faults are complex features with unique and variable hydrogeological characteristics comprising zones of brittle deformation, which displace rocks on either side (Caine et al., 1996; Wibberley et al., 2008; Yielding et al., 1997).

Figure 1 shows a simplified representation of the architecture and structure of fault zones (Chester & Logan, 1987). This conceptualisation divides fault zones into a central fault core and a surrounding fault damage zone, typically characterised by a distributed network of fractures. A fault zone may contain one or more fault cores.

Observations show that the geometry, architecture and structure of the fault core and damage zone are highly controlled by the geo-mechanical properties of the fractured rocks themselves. One study, comparing the fracture attributes from different rock types, has shown that litharenites (rocks with >5% lithic fragments) produce isolated, widely spaced fractures in the damage zone, which gradually increase in density towards the fault core (Laubach et al., 2014). Faulting of such rocks also tends to result in a dense and clay-rich fault core. Conversely, faulting of rocks with greater proportions of quartz tends to result in interconnected, closely spaced fractures in the damage zone and more permeable fault cores filled with fault breccia (Laubach et al., 2014).

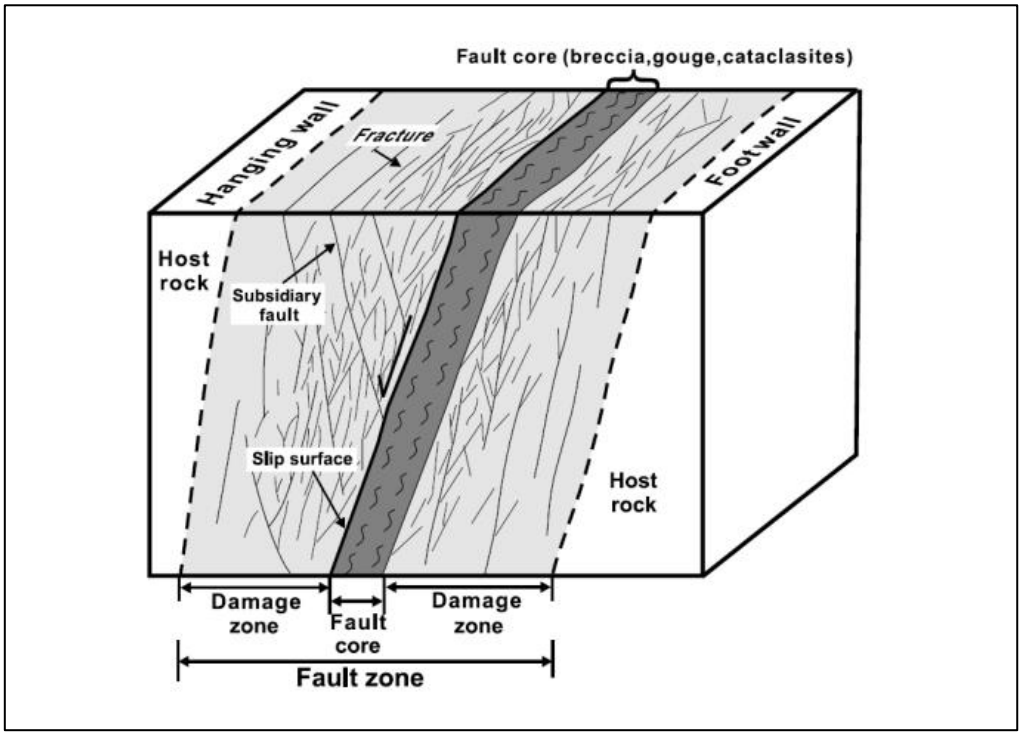

Figure 1 Fault architecture showing the fault core, damage zone and protolith (host rock)

Fault geometries are often characterised with reference to the type of movement along the fault plane (e.g. normal, reverse or strike-slip movement (Park, 2000)) and this movement is usually a result of changes in stress and strain in the protolith (i.e. unfaulted host rock). Normal faults tend to be the result of an extensional stress regime, which allows material on one side to slip down relative to the

other (Figure 2). Reverse faults are usually formed in compressional stress regimes by 'thrusting' a fault block upwards relative to the other side. Strike-slip faults are where displacement occurs in the horizontal direction.

In many cases, a combination of different types of movement can occur (e.g. oblique strike slip faulting), resulting in complex geometries. However, this can be simplified somewhat through reference to the dominant displacement type.

It is important to note that reactivation of a given fault in a different stress regime may produce complex geometries (Krantz, 1991; Peacock & Sanderson, 1997).

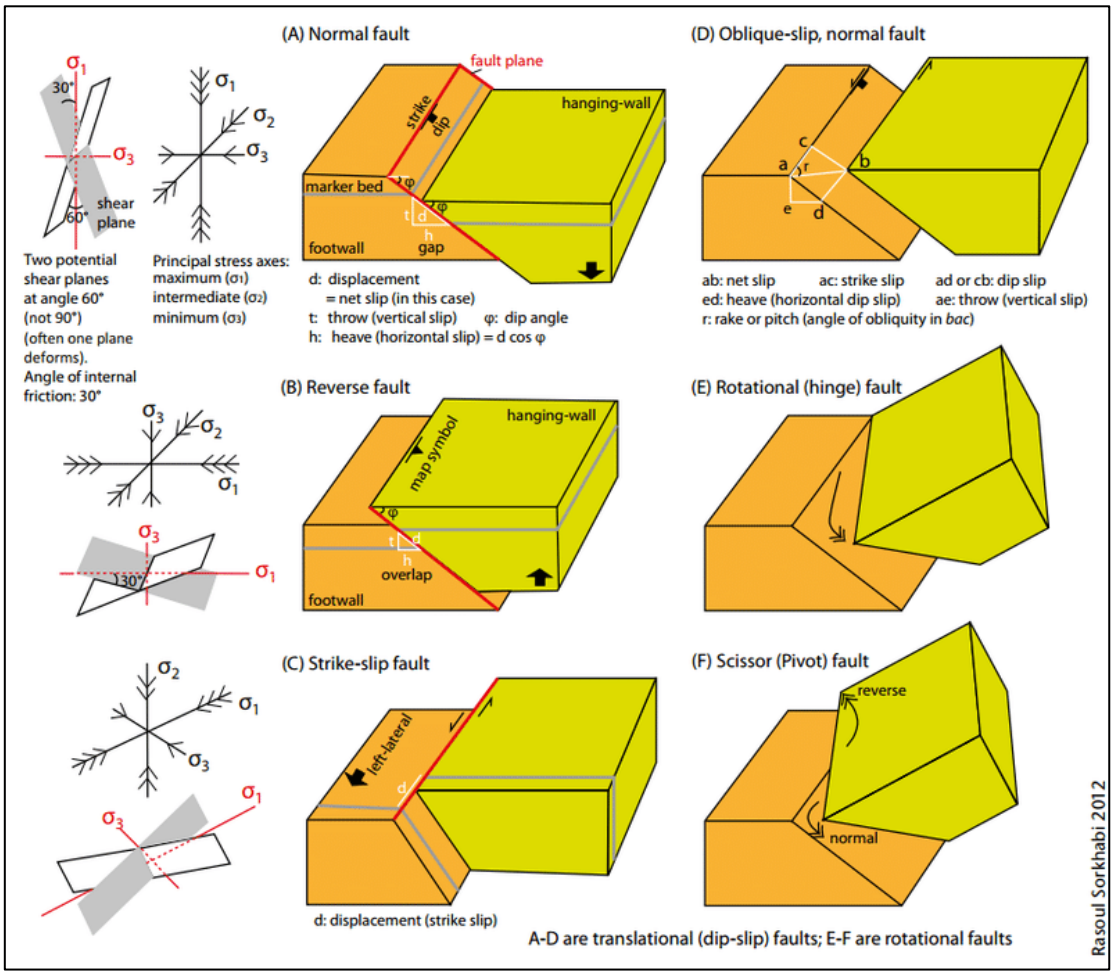

Figure 2 Types of faults and associated stress regimes (taken from Underschultz et al., 2018)

A meta-analysis combining global results of the maximum fault displacement (D_{max}), plotted against the corresponding fault length (Figure 3), suggests an approximately linear relationship (Kim & Sanderson, 2005). Separate relationships have been derived for normal and thrust faults and are widely used for estimating the length of faults from known displacements (Kim & Sanderson, 2005).

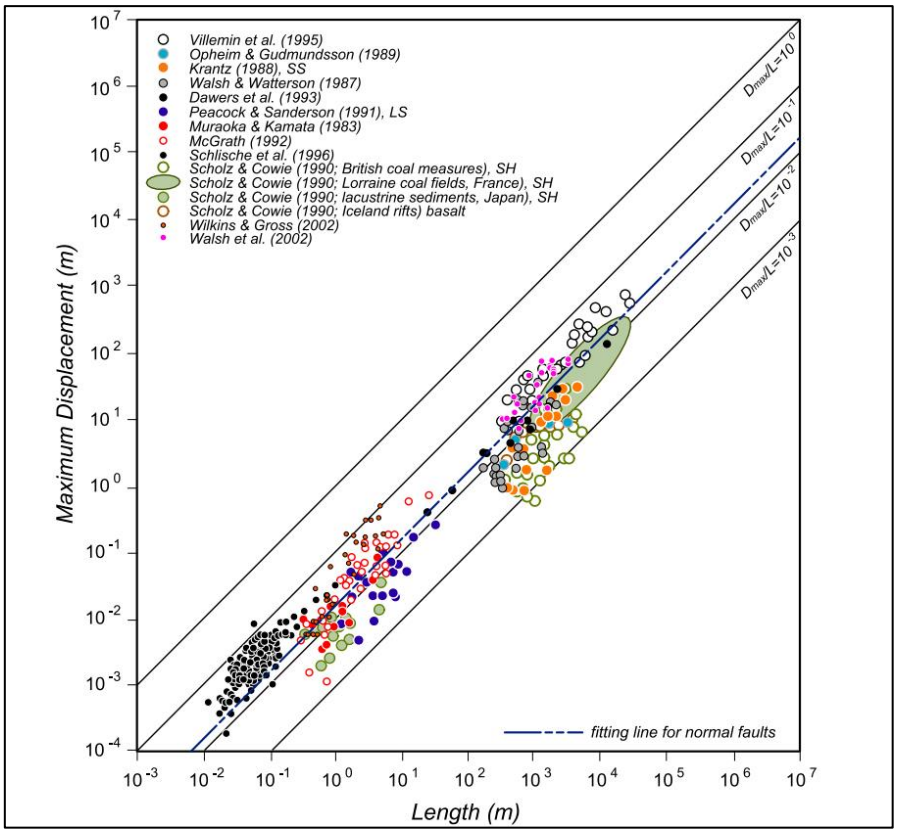

Figure 3 Maximum fault displacement vs length from various global studies (taken from Kim & Sanderson, 2005)

Fault displacements will vary along the fault plane, reducing to zero at the limit of the fault. One study, carried out in the Dan River rift basin, utilised high-precision instrumentation (micro rulers and a profilometer) to measure fault displacements and fault length (Schlische et al., 1996). The study found that the greatest displacement tended to be in the centre of the faults, with displacement tailing off towards the ends, resembling a parabolic shape. Similar observations have been made in other studies (e.g. Grasemann et al., 2011). In some cases, the fault systems are more complex and have multiple displacement maxima (Adiotomre, 2014). This highlights the need to break large fault systems into several segments, each with its own displacement profile. As shown in Figure 3, the maximum displacement of a fault can be related to the length of the fault through equation $Dmax=cL^n$, where c and n are constants and L is the maximum length of the fault (Kim & Sanderson, 2005). The parabolic shape of displacement profiles provides the foundation for complex analysis of the relationship between fault length and displacement. When multiple fault segments are present, significant stresses are formed in the zone between fault segments (referred to as the transfer zone). These zones often contain relay ramps which accommodate offsets between fault segments (Peacock & Sanderson, 1994).

2.2 Structural processes

This section outlines the key mechanisms and processes that generate faults and thereby affect their likely hydraulic behaviour.

2.2.1 Tectonic history

One important consideration in the analysis of faults is their often complex tectonic history. This involves developing a detailed understanding of the tectonic and neo-tectonic processes contributing to the architecture and geometry of the current-day structural framework of a basin.

The tectonic history will determine the type and overall geometry of fault systems present. A good example in the Surat Basin is the Hutton-Wallumbilla Fault, which is a large basement thrust fault system extending through the Bowen Basin sediments as far as the Surat Basin unconformity (i.e. the base of the Surat sediments) (OGIA, 2019f). As shown in Figure 4, this fault appears to have been reactivated in an extensional style following deposition of the Surat sediments. The fault zone extends into the shallower portions of the Surat Basin as negative 'flower' structures located to the east of the basement fault. As such, the complex reactivation history strongly controls the final geometry of faults in the area. Neo-tectonic reactivation will also control the extent of faulting in shallow, near-surface formations (Lawrie et al., 2012).

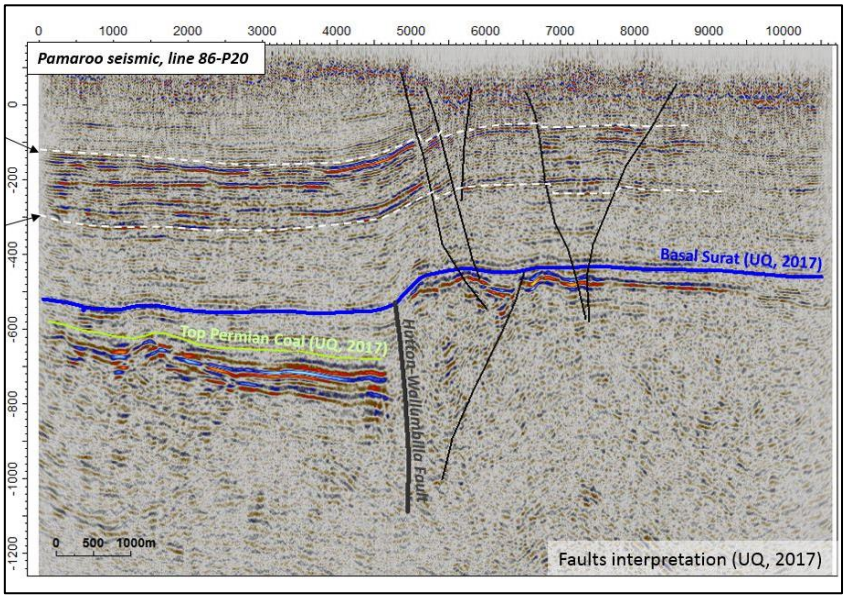

Figure 4 Seismic section showing the Hutton-Wallumbilla thrust fault

2.2.2 Deformation processes

Cataclasis is the brittle fracturing, shearing and grinding of rocks in a fault zone (Engelder, 1974). The process that generally affects consolidated sediments includes grain rotation and dragging of mineral grains into the fault core (Engelder, 1974).

The initial failure of the matrix on the fault plane causes the breaking up of clay fractions as well as progressive milling of mineral grains into a clay gouge (Holland et al., 2005). Cataclasis generally results in grainsize reduction due to stress concentrations on the corners of angular grains (Engelder, 1974). This produces an additional abundance of fine-grained material in the fault core and some studies suggest that faults in poorly lithified sandstones can accommodate a 10% increase in clay fractions in fault zones relative to the protolith (Schwenck Galvão et al., 2018).

When low proportions of clay are present in the protolith, fault breccias dominate the fault core material. However, when higher proportions of clay are present in the protolith, rocks in the fault core are more likely to include foliated strata formed by clay-smearing. Ductile flow of clay and shale layers

along the plane of a fault can result in the smearing of these clay/shale layers along the length of the fault plane (Smith, 1966), as illustrated in Figure 5.

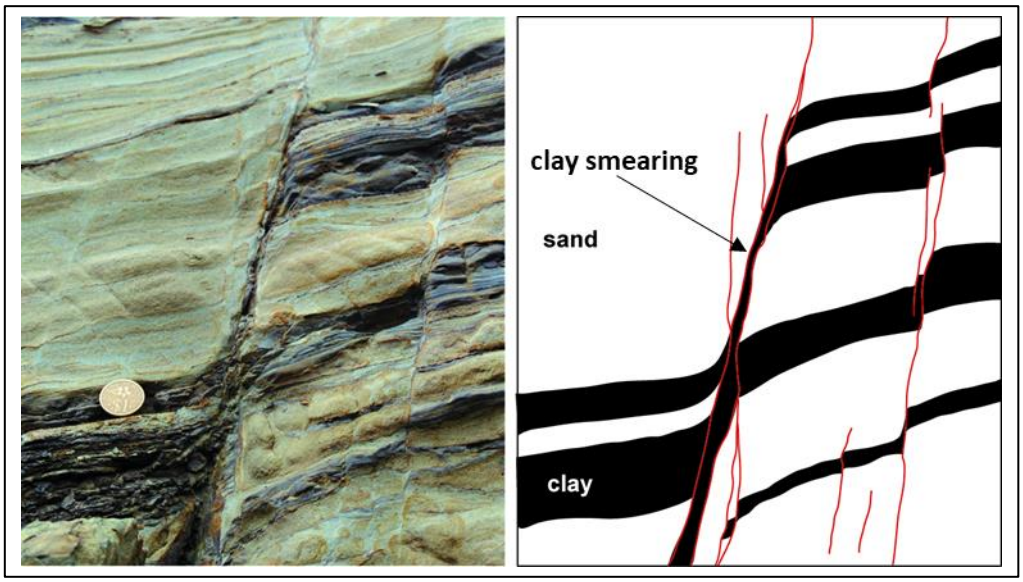

Figure 5 Clay smearing on a fault in clay containing rocks (taken from van der Zee & Urai, 2005)

2.2.3 Rheology

Faults and associated fractures are subject to the same stresses as the protolith (i.e. the unfaulted rock) and their responses to these stresses depend largely on their orientation with respect to these principal stresses (Ferrill & Morris, 2001).

Fractures that are favourably oriented to fail in shear under the present-day stress field are said to be critically stressed. These fractures exhibit very good fluid-flow characteristics.

Faults that are oriented perpendicular to the principal stress direction are under compressional forces. Conversely, faults oriented parallel or subparallel to the principal stress direction are likely to be subjected to dilation forces (Ferrill & Morris, 2001). This is particularly important in the fault damage zone, where fractures are more likely to be open and hence permeable, where they are experiencing dilation rather than compression (Faulkner et al., 2010).

2.3 Hydrogeological processes

Studies of the geometry and internal structure of faults has led to improved understanding of fluid flow in faulted zones (Faulkner et al., 2010). Several key mechanisms have been identified by which groundwater flow can occur within the fault core and/or the surrounding rock damage zone.

The hydraulic behaviour of faults can vary between the horizontal and vertical directions. They may act as horizontal barriers (while simultaneously allowing for vertical connection between units), enhance horizontal connectivity (while acting as vertical barriers), or act as barriers in both directions. Importantly, the behaviour of a fault can also vary along the strike, as the displacement of the fault changes and the lithological and geological structure varies (Underschultz et al., 2018).

2.3.1 Horizontal effects

2.3.1.1 Enhanced horizontal connectivity

Faults may create connections between formations that are otherwise separated, by juxtaposition of the two formations. This has long been acknowledged in fault seal analysis workflows (Allan, 1989; Bouvier et al., 1989).

Faults may juxtapose permeable sediments from different formations, such as sand against sand or sand against coal. These contacts may allow fluid transfer across a fault. The extent of this connectivity will depend in part on the permeable contact area on the fault plane, which will in turn depend on the displacement profile of the fault. Figure 6 shows a diagrammatic example of this type of fault-induced connectivity.

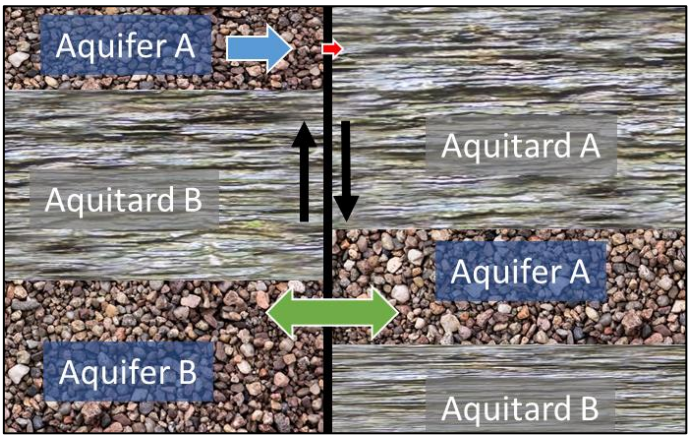

Figure 6 Schematic showing the connection between two aquifers

Reliable assessment of the potential for horizontal connections through juxtaposition requires that the fault geometry is well understood – a requirement that becomes more onerous as the complexity of the fault increases.

2.3.1.2 Horizontal barrier effects

Faults can also act as horizontal flow barriers, impeding flow across faulted zones and potentially compartmentalising local and regional groundwater systems (Bense & Person, 2006).

As shown in Figure 7, where the maximum displacement of a given fault approaches or is larger than the thickness of a permeable unit within the faulted zone, horizontal flow may be impeded and the unit may become disconnected from itself.

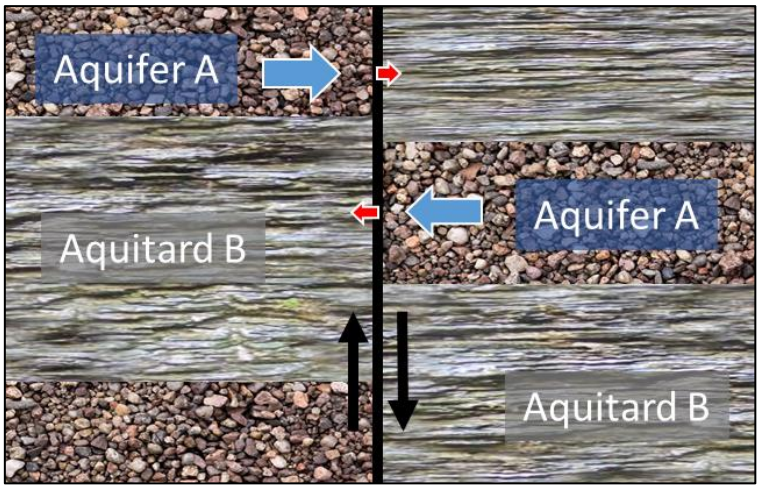

Figure 7 Schematic showing a fault displacement resulting in a local disconnected Aquifer A

The potential horizontal barrier effects of a fault vary along the strike of a feature, since displacement varies along the strike and, consequently, so will the juxtaposition of different sediments.

If the fault length is relatively short or the maximum displacement small, then any associated barrier effects may be more localised. However, if the maximum displacements significantly exceed the thickness of an aquifer and the fault extends for several kilometres, then the potential impact on groundwater flow may be regional.

As discussed above in section 2.2.2, faulting of clay-rich sedimentary formation is often accompanied by clay-smearing within the fault core. The degree to which clay is smeared into the fault core represents an important mechanism controlling the horizontal permeability of the fault plane (Egholm et al., 2008; Vrolijk et al., 2016). It is important to note that the degree of clay-smear along a fault plane varies and will be dependent on the clay content of a given section of entrained sediment, as well as the fault displacement. Intuitively, formations characterised by relatively low clay proportions will undergo limited clay-smearing and, in such cases, the horizontal permeability across the fault will be controlled largely by the juxtaposed protolith. The degree of clay-smearing represents a potentially important control on the migration of oil and gas across faults and much of the literature on this topic emanates from the oil and gas industry (Dolson, 2016).

The degree of clay-smearing is typically quantified through reference to the Shale Gouge Ratio (SGR), which is a measure of the percentage of clay within the entrained sediment along the fault plane. When faulted rocks contain low clay proportions and the resulting SGR is low (<20%), the fault core is likely to be dominated by brecciated protolith and the fault properties are likely to approach those of the entrained protolith. Conversely, where the host rock includes higher proportions of clay and the SGR is relatively high (20–50%), clay-smear is likely to significantly reduce the horizontal permeability of the fault plane (Yielding et al., 2010).

2.3.2 Vertical effects

In addition to horizontal effects, faults may also enhance or impede flow in the vertical direction. Faults may form vertical preferential flow paths even where horizontal barrier effects are observed (Bense & Person, 2006).

Evidence for vertically assisted flow through faults has been found from fault-zone cements (Mozley & Goodwin, 1995), contaminated groundwater (Mal'kovskii & Pek, 2001) and oil migration along fault zones (Moretti, 1998). There are also examples from the Surat Basin where faults are likely to provide

vertical conduits for flow, such as the Condamine river gas seeps, where gas has been observed bubbling in the river (APLNG, n.d.). Another example is from springs, where faults have been conceptualised as providing localised conduits for pressurised groundwater to move to the surface (OGIA, 2016d).

The main mechanism by which faults facilitate vertical flow between formations is predominantly via fractures in the damage zone, rather than along the fault core, which is typically thin and characterised by low permeability (Faulkner et al., 2010). Some of the primary characteristics affecting the vertical flow are described in the sections below.

Conversely, precipitation of calcite, quartz and pyrite will tend to reduce fracture permeability over time (Gale et al., 2004). Cement accumulation in fault zones is known to fill fracture apertures and strengthen faults (Fisher & Knipe, 2001; Hippler, 1993; Laubach et al., 2014; Robertson & Chilingar, 2000).

2.3.2.1 Rock type and composition

Rock type and composition are key factors that affect the formation of the fault damage zone. In unconsolidated sediments, particulate flow will be the dominant mechanism in fault zones and as such, the vertical hydraulic properties of the damage zone will be determined by features such as deformation bands (Rawling et al., 2001). In consolidated sediments, fractures are more likely to have the primary control on vertical hydraulic properties in the fault zone (Bense et al., 2003).

The mineralogy of the faulted and fractured rocks also represents an important secondary control on water movement, especially within the damage zone. The tendency for certain clay minerals (primarily smectite) to swell as a result of their capacity to adsorb water is well documented in the literature (Van Olphen, 1964). This swelling results in a volumetric expansion (Shakoor & Sarman, 1992), contributes to the reduction of fracture apertures and subsequently results in permeability reduction (Ingraham et al., 2015).

Adsorption, which also reduces fracture permeability, occurs when swelling clays are exposed to low-salinity solutions (Himes et al., 1991). Rocks containing significant proportions of these minerals have the ability to take on large quantities of water in addition to their naturally saturated state, due to adsorption effects (Hensen & Smit, 2002). Additionally, the permeability of fractures that are generated in rocks with high smectite proportions is likely to reduce over time, as the passage of water leads to swelling of the constituent clays.

Zhang (2013) measured permeability decreases of two orders of magnitude as a result of smectite swelling. Additional insight into this process in the Surat CMA was gathered via laboratory experiments conducted by CSIRO for OGIA (Esteban et al., 2015). It was shown that dried rock samples from the Walloon Coal Measures are able to self-heal over a period of days after resaturation with a fluid resembling in situ formation fluid. The experiments aimed to mimic in situ conditions, including pressure and water chemistry. It is noted that the experiments were conducted with air-dried core, which will likely increase the effect of swelling clays. There is additional insight from operational experience with in situ hydraulic fracturing, where swelling clays have been attributed to permeability reduction of interburden (Mahdi et al., 2017).

2.3.2.2 Stress and strain

Fractures can range widely in permeability, with the primary property that controls this being the fracture aperture (Gong & Rossen, 2017). Zhang (2013) demonstrated the dependence of fracture permeability in claystones on confining pressure and stress orientation. It was shown that fracture

aperture and permeability are highly dependent on the normal stress magnitude. Fractured samples subjected to varying normal stresses were shown to have very low permeabilities that were less than or approaching background permeability, while fractures oblique to extensional stresses were shown to have significantly increased permeability associated with larger fracture apertures. This principle also applies to other consolidated rock types including sandstone, limestone and coal; hence, fractures in the fault damage zone that are oriented parallel or subparallel to the principal stress direction are more likely to provide vertical connectivity pathways, due to increased fracture apertures.

Analysis of coal permeability in the Surat Basin, as a function of angle difference between fracture orientation and maximal horizontal principal stress direction, suggests that maximum permeability is observed at about 30 degrees differential angle (the angle between the fracture orientation and maximum principal horizontal stress direction) (Copley et al., 2017).

Fractures also tend to close with increasing depth, due to the lithostatic pressure component. This reduction in fracture permeability with depth corresponds to approximately one order of magnitude every 100 m (Lin et al., 2007).

The behaviour of fault-related fractures in damage zones is therefore largely controlled by:

- **fracture network connectivity**, which is largely controlled by rock type and mineralogy (Jing & Stephansson, 2007)
- **fracture aperture**, which is controlled by the resolved normal stress (a function of lithostatic and tectonic stresses as well as fluid pressure) (Bradley Thomas Grosser, 2012).

In summary, where ubiquitous aquitards with high clay proportions separate units of interest and fault displacement does not exceed the aquitard thickness, fracture network connectivity may be low and connectivity is likely to be low.

Where no or limited aquitard material is present, fractures oriented sub-parallel with respect to current-day principal horizontal stress directions may be critically stressed and enhance vertical connectivity.

2.4 Geological framework of the Surat Basin

This section provides an overview of key geological formations discussed in this report, as well as a description of the structural setting of the Surat Basin, which is discussed in further detail in a separate report on geology (OGIA, 2019f). A more generalised representation of the stratigraphic framework of the Surat Basin is shown in Figure 8.

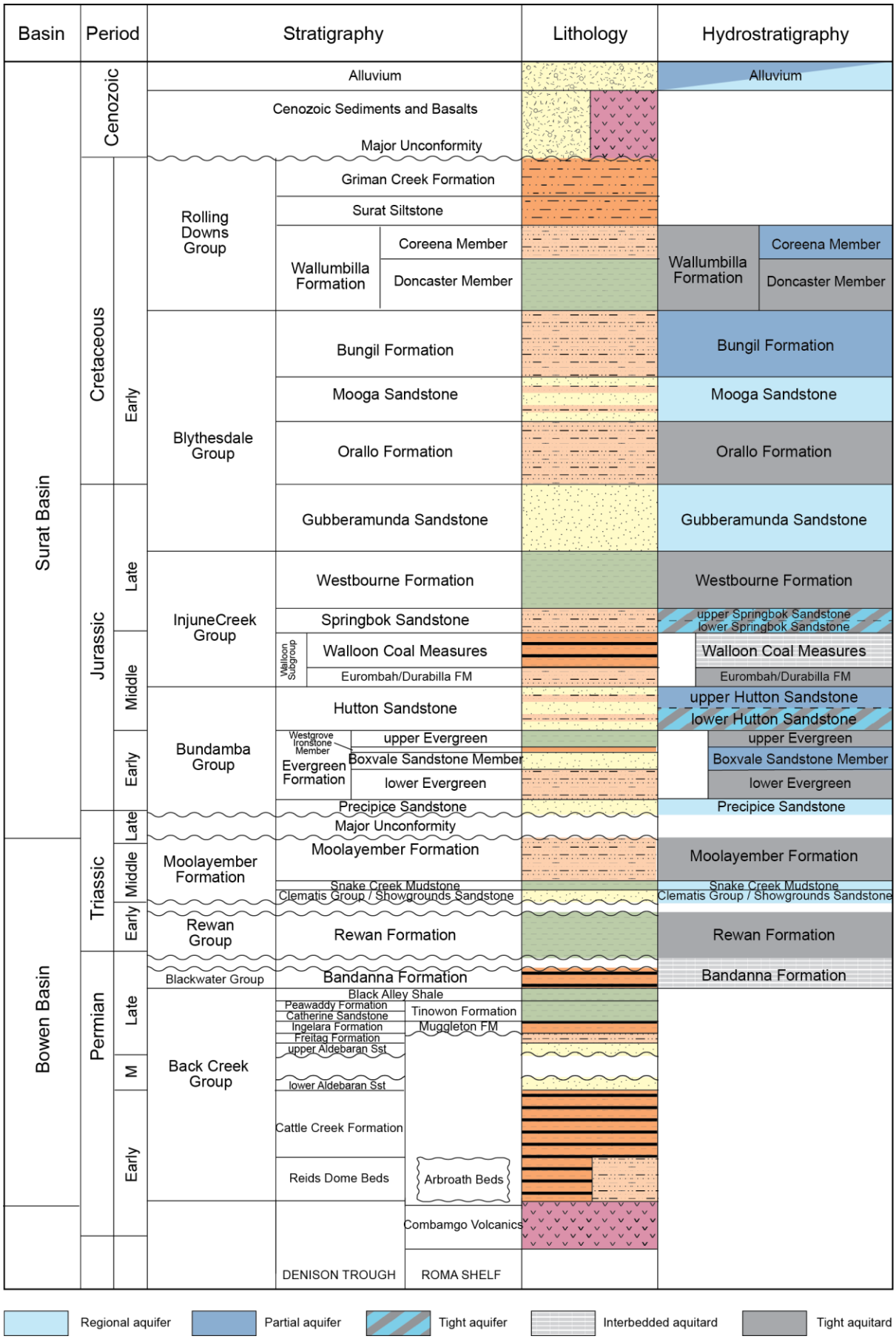

Figure 8 Generalised hydrostratigraphic classification in the Surat Basin

2.4.1 Stratigraphy

2.4.1.1 Condamine Alluvium

The Condamine Alluvium is one of the more significant accumulations of alluvial sediments within the area. This alluvial groundwater resource is extensively developed for agriculture and forms a broad alluvial plain (more than 20 km wide), stretching between Millmerran and Chinchilla. The thickness of alluvium ranges from less than 10 m in the headwaters and along the floodplain margins, to more than 120 m in the central floodplain near Dalby. The sediments within the Condamine Alluvium are dominated by fine to coarse-grained gravels and channel sands interbedded with clays. The Condamine Alluvium is underlain by a low-permeability undifferentiated clay-dominated horizon referred to as the 'transition zone'.

2.4.1.2 Springbok Sandstone

The Springbok Sandstone is composed of upper and lower units. The upper Springbok Sandstone typically comprises interbedded fine to coarse-grained feldspathic to lithic sandstone, siltstone and mudstone, while the lower Springbok Sandstone typically comprises course to very coarse-grained sandstone and excludes significant coal seams. Stacked channel sandstones comprise more than 80% of the lower unit and the permeability is therefore higher than the upper unit. The lower Springbok Sandstone unconformably overlies the Walloon Coal Measures.

2.4.1.3 Walloon Coal Measures

The Walloon Coal Measures is the primary reservoir for gas extraction in the Surat Basin and is unconformably overlain by the Springbok Sandstone, which is incised into the coal measures in places, completely removing the upper coal seam groups in some areas (Hamilton et al., 2014). The internal structure of the Walloon Coal Measures can be separated into the Upper Juandah, Lower Juandah, Tangalooma Sandstone and Taroom coal measures. Gas-producing coal seams are primarily situated in the Upper Juandah, Lower Juandah and Taroom coal measures.

The upper non-coal zone is the portion of the upper Walloon Coal Measures that sits above the uppermost coal seam. This unit acts as the 'upper aquitard' and typically provides some resistance between the Walloon Coal Measures and the lower Springbok Sandstone. This zone is not present where coal is directly sub-cropping against the unconformity. Furthermore, the upper non-coal zone has variable lithological composition and permeability characteristics.

2.4.1.4 Durabilla Formation

Underlying the Walloon Coal Measures, the Durabilla Formation comprises an upward-fining sequence of thickly cross-bedded, fine-grained, labile to sublabile sandstones and interbedded siltstones and mudstones, and is largely devoid of coal (Green et l., 1997; QGC, 2014; Ryan et al., 2012). The Durabilla Formation conformably overlies the Hutton Sandstone.

2.4.1.5 Hutton Sandstone

The Hutton Sandstone underlies the Durabilla Formation. Deposition of the Hutton Sandstone occurred from a system of meandering rivers on a broad floodplain (Exon, 1976). The Hutton Sandstone is therefore highly heterogeneous, with significant lateral and vertical facies changes, especially towards the eastern margin of the Surat CMA (OGIA, 2016c). The dominant lithology comprises sublabile to quartzose sandstone interbedded with siltstone and shale. Like the Springbok Sandstone, the Hutton Sandstone is subdivided into upper and lower units. The upper Hutton

Sandstone generally includes greater proportions of permeable quartzose sandstones compared to the lower Hutton Sandstone, which contains higher proportions of lithic fragments (QGC, 2014).

2.4.2 Structure

The Surat Basin comprises a non-marine Jurassic succession and a mixed non-marine to marine Early Cretaceous sequence. Structures in the Surat Basin are predominantly controlled by the underlying basement structures of the Bowen Basin and older basement rocks (DNRM, 2005). Structural features of the Bowen Basin are generally reflected in the overlying Surat Basin sediments in a subdued manner, through the reactivation of deep basement faults in a different tectonic style (OGIA, 2016c). An example of this is the Hutton-Wallumbilla fault, where significant displacements of several hundred metres are observed in the basement sediments. Reactivation of the fault in an extensional manner has then led to the propagation of normal faults in the shallower Surat Basin sediments (OGIA, 2016c).

Several tectonic events are responsible for the current configuration of the Surat Basin. The Goondiwindi Event (Korsch & Totterdell, 2009) resulted in major regional compression during the Middle to Late Triassic. This event concluded sedimentation of the underlying Bowen Basin and resulted in significant extensional and thrust faults in the Bowen Basin.

During the Middle Cretaceous, a regional uplift and tilting event terminated deposition in the Surat Basin and resulted in large-scale erosion of Jurassic–Cretaceous sediments (Raza et al., 2009). This is often referred to as the Moonie event (Korsch et al., 2009) and caused only minor deformation, with reactivation of Triassic thrust faults generally manifested as folding in the Surat Basin succession.

Following this, a regional extensional event occurred associated with the cessation of rifting in the Tasman Sea. Both extensional and trans-tensional styles are observed in the Surat Basin associated with this event (Ryan et al., 2012).

A subsequent uplift and compression event in the Late Cretaceous caused significant folding and small-scale faulting. The displacement of faults associated with this event is generally less than 50 m.

3. Methodology

The assessment focuses on faults that are likely to affect groundwater flow between or across the aquifers adjacent to the Walloon Coal Measures, the overlying Springbok Sandstone and the underlying Hutton Sandstone. The analysis aims to explore the location and extent of possible increased connectivity caused by faults affecting the contact between the Walloon Coal Measures and these adjacent aquifers, and to assess potential depressurisation risks that may arise.

Given the key processes and considerations outlined in Chapter 2, the approach involved three main steps:

- **Fault mapping (section 4.1)**

  The first step involves a thorough review of existing fault picks, followed by supplementary interpretation of available seismic data to identify structures that may cause connectivity between key aquifers in the Surat Basin and the Walloon Coal Measures.

- **Multi-disciplinary case studies (section 4.2)**

  Sites were selected where faults potentially impact groundwater connectivity and where sufficient data were available to carry out a more detailed investigation. Multidisciplinary case studies were then conducted in order to understand the likely processes occurring at each site. This step includes the validation of conceptual models through numerical models. These investigations also serve as a basis for a regional analysis of fault-induced connectivity.

- **Regional analysis (section 4.3)**

  Based on the key findings from the case studies, regional analysis was undertaken to evaluate the potential for fault-induced connectivity between the Walloon Coal Measures and the Springbok and Hutton sandstones. The analysis includes an assessment of key fault attributes such as displacement, stratigraphic and lithological contact and fault permeability. These attributes are then assessed in a regional context to understand the scale of potential connectivity risks and to help identify sites for further investigation.

Three fault attributes are assessed as part of both the multi-disciplinary case studies and regional analysis[1]:

- **Leakage windows:** the likelihood of a fault transmitting flow horizontally between two formations will depend partially on the contact of permeable units either side of the fault plane. Leakage windows are areas on the fault plane where permeable units are juxtaposed against one another. Leakage windows are estimated as part of a leak point analysis, as described in section 3.3.
- **Horizontal resistance:** as well as the contact of permeable units, cross-formational flow because of faulting is also likely to be controlled by the resistance experienced on the fault plane itself. As such, a fault seal analysis was undertaken to estimate this cross-fault resistance (see section 3.4)

[1] Due to a lack of relevant data, some of the processes discussed in Chapter 2 (e.g. mineral precipitation/dissolution, time variant properties and a comprehensive assessment of critically stressed faults) are not able to be represented in this assessment. Future assessments may focus on these processes.

- **Stress conditions:** to assess the potential for faults to transmit impacts vertically through damage zones, fault orientations were assessed with respect to the principal horizontal stress directions. This part of the analysis is discussed in section 3.5.

Leakage windows and horizontal resistance attributes were used to assess the potential for cross-formation flow on a given fault, while the in situ stress conditions were used to infer where some faults may be critically stressed.

3.1 Area of interest

As this assessment is focused on faults that may transmit CSG impacts, the area of interest has been defined around the extent of current CSG developments within the Surat CMA. There are broadly four sub-areas, however this report will focus on a regional-scale assessment across these different subregions (see Figure 9 below).

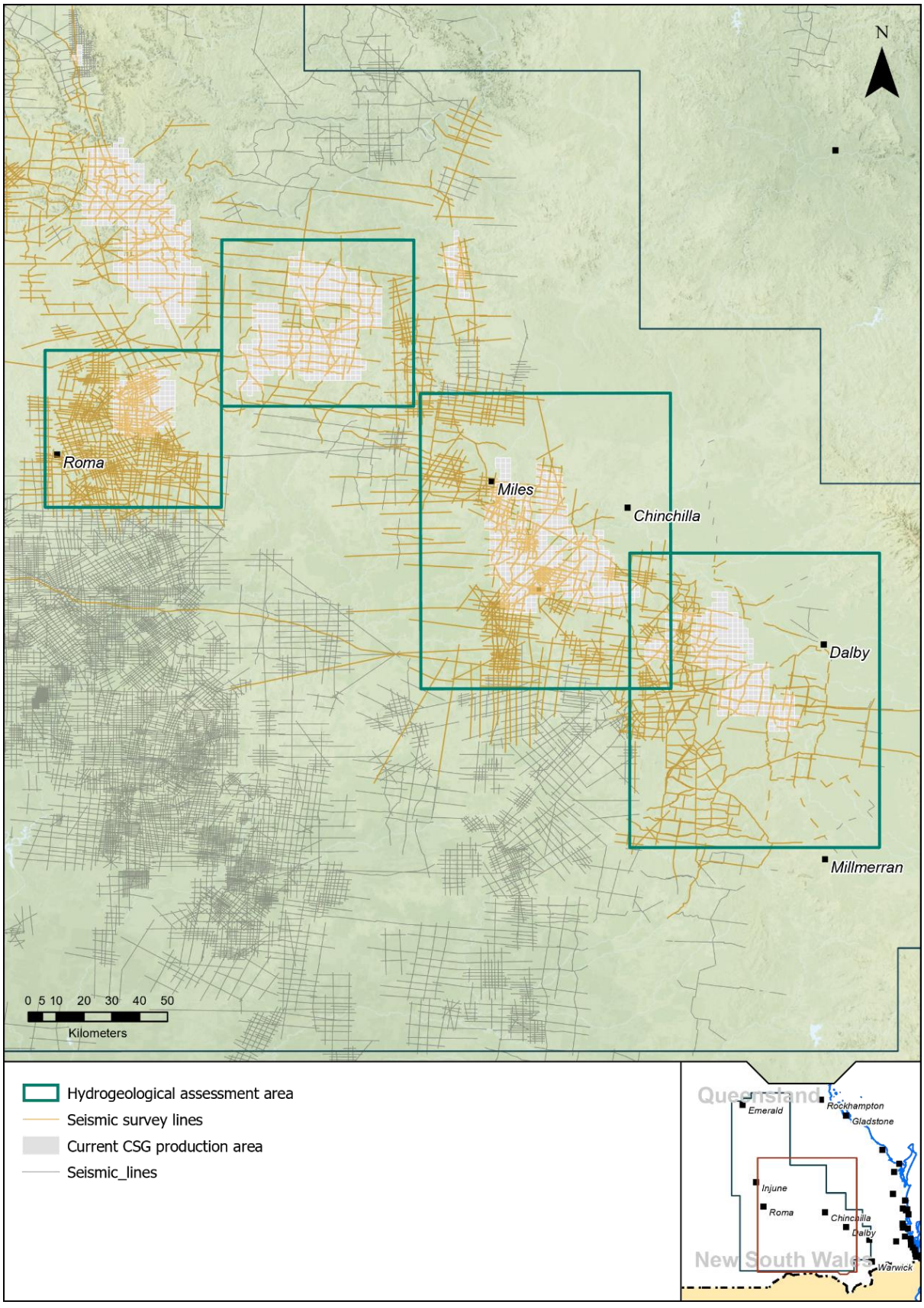

Figure 9 Map of the assessment area in the Surat CMA

3.2 Fault mapping

The main data set used for mapping of the location of faults in the Surat Basin is a repository of seismic data (2D and 3D) and associated interpretations, which were combined into a Petrel project (Schlumberger Pty Ltd platform) created by the University of Queensland (UQ) as part of its fault and fractures research (Copley et al., 2017). Available seismic lines are shown in Figure 9. The Petrel project contains all available seismic data, which includes 800 2D seismic lines and four 3D seismic surveys in the Surat CMA, together with a number of interpreted Surat Basin fault picks (Copley et al., 2017). This work did not, however, determine fault throws and as such, OGIA has independently reviewed this seismic data set for the purpose of picking and correlating faults that affect the interfaces between the Walloon Coal Measures and the Hutton and Springbok sandstones.

The faults discussed and shown in this report therefore pertain to these interfaces. Several smaller intra-formational faults have also been picked in the Walloon Coal Measures but are not presented in this report as these are considered to pose reduced risk of aquifer interconnectivity.

Furthermore, basement faults were not picked as part of this work, since the location of these faults is well understood and documented (Babaahmadi et al., 2015, 2016; OGIA, 2016c). A similar approach has been previously adopted for picking faults in the Eastern Surat Basin (Sliwa, 2013).

Two categories of faults have been interpreted (Figure 10 shows an example of both):

- **Mappable faults:** in some cases where 3D seismic data are available or where the faults can be mapped across multiple 2D seismic lines, these faults are shown as lines and labelled as “mappable faults”. These are present largely as complex fault systems, such as negative flower structures.
- **Fault intersections:** these are isolated faults that are not present in other nearby seismic lines. The key challenge with these faults is the determination of their orientation, as the faults may intersect seismic lines within a range of relative orientations.

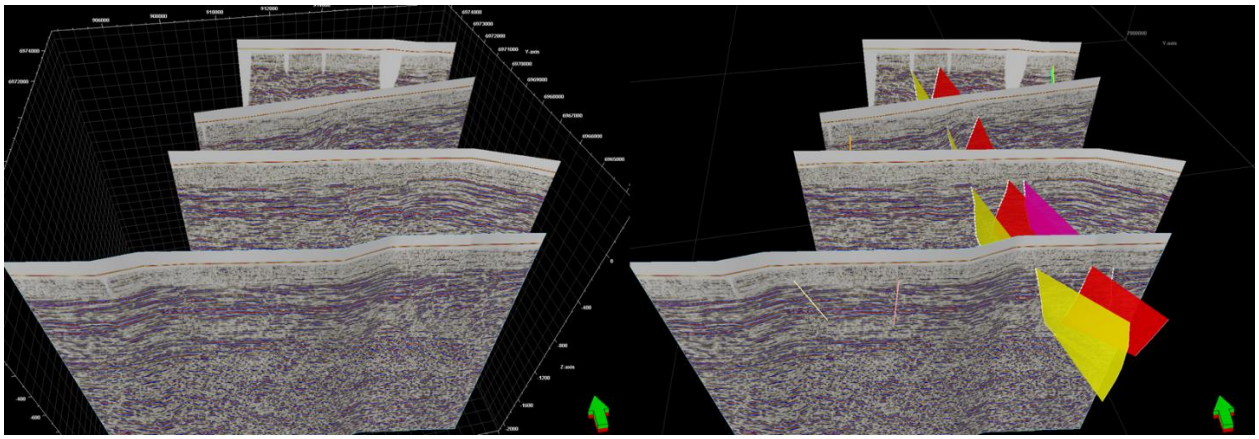

Figure 10 3D images of the Horrane Fault seismic data a) with no faults picks and b) with mappable faults and fault intersections

When estimating the displacements on all picked faults, a simple relationship assuming a uniform seismic velocity of 2,800 m/s was used to convert Two Way Time (TWT) to depth. The same relationship was previously applied for estimating displacements in the Surat Basin (Babaahmadi et al., 2015).

Fault displacements were estimated by first marking a single reflector on both sides of a fault intersection and then measuring the vertical TWT between these points, which was subsequently converted to depth using the aforementioned TWT-to-depth conversion. This analysis was done for faults intersecting the top and base of the Walloon Coal Measures.

Where the seismic coverage and quality allowed it, faults were mapped spatially across adjacent seismic lines, providing key information on fault orientation and subsequently on likely stress regimes. While fault orientation is not easily determined for fault intersections, the following data sets were used to infer the likely orientation:

- **Nearby mappable faults:** where mappable faults were present, nearby fault intersections were assigned similar orientations.
- **Formation curvature maps:** linear trends in formation curvature maps derived from stratigraphic surfaces may indicate the likely orientation of fault intersections. These lineaments were used as proxies for fault orientation (see Appendix B).
- **Basement structural map:** where strong lineaments or basement structural features were present, fault intersections may have similar orientation. In the Surat Basin, this is particularly true, as faults in the Surat Basin tend to form above basement features (OGIA, 2016).
- **Seismic line orientation:** faults that are visible on seismic lines are assumed to intersect at angles between ±45 to the orientation of the seismic line. However, where no other information is available, faults were assumed perpendicular to the line.

A combination of these methods was used where multiple lines of evidence were available.

3.3 Leak point analysis

In order to evaluate the likelihood of permeable sections of different formations being juxtaposed along a fault plane, leak point analyses were performed. 2D analysis was undertaken for the targeted case studies presented in section 4.2 and a simplified 1D analysis was also conducted for all faults in this study.

For both 1D and 2D scenarios, this involved using the closest available lithology log (from borehole wireline data) to infer the likely lithological context of a given fault. A maximum search distance of 2 km was applied to borehole data, to ensure the lithology was representative of the fault protolith.

For the 1D case, the displacement of a given fault intersection was then applied to the lithology log and subsequent leakage windows identified.

Leakage windows are sections of the fault plane where permeable units are in contact. In this analysis, leakage windows are created where coal in the Walloon Coal Measures is directly in contact with sandstones in either the Springbok Sandstone or the Hutton Sandstone. Results for this regional analysis are presented in section 4.3.

For the 2D case, simple fault displacement profiles were first generated using the quadratic equation:

$$f_{(x)} = -a(x-b)^2 + c \qquad \textbf{(1)}$$

Where:

$$c = D_{max}\ ,\ b = \frac{L}{2} \text{ and } a = \frac{c}{b^2}$$

Where:

D_{max} is the maximum displacement;

L is the length of the fault derived from the D_{max} /L ratio as derived from (Kim et. al, 2004);

$f_{(x)}$ defines the displacement as a function of distance (x). This is discussed in section 2.1.

Separate scenarios must be considered for the fault-induced connectivity between the Springbok Sandstone and Walloon Coal Measures, and between the Hutton Sandstone and Walloon Coal Measures. This is due to the presence of an aquitard, the Durabilla Formation, between the Walloon Coal Measures and the Hutton Sandstone, whereas the Springbok Sandstone directly overlies the Walloon Coal Measures.

The contact area between the Springbok Sandstone and Walloon Coal Measures is described by the entire area of the displacement profile, as no aquitard is present. Figure 11 represents this scenario.

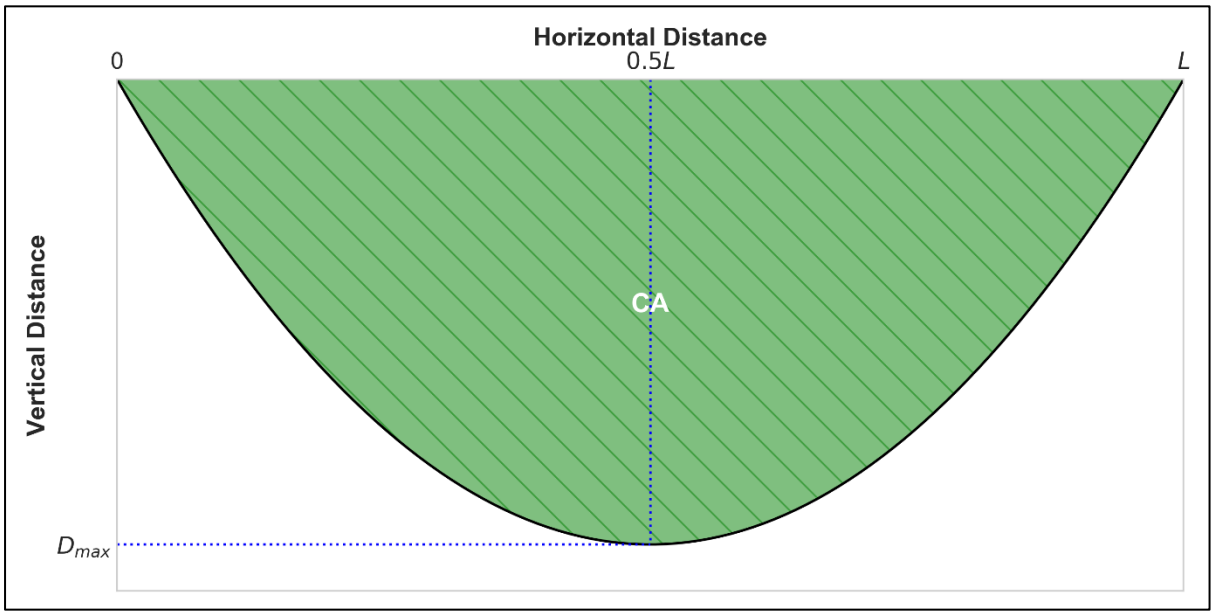

Figure 11 Hypothetical displacement profile and contact area between two formations where no aquitard is present

In this case, the contact area (*CA)* is described by:

$$CA = \int_0^L f_{(x)}\, dx \qquad \textbf{(2)}$$

A different model is required where an aquitard is present between the two formations of interest, such as the Durabilla Formation between the Walloon Coal Measures and Hutton Sandstone. Figure 12 represents this scenario.

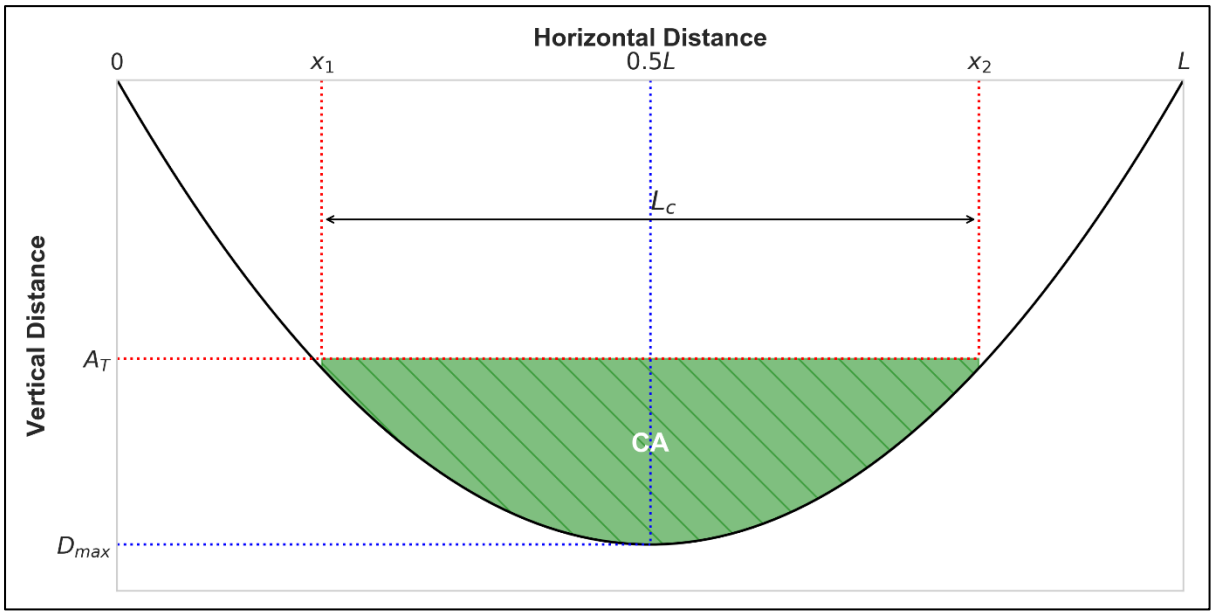

Figure 12 Hypothetical displacement profile and contact area between two formations where an aquitard separates the two formations of interest

In this case, the CA can be described by:

$$if\ D_{max} > A_T$$

$$CA = \int_{x1}^{x2} f_{(x)}\, dx - (L_c * A_T) \quad \textbf{(3)}$$

Where:

$$L_c = x_2 - x_1 \quad \textbf{(4)}$$

Where:

A_T is the aquitard thickness

x_2, x_1 are the x intercepts of the parabola where *f(x)* = A_T

L_c is the length of the fault that corresponds to CA.

Since only a proportion of the CA between the two formations on the fault plane will be dominated by sediments considered to be reasonably transmissive, further calculations are then necessary to obtain the leakage area (*LA*). This will largely be determined by the contact between highly permeable sediments on the fault plane. The following approach for determining LA is derived from (Allan, 1989).

Lithology data from a nearby borehole was extrapolated onto the fault plane to represent the up-thrown side of the fault (Figure 13a). The displacement profile was then applied to lithology data to represent the down-thrown side of the fault (Figure 13b).

Connected permeable units were then identified considering lithological profiles from both sides of the fault, and the areas of overlap were obtained in terms of potential leakage windows (*lw*) (Figure 13c). In this case, each leakage window represents a 1×1-m area of contact on the fault plane between these permeable units. The resulting map is referred to as an Allan Map (Allan, 1989).

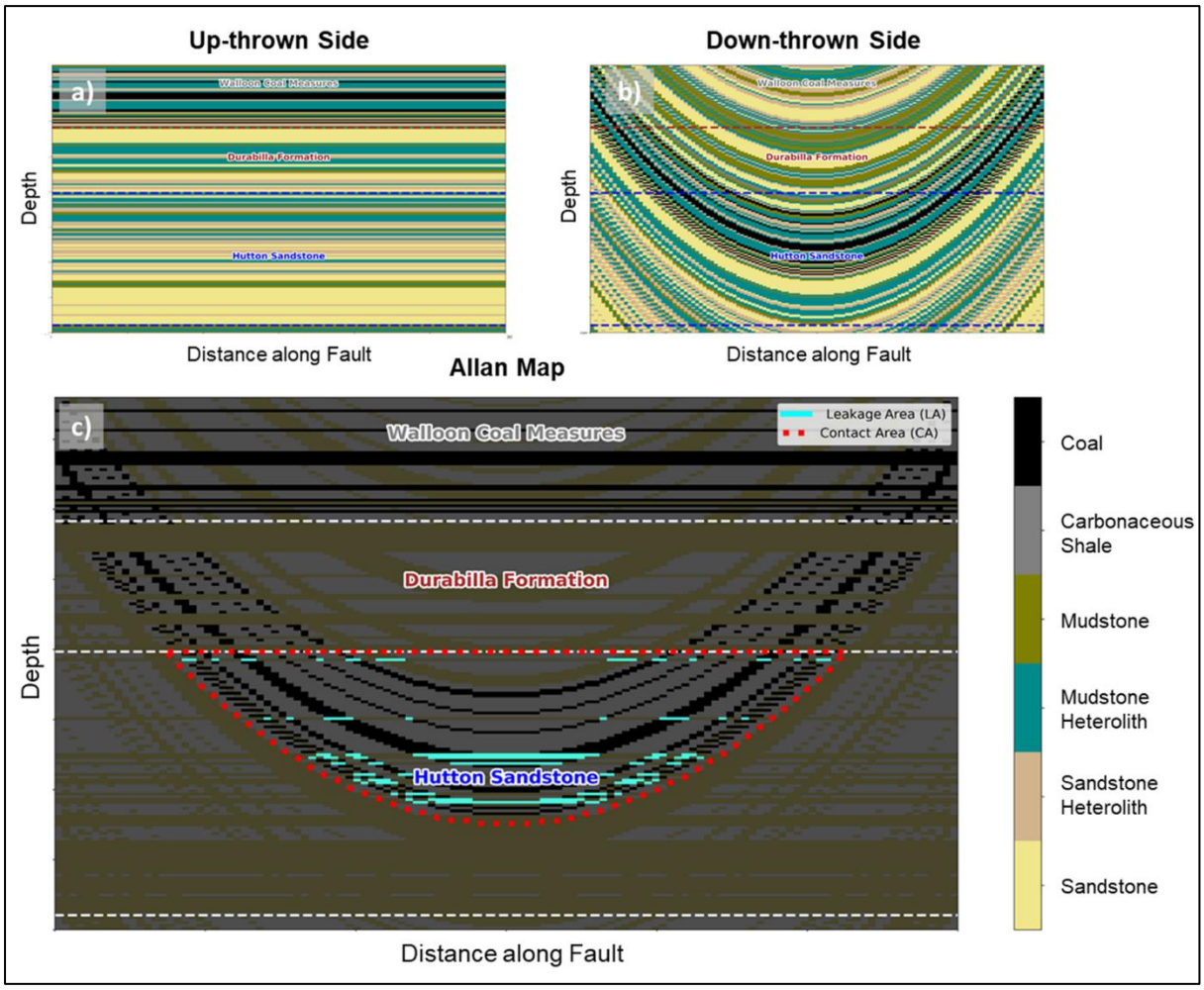

Figure 13 Lithology profile of a fault on a) up-thrown side, b) down-thrown side, and c) Allan Map showing estimated contact and leakage areas

From this, the total leakage area (*LA)* was calculated:

$$LA = \sum_{AT}^{D_{max}} lw \qquad \textbf{(5)}$$

3.4 Fault seal analysis

In the event that a fault places two permeable units against one another, clay-smearing may reduce the cross-fault permeability. Alternatively, if there are no significant proportions of clay in the entrained sediment, cross-formational flow may not be inhibited.

The Shale Gouge Ratio (SGR) is a quantitative proxy for the amount of clay-smearing likely to occur on a fault plane and can further be related to the horizontal resistance imparted by the fault. SGR can be calculated using (Yielding et al., 1997):

$$SGR = \frac{\sum Shale\ Bed\ thickness}{fault\ displacment} \cdot 100\% \qquad \textbf{(6)}$$

For this assessment, the shale bed thickness has been calculated as the total thickness of mudstone and siltstone (from lithology logs). The fault displacement was obtained from seismic interpretation as described in section 3.2.

For targeted case studies and the 2D analysis, the SGR was calculated along the entire fault plane and the results are presented in section 4.2.

For the 1D case, the SGR was calculated along the contact with the Walloon Coal Measures using lithology data for the nearest borehole within 2 km. Results for this are presented in sections 4.3.1.1 and 4.3.2.1.

A meta-analysis of permeability measurements in fault cores was used to derive the following relationship between the permeability of the fault core material (k_f) and SGR (Wibberley et al., 2008):

$$log k_f(mD) = -1.01 - 5.34 \cdot SGR \quad \textbf{(7)}$$

This relationship was used to estimate the horizontal permeability of each fault plane accounting for the SGR. Values for k_f ranging between 8.6×10^{-02} and 1.8×10^{-5} mD (or 1.1×10^{-4} to 2.3×10^{-8} m/day) were obtained for the range of SGR calculated for Surat Basin faults (10–70%). Several additional parameters were then also estimated in order to further understand the likely resistance to horizontal flow imparted by each fault.

Ignoring the fault core, the permeability across the fault would be described by the permeability of the juxtaposed material across the fault. This can be calculated by the harmonic mean of the permeability on either side of the fault (K_1 upthrown side and K_2 downthrown side):

$$k_{12} = \frac{2}{\frac{1}{k_1} + \frac{1}{k_2}} \quad \textbf{(8)}$$

The permeability across the fault (cross-fault permeability) depends not only on the nature of the juxtaposed material, but also on the permeability of the fault core, which can be affected by clay-smearing. As such, the cross-fault permeability was estimated using the harmonic average of all three sides. This represented the cross-fault permeability including the effect of the fault core[2]:

$$k_{fault} = \frac{3}{\frac{1}{k_1} + \frac{1}{k_2} + \frac{1}{k_f}} \quad \textbf{(9)}$$

From here, the transmissibility multiplier TM_{fault} was used to quantify the effect of the fault core on overall cross-fault permeability. Transmissibility multipliers are commonly used in reservoir models to represent fault zone properties and requires:

$$TM_{fault} = \frac{k_{fault}}{k_{12}} \quad \textbf{(10)}$$

A TM_{fault} of 1 therefore implies that the fault has no effect on cross-fault permeability, while numbers less than 1 reflect a cross-fault permeability reduction. This is useful in assessing the potential for cross-formation flow at a given fault intersection.

[2] Equations 8, 9 and 10 are commonly utilised in reservoir modelling as part of upscaling workflows (Manzocchi et al., 1999). In that context, these equations usually account for the fault thickness relative to cell size in equation 9. However, for the purposes of this report, they are only used as indicative measures of the effect of the fault on cross-formational flow.

An additional metric (kc) or the contact permeability can be calculated as the harmonic mean of horizontal permeability on the up-thrown side of the fault (k) and the estimated horizontal permeability of the fault core (k_f). kc is calculated along the entire fault plan and is obtained by:

$$kc = \frac{2}{\frac{1}{k_1} + \frac{1}{k_f}} \quad \textbf{(11)}$$

The leak point analysis and fault seal analysis were undertaken together as part of a “cross-fault leakage analysis”. Results are presented for two faults in sections 4.2.1.2 and 4.2.3.4.

3.5 Vertical connectivity assessment

As discussed in section 2.3.2, the primary pathway by which faults may propagate impacts vertically is via fractures in the damage zones. The key attribute likely to affect whether or not a fault acts as a vertical conduit is therefore the fracture permeability. This will largely be a function of fracture aperture.

This attribute is strongly controlled by the orientation of fault-related fractures with respect to the principal horizontal stress direction, i.e. whether the fractures are subject to compressional or dilatational forces. While this is ultimately a three-dimensional problem, a simplified assessment was conducted due to the lack of data.

Principal horizontal stress data (SHmax) were compiled from various sources for the Surat and Bowen basins, yielding 146 stress orientation measurements. These data were interpolated using a natural-neighbour algorithm to create the regional principal horizontal stress map shown in Figure 14.

A simple approach was adopted to evaluate whether a given fault’s damage zone is likely to be subject to compressional or dilatational forces. The relative angle between fault orientation and SHmax was utilised as a proxy for potentially critically stressed conditions.

Additionally, the depth to Walloon Coal Measures was incorporated into the analysis to account for the depth dependency of fracture permeability, as discussed in section 2.3.2.2.

The assumptions in this approach are as follows:

- fractures in fault damage zones are oriented similarly to the main fault
- regional SHmax orientations are a reasonable proxy for local conditions at the fault.

No stress data were available for the eastern gas fields and as such, the analysis could not be carried out in this area. Results for this analysis are presented in section 4.3.2.2.

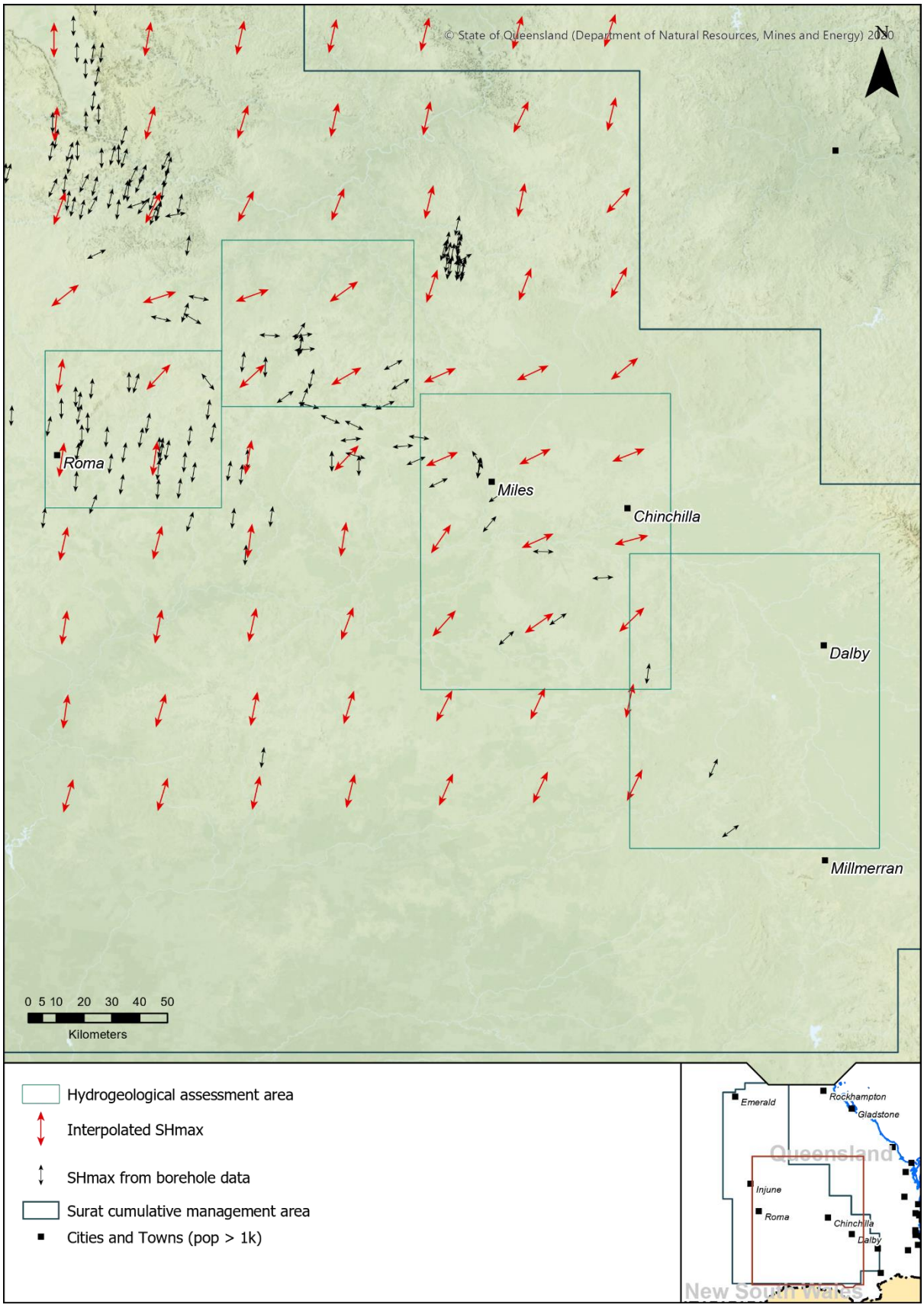

Figure 14 Map of available principal horizontal stress data and the interpolated stress map

4. Results and discussion

4.1 Fault mapping

Based on the available seismic information, a total of 61 mappable faults and 1,230 fault intersections are identified in focus areas in and around the CSG development. These faults have currently been picked in Two Way Time (TWT) from key seismic surfaces, such as the top and bottom of the Walloon Coal Measures.

All identified mappable faults and fault intersections are shown in Figure 15. Both types of faults have been picked in 3D and some information is therefore available about fault geometry (dip angle, displacement and structural style).

594 faults have been identified which affect the Walloon Coal Measures and Hutton Sandstone and 560 have expression across the Walloon Coal Measures and Springbok sandstone.

The displacements on fault intersections are generally small (<50 m).

Mappable faults generally follow the orientation of larger basement structures, such as the Hutton-Wallumbilla Fault in the west and the Taroom Trough in the central part of the basin. There are also less mappable faults in the northern part of the basin, however the density of fault intersections is consistent across the basin.

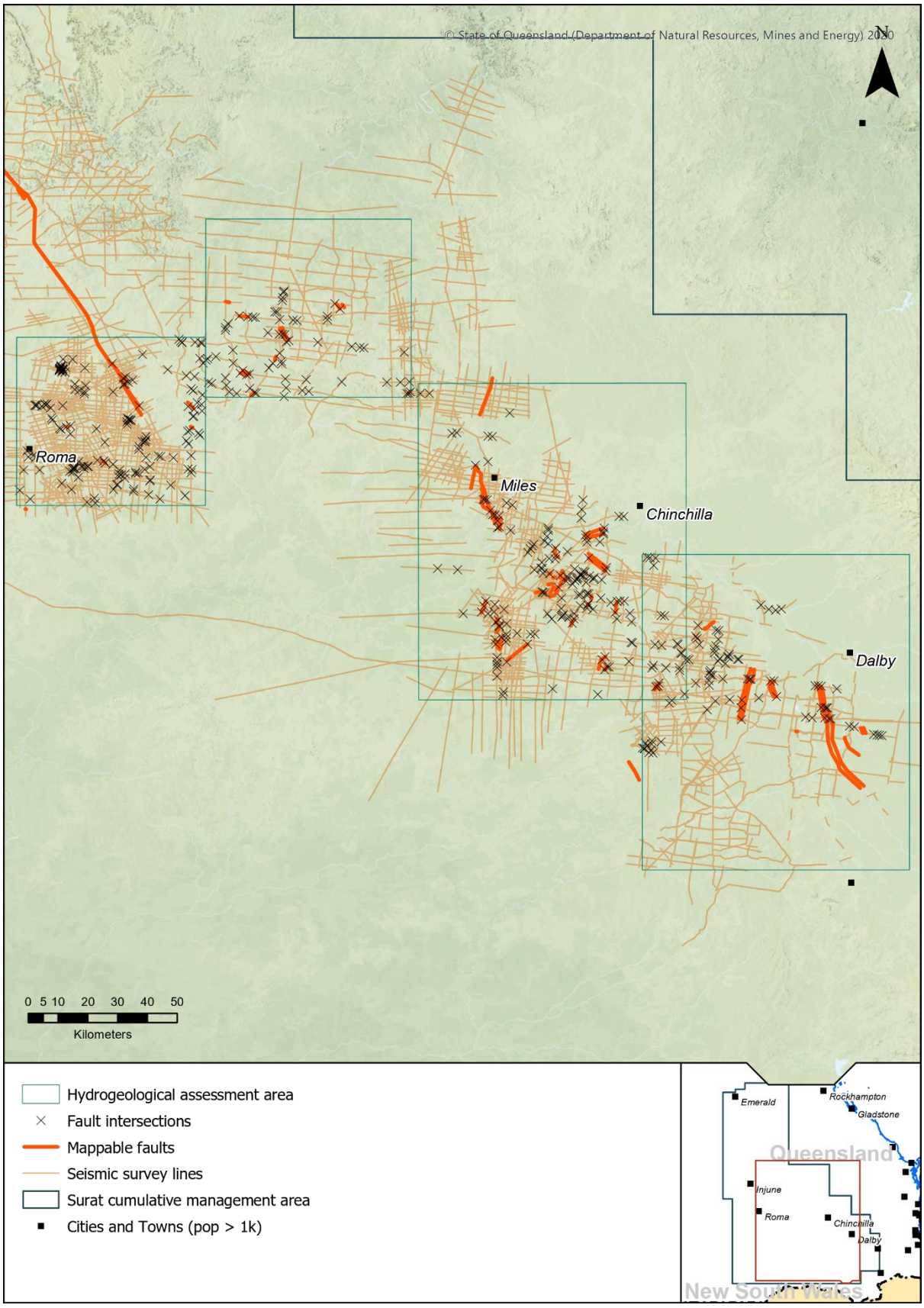

Figure 15 Mappable faults and fault intersections within the assessment area

4.2 Case studies

Several locations have been identified in the Surat Basin where faults have the potential to alter groundwater flow locally. This section outlines some selected sites where sufficient data are available to allow further assessment of the likely hydrogeological behaviour of the mapped faults. These investigations will serve as a basis for conceptualisation of similar faults in the Surat Basin.

4.2.1 Horrane Fault

The Horrane Fault is a regionally significant structural feature in the eastern part of the Surat Basin. The fault originates from a basement fault system and has subsequently propagated into the Surat Basin, with a normal tectonic style consistent with keystone structures described by Copley et al., 2017. The Horrane Fault is significant due to its relatively large displacements (~100 m) and proximity to active CSG production as well as the Condamine Alluvium. The large displacement increases the likelihood of juxtaposing aquifers with the Walloon Coal Measures. Figure 17 shows the fault mapping and proximity to CSG production.

4.2.1.1 Seismic interpretation

Several existing seismic lines are utilised to interpret the Horrane Fault zone, orientation and displacement, including those lines provided by Arrow Energy during the course of the current study. The interpreted length of the fault zone is nearly 40 km, trending north–south and exhibiting a normal tectonic style. The main fault forms the western margin of the zone, accompanied by smaller synthetic and antithetic faults forming a negative flower structure. Some seismic sections show a compressional feature in the centre of the structure, referred to as a keystone structure (Copley et al., 2017). There are also a number of synthetic and antithetic faults along the periphery of the main fault zone. The seismic interpretation and mapped extent of the fault are shown in Figure 16 and Figure 17.

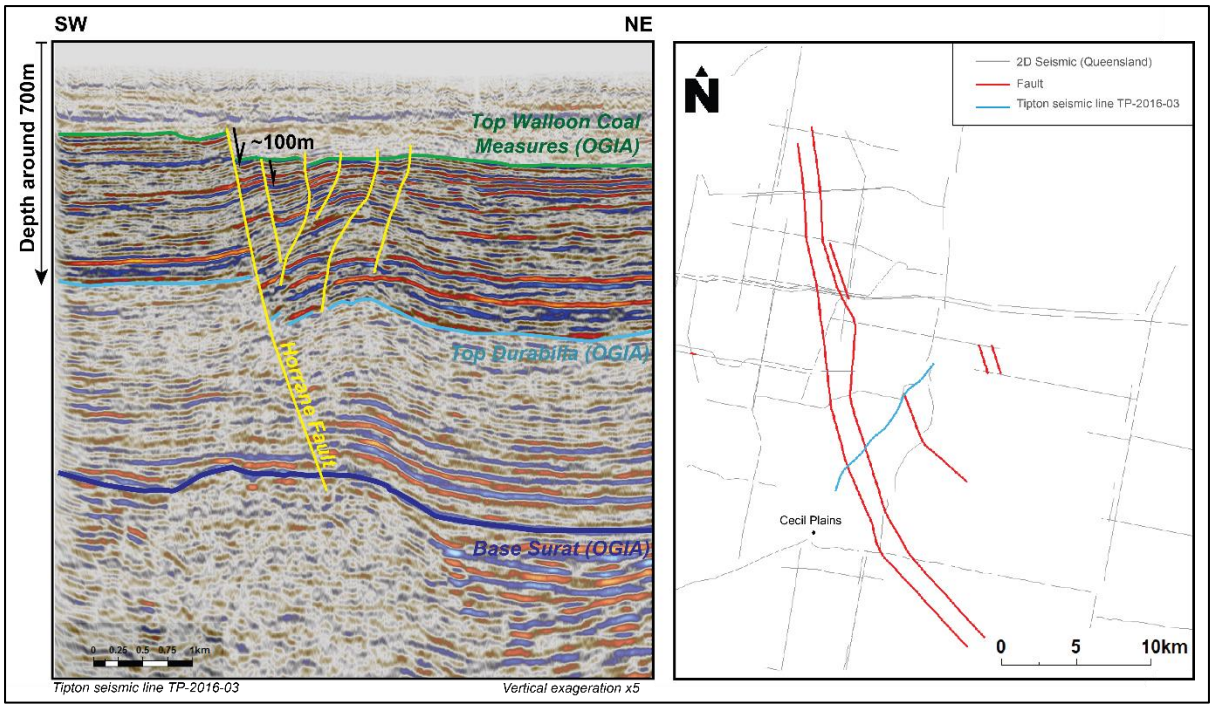

Figure 16 Seismic Interpretation of the Horrane Fault

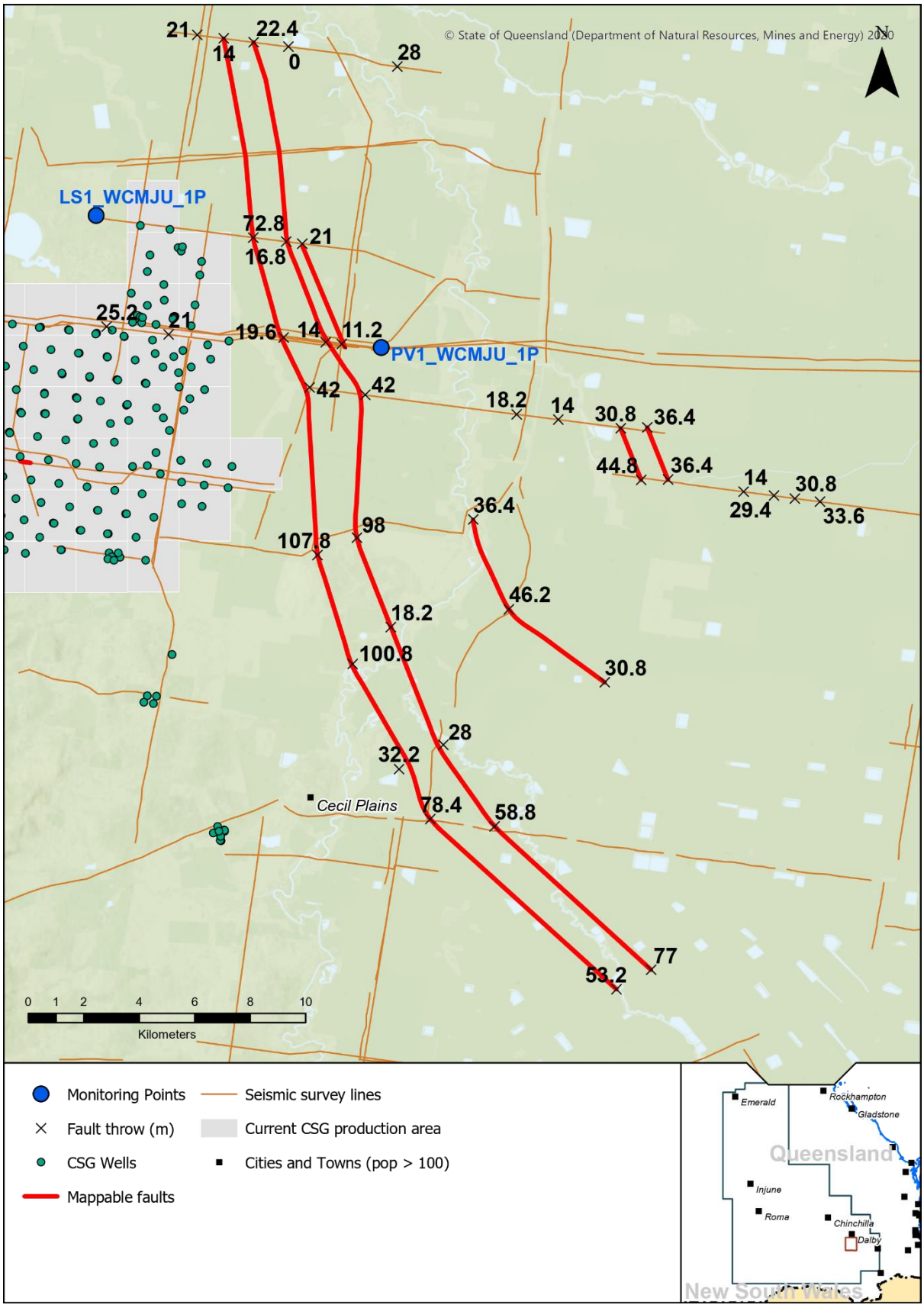

Figure 17 Map of the Horrane Fault, associated observed fault displacements and nearby CSG wells

The Horrane Fault has maximum interpreted displacement of 108 m. Based on a correlation of fault length to maximum displacement from several studies, a normal fault of this length is likely to result in an unrealistic displacement of about 1,000 m (Kim & Sanderson, 2005). This suggested that the fault may comprise a number of smaller segments, rather than a single fault. To test this, a profile of seismic interpreted displacement was developed along the fault (Figure 18), which confirmed the multiple troughs and highs in displacement along the fault length.

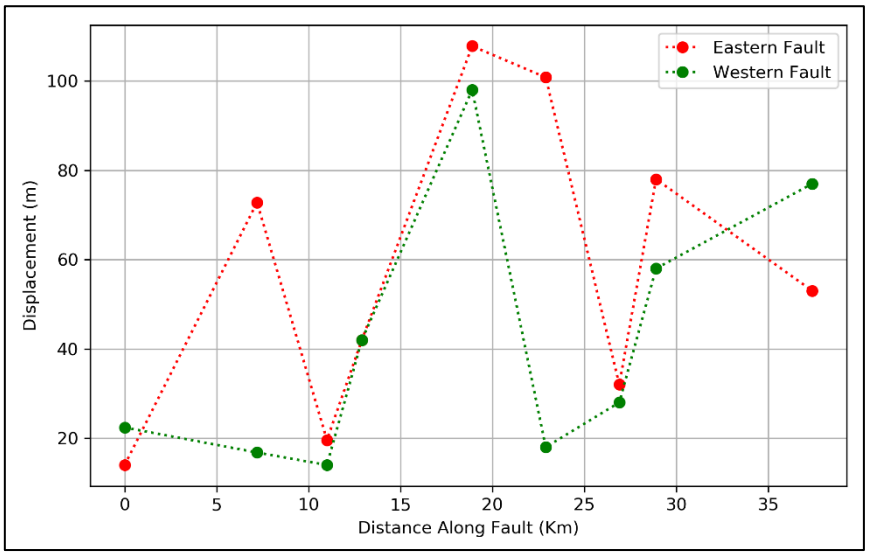

Figure 18 Displacement distribution along strike of the Horrane Fault zone; both eastern and western faults are shown

Displacement data were split at local minima and a parabolic function was fitted to each segment and normalised, such that each segment had no displacement at each end. Results suggest that fault segments are between 12.5 and 17.5 km in length, while maximum displacement generally increases with segment length (Figure 19). These values are consistent with the literature length–displacement relationship referred to earlier (Kim & Sanderson, 2005).

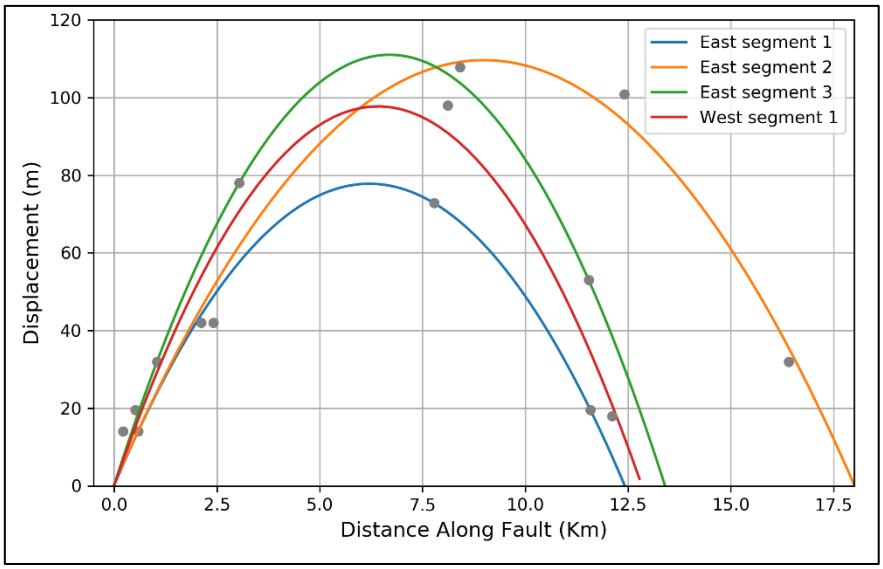

Figure 19 Normalised displacement profile for segments along the Horrane Fault

This variability in displacement along the Horrane Fault suggested the likely presence of either relay ramps along the strike of the fault, or transfer faults that may be perpendicular to the main fault.

However, the available data do not indicate the presence of perpendicular faults, and so relay ramps are more likely to occur here.

4.2.1.2 Cross-fault leakage

A cross-fault leakage analysis was undertaken for the Horrane Fault. Figure 20 below shows the leakage windows, estimated permeability and associated SGR (see section 3.3). The Durabilla Formation at this location is approximately 30–50 m thick; as such, displacements of more than 50 m have the potential to connect permeable sandstones in the upper Hutton Sandstone with coal seams in the Taroom Coal Measures (lower part of the Walloon Coal Measures). Nearby bore logs suggest the Hutton Sandstone at this location is highly heterogeneous and has limited sandstone (Figure 20 a, b), which would limit leakage windows on the contact zone with the Taroom Coal Measures (Figure 20d). Figure 20c shows the SGR approaches 50% along the entire section of the fault; as such, the transmissibility multiplier is generally less than 1 on leakage windows (Figure 20f). This indicates that the fault core here is likely to offer some resistance to cross-formational flow.

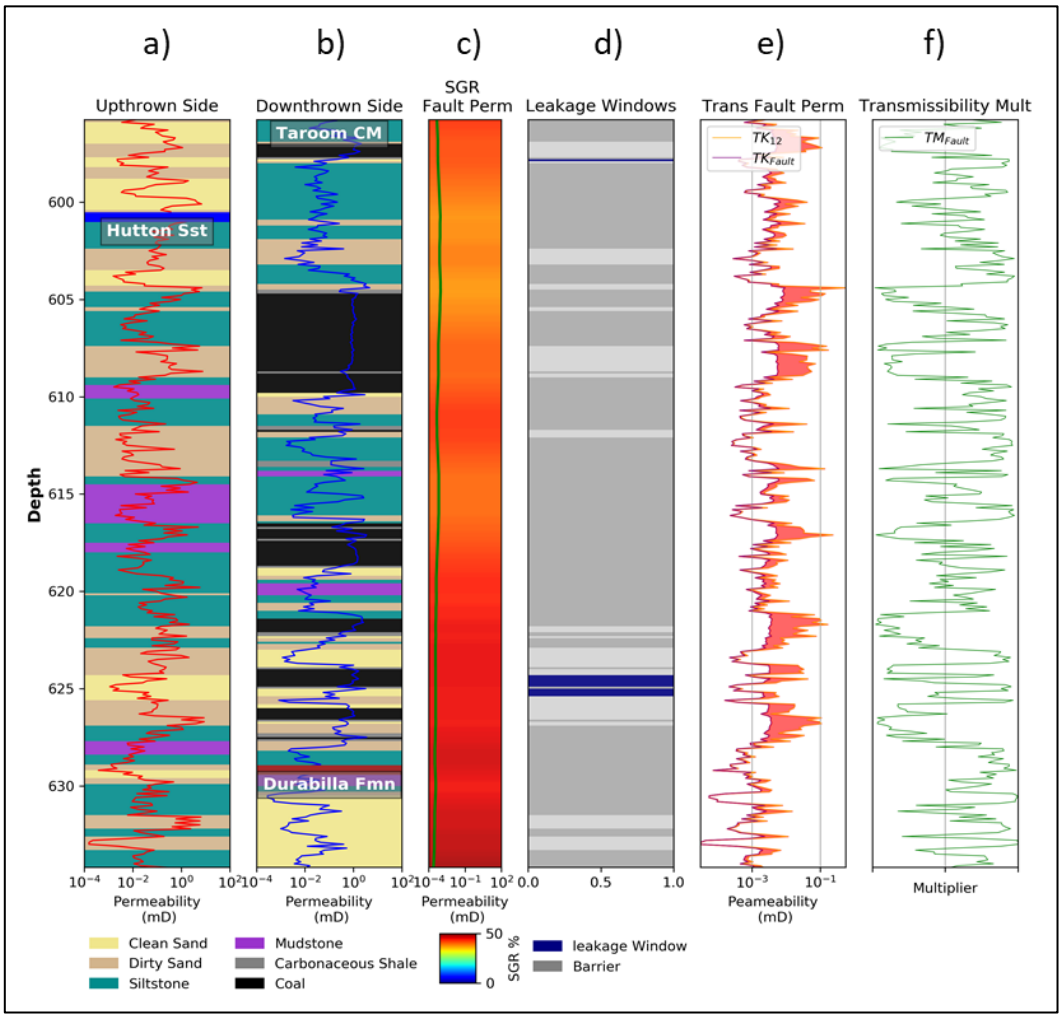

Figure 20 1D cross-fault leakage analysis for a fault intersection along the Horrane Fault

As outlined in section 3.4, a 2D fault seal analysis was undertaken for the Horrane Fault, as presented in Figure 21. This shows the combination of leakage windows and the SGR across the contact area between the Hutton Sandstone and Walloon Coal Measures (refer to sections 3.3 and 3.4). In this case, Figure 12 shows the appropriate representation of the contact area. The leakage windows comprise approximately 5% of the contact area between the Walloon Coal Measures and

the Hutton Sandstone. The SGR is also consistently high (average ~36%). As a result, a combination of limited leakage windows and the clay-smearing on the fault plane will collectively reduce the potential for cross-formational flow.

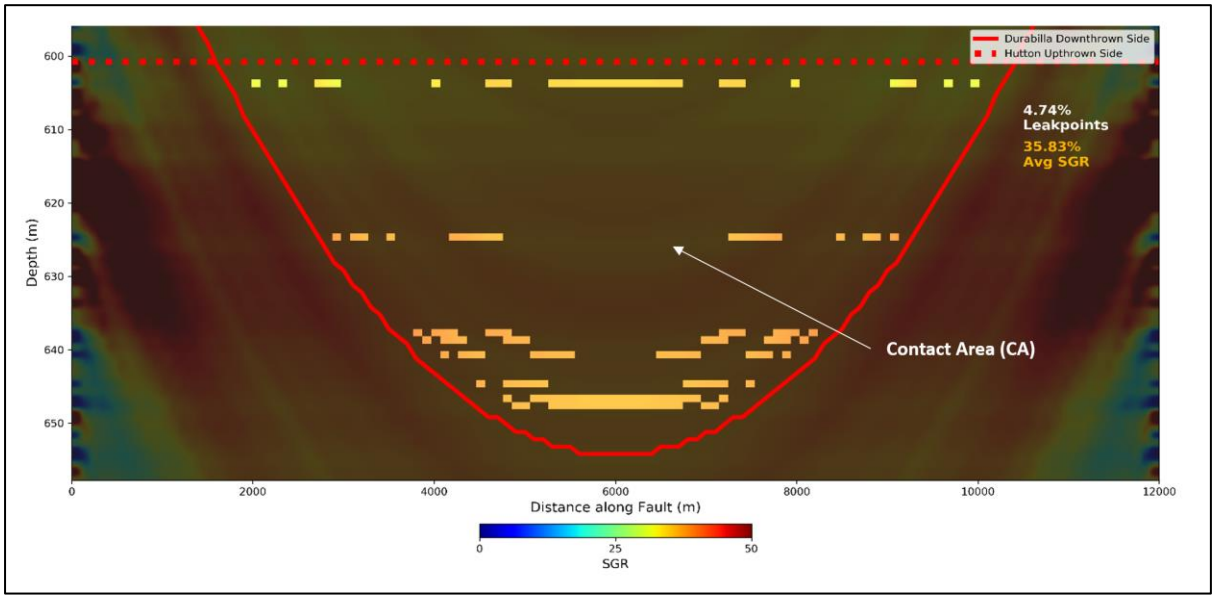

Figure 21 2D cross-fault leakage analysis for a segment of the Horrane Fault

As it is possible that seismic lines have not intersected the maximum displacement of the fault segment, a sensitivity analysis subsequently evaluated the potential effects of underrepresenting the maximum displacement of this fault. The total contact area, leakage area and average SGR were estimated for a range of maximum displacements up to 140 m (larger than any observed displacements in the Surat Basin, and as such, a conservative upper bound). Figure 22 presents the results of this analysis. The leakage area is consistently low for maximum displacements below 80 m on this fault (compared to other faults such as the Kenya East fault, discussed in section 4.2.3.4) and there is only marginal increase in potential for horizontal flow across the fault plane with increasing displacement. This is likely due to the highly heterogeneous nature of the upper Hutton Sandstone at this location.

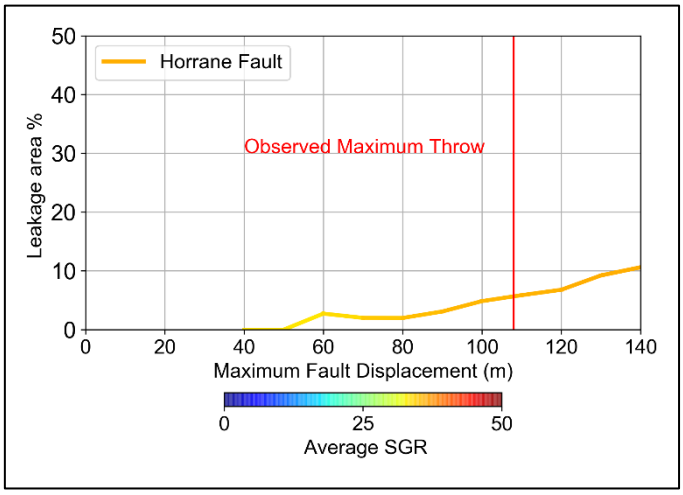

Figure 22 Results from a sensitivity analysis, evaluating total contact area as a function of varying maximum displacement at the Horrane Fault

4.2.1.3 Groundwater monitoring

Additional insight on the hydrogeological behaviour of the Horrane Fault can be derived from two groundwater monitoring points in the Upper Juandah Coal Measures either side of the fault: LONG SWAMP 1 (LS1_WCMJU_1P) on the western side and PLAINVIEW 1 (PV1_WCMJU_1P) on the eastern side (Figure 17). LONG SWAMP 1 is also close to the CSG production fields.

As shown in Figure 23, data for LONG SWAMP 1 on the western side exhibits 15 m of drawdown between 2009 and 2017, while PLAINVIEW 1 on the eastern side of the fault shows no change or even a slight increase in groundwater pressure. The eastern monitoring point also has consistently higher groundwater pressures (almost 40 m higher) than on the western side. These data suggest limited connection between these monitoring points, consistent with the likely horizontal barrier effects caused by the Horrane Fault (at least within the Walloon Coal Measures).

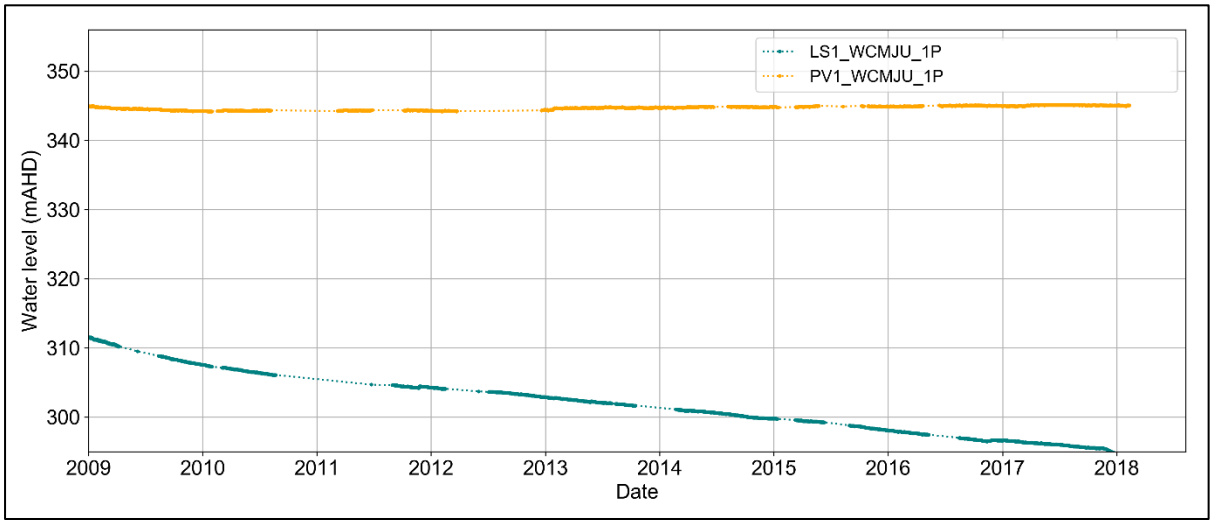

Figure 23 Monitoring in the Walloon Coal Measures, either side of the Horrane Fault

4.2.1.4 Key findings

The Horrane Fault is one of two instances where a fault in the Surat Basin is thought to have sufficient displacement to juxtapose the Hutton Sandstone with the Walloon Coal Measures. The displacement on this fault generally exceeds the thickness of the Durabilla Formation (~55 m), which allows for the juxtaposition of the two units. However, a cross-fault leakage analysis suggests that the heterogeneous nature of the Hutton Sandstone may result in a leakage area of less than 5% of the fault plane. Furthermore, clay-smearing is expected to produce low-permeability fault core material across the Hutton Sandstone to Walloon Coal Measures contact, as evidenced by high SGR values.

Although there are currently no groundwater level data for the Hutton Sandstone near the Horrane Fault, large pressure differences are observed in the Walloon Coal Measures on either side of the fault, suggesting the fault may act as barrier for that formation.

The displacement of the fault at some locations exceeds the thickness of the overlying Springbok Sandstone and, hence, there is some potential for coal seams in the Walloon Coal Measures to be in contact with the Condamine Alluvium. This will largely depend, however, on the extent of neo-tectonic reactivation of the Horrane Fault. If faulting occurred syndepositionally or postdepositionally, then it may be possible for coal seams in the upper portion of the Walloon Coal Measures to be juxtaposed against the Condamine Alluvium. However, if deposition of the Condamine Alluvium occurred after the last fault reactivation event, connectivity will be less likely, due to the intact nature of the transition

zone at the base of the alluvium. If faulting does extend into the Condamine Alluvium, vertical flow through the fault damage zone may play a role in connectivity.

Arrow Energy has also conducted an investigation around the Horrane Fault to better understand the reservoir characteristics of the Walloon Coal Measures and establish hydraulic characteristics of the fault (Viljoen et al., 2020).This work included a 2D seismic survey, coring through the fault zone and hydraulic testing across the fault zone. Results indicate that above the fault zone (eastern side), the pressure in the Walloon Coal Measures is close to hydrostatic conditions with high gas content, while below the fault zone (western side), the pressure is 50% below hydrostatic pressure with lower gas content. This suggests limited connectivity across the fault zone within the Walloon Coal Measures. However, there is currently no pressure data from the Hutton Sandstone to infer this behaviour in the underlying Hutton Sandstone or any potential interaction with the Walloon coal Measures.

4.2.2 The Hutton-Wallumbilla Fault

The Hutton-Wallumbilla Fault is a near-vertical thrust fault dividing the Comet Ridge Platform from the lower Roma Shelf (Green, 1997). The main thrust fault event occurred in the Early Permian during the back-arc extension phase of the Bowen-Gunnedah Basin, which produced a series of graben and half-graben structures along the eastern margin of the Australian continent (Jones & Veevers, 1983). Periods of reactivation have extended the fault through the overlying sediments and have resulted in pervasive en echelon faulting with evidence of reactivation in the near surface (Coote, 1984; Jensen et al., 1964). While the fault system exhibits more than 300 m of displacement in the Bowen Basin, faulting in the Surat Basin is more subdued.

There are a number of important connectivity features associated with this fault, including the regionally significant Precipice–Bandanna contact zone (OGIA, 2019f). This section, however, will focus on a multidisciplinary case study around a group of springs that are found in the vicinity of the Hutton-Wallumbilla Fault (OGIA, 2015d). This site has been selected due to several lines of evidence for structural control on local groundwater dynamics.

The Lucky Last and Abyss spring complexes are located approximately 20 km north of Injune (Figure 24). OGIA has undertaken a detailed conceptualisation of these sites as part of a spring wetland conceptualisation project (OGIA, 2015d). A multidisciplinary investigation was conducted to test several hypotheses regarding the water source and mechanism of flow at this site. Investigations included geological mapping, geophysical surveys, well logs, water chemistry and water level information (OGIA, 2015b).

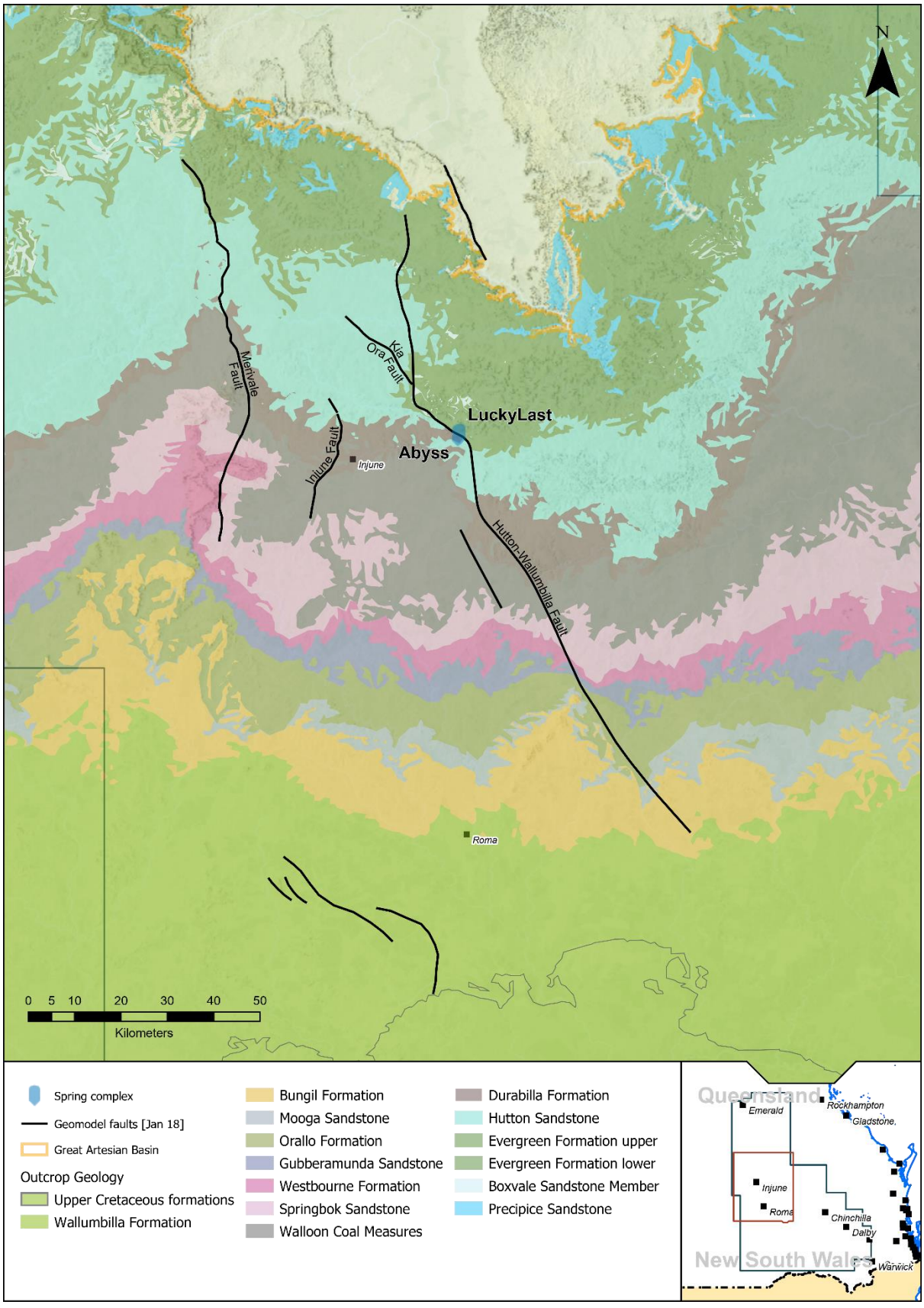

Figure 24 Map showing Hutton-Wallumbilla Fault and location of the springs

4.2.2.1 Seismic Interpretation

Seismic data in vicinity of the Lucky Last and Abyss spring complexes (Figure 25a) were collected in the 1970s and the resolution of near-surface sediments is therefore poor. It is clear, however, that there is a complex deformation zone associated with the fault in this area. Both the lower resolution in the near surface and the complex deformation add to the challenge of determining the influence of faulting on the Surat Basin formations. While individual faults are not able to be mapped, a deformation zone can still be delineated from the available seismic data (Figure 25b). In this case, both springs of interest are located within this deformation zone.

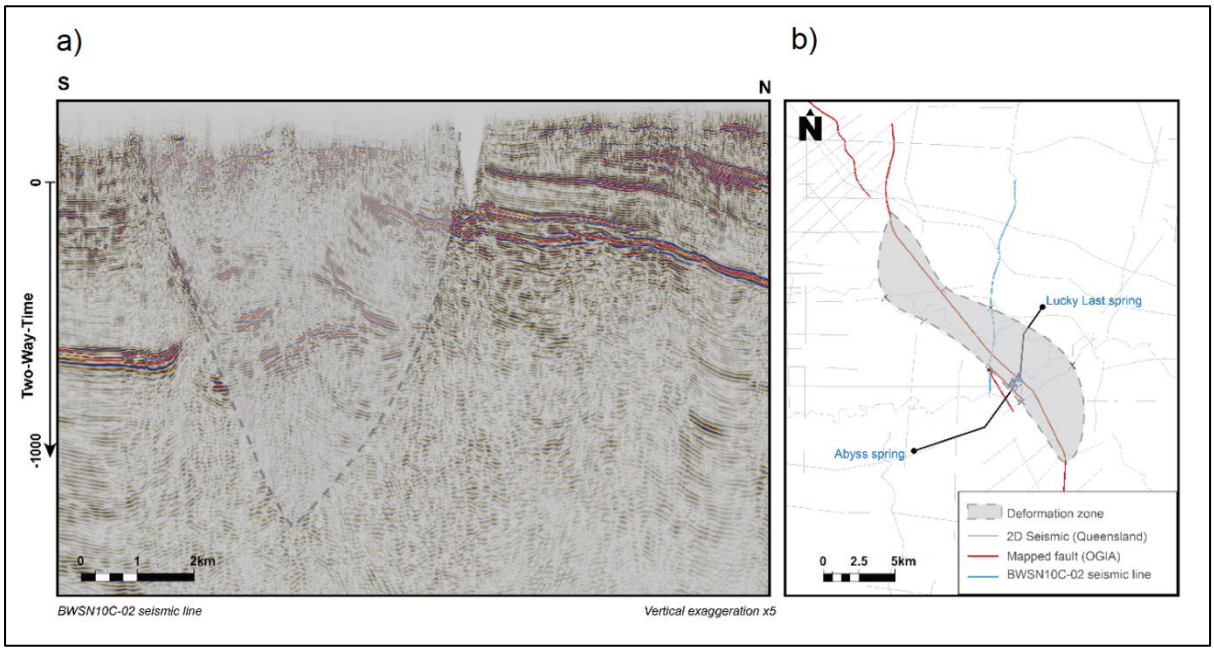

Figure 25 a) nearby seismic line with the deformation zone, and b) map showing the Hutton-Wallumbilla Fault zone and spring locations

Some more recent seismic data over this fault zone are available to the south of the site. These data can be used to infer the likely geometry of faulting in the Surat Basin formations (Figure 26) and show that the Hutton-Wallumbilla thrust fault terminates in the lower Surat Basin, overlain by folding sediments at the unconformity. Faulting in the Surat Basin formations originates at the “shoulder” of the basement fault where Surat Basin sediments roll over the unconformity. The structural style in the Surat sediments is predominantly normal, forming negative flower structures and extending into shallow formations of the Surat Basin. This type of faulting is common in the Surat succession along the strike of basement faults.

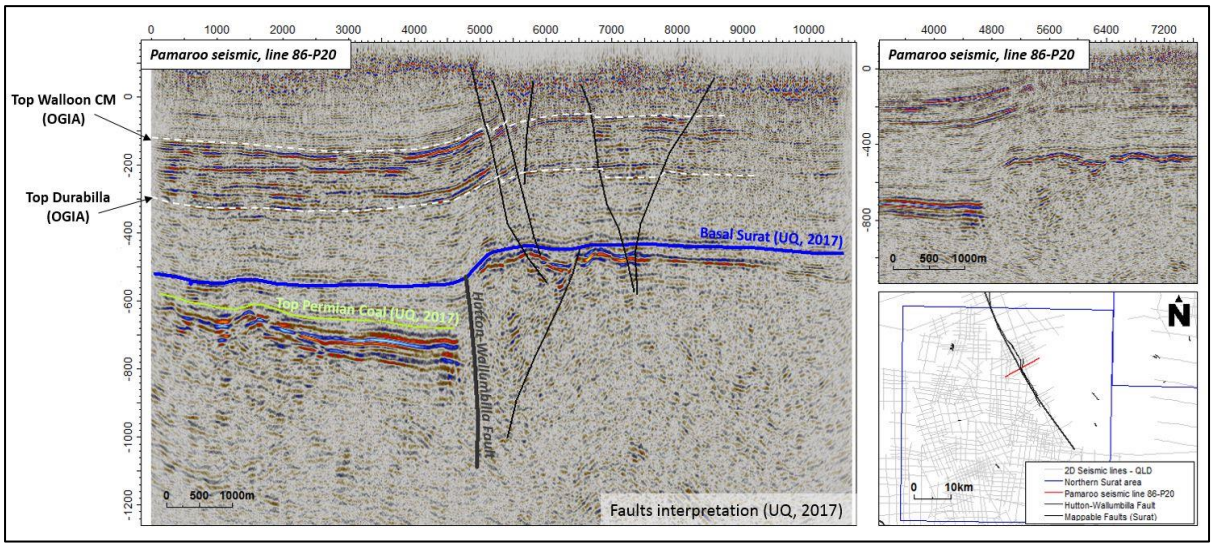

Figure 26 Seismic section showing the structural style of Hutton-Wallumbilla Fault within the Surat Basin sediments

4.2.2.2 Geology

Investigation bores were used to infer the Hutton Sandstone as the underlying formation for the Abyss springs. However, outcrop mapping suggested the lower Evergreen Formation to be present at surface at the Lucky Last springs. The Boxvale Sandstone is not observed at outcrop, the mapping of which also reveals a lineament aligned with the wetlands area. This sharp change in geology could be explained by the presence of local faulting. Additionally, the bedding dip was observed to be different on either side of the inferred fault zone. Due to the resolution of seismic data in the near surface, it is difficult to determine the exact geometry and influence of faulting in this region; however, the deformation is likely to be complex, as is observed in deeper sediments at this location (Figure 25). The surface geology for the area is presented in Figure 27a, with a conceptual stratigraphic cross-section in Figure 27b.

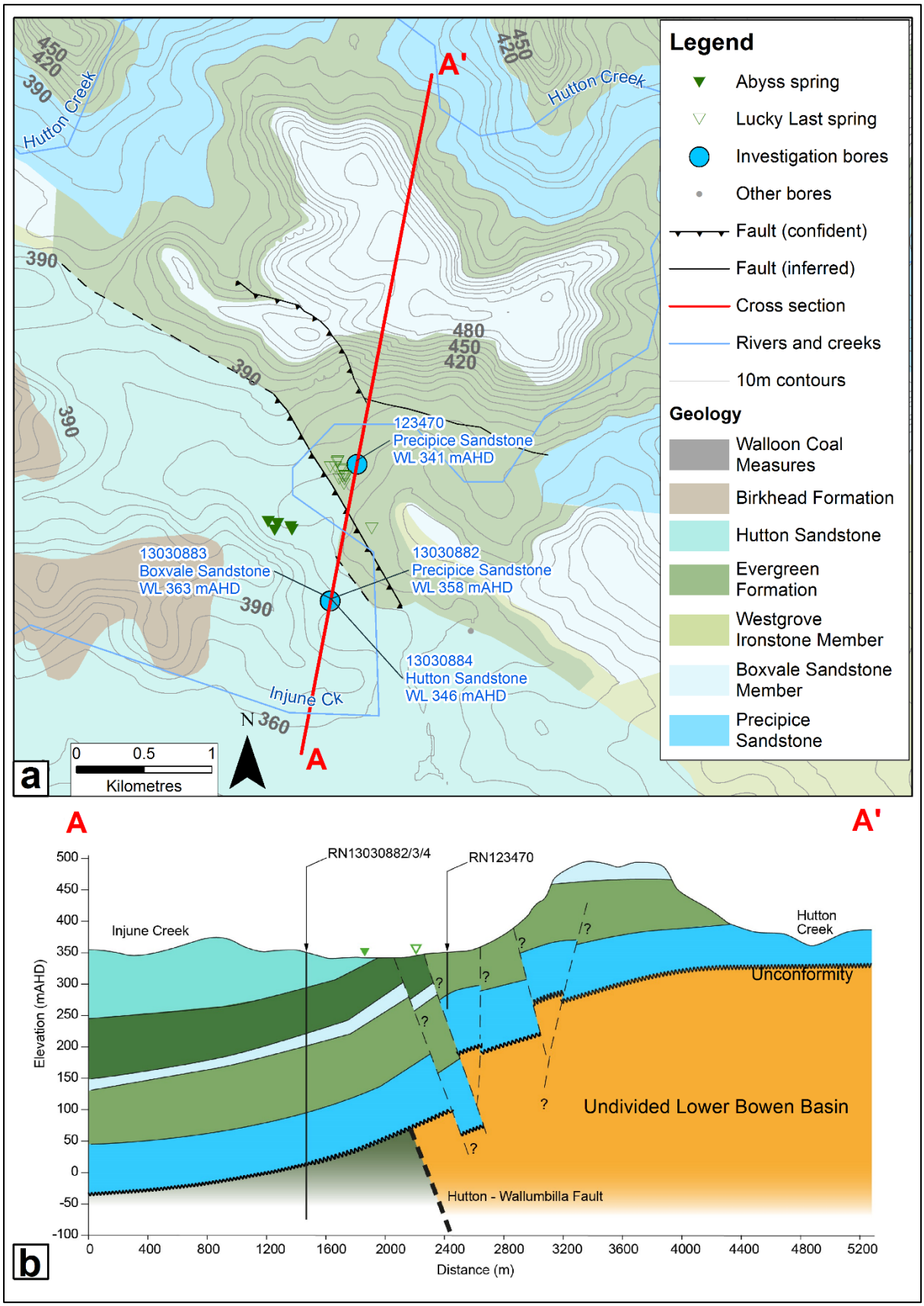

Figure 27 Mapped surface geology and inferred Hutton-Wallumbilla Fault

4.2.2.3 Geophysics

Ground geophysical surveys, including resistivity and transient electromagnetics (TEM), were carried out over the spring site in order to better understand subsurface geology and groundwater flow. The effective depth of investigation ranged between 30 and 50 m. As can be seen in Figure 28, a clear conductivity contrast is present either side, with a conductive zone on the northern side of the fault and a less conductive zone on the southern side. This is further illustrated by the vertical cross-section in Figure 28, which shows a less conductive area on the southern side of the interpreted fault, extending up to the surface where the springs are present. The data are consistent with fresher water on the southern side of the fault flowing vertically to the surface (likely through the damage zone). The sharp conductivity contrast across the fault zone also suggests the fault may provide some horizontal resistance to groundwater flow.

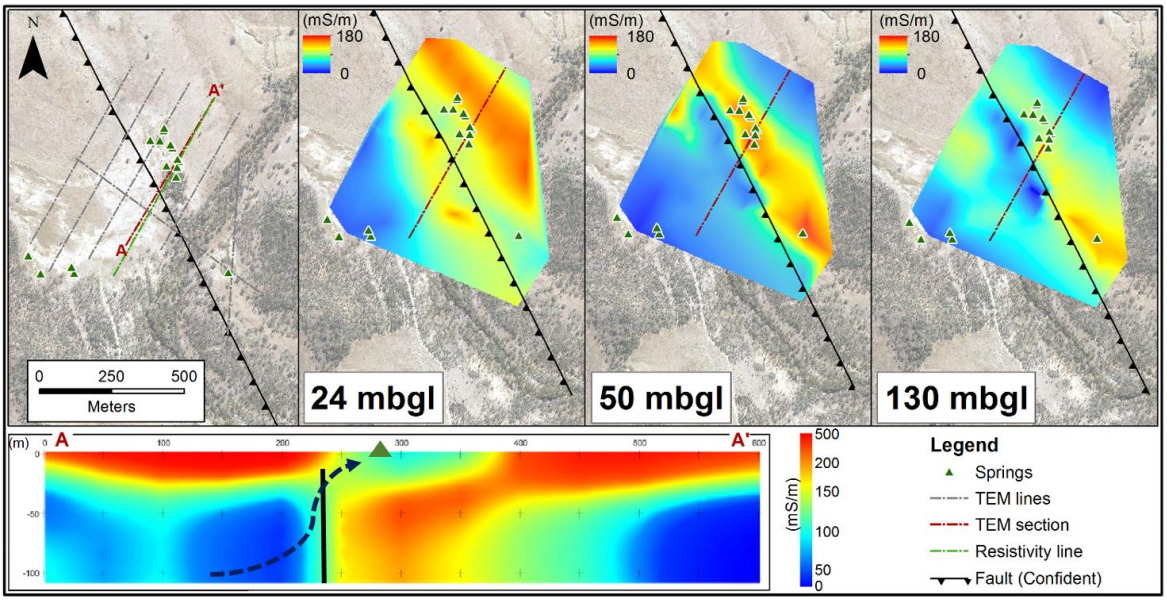

Figure 28 TEM conductivity model results for the Lucky Last and Abyss springs area

4.2.2.4 Monitoring

Groundwater level monitoring at this site shows that water levels in the Precipice Sandstone are at significantly different elevations either side of the fault (Figure 29), suggesting at least local disconnection of the system. There may be similar effects in the overlying Evergreen Formation and Hutton Sandstone. The location of these bores is shown in Figure 27.

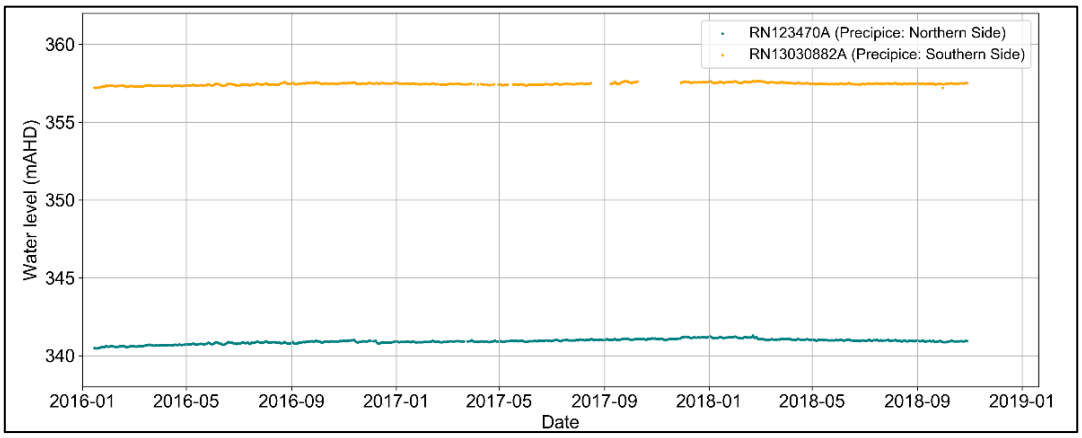

Figure 29 Monitoring data in the Precipice Sandstone, either side of the fault zone

4.2.2.5 Hydrochemistry

The available hydrochemistry data for the Lucky Last and Abyss springs and nearby bores within different formations are shown in a Durov plot (Figure 30).

The Abyss springs have a relative major ion composition similar to the Hutton Sandstone, the exception being the TDS, which is much higher for the Abyss springs (likely due to evaporation).

The Lucky Last springs exhibit a chemistry similar in composition to the Boxvale Sandstone and discernible from the Precipice Sandstone by a higher abundance of monovalent cations ($Na^+ + K^+$) and very low proportions of divalent cations (Ca^{2+} and Mg^{2+}).

These composition data suggest that the origin of groundwater for the Abyss spring complex is local groundwater flow from the Hutton Sandstone (Hypothesis A), while regional groundwater flow from the Boxvale Sandstone Member is the likely source for the Lucky Last springs.

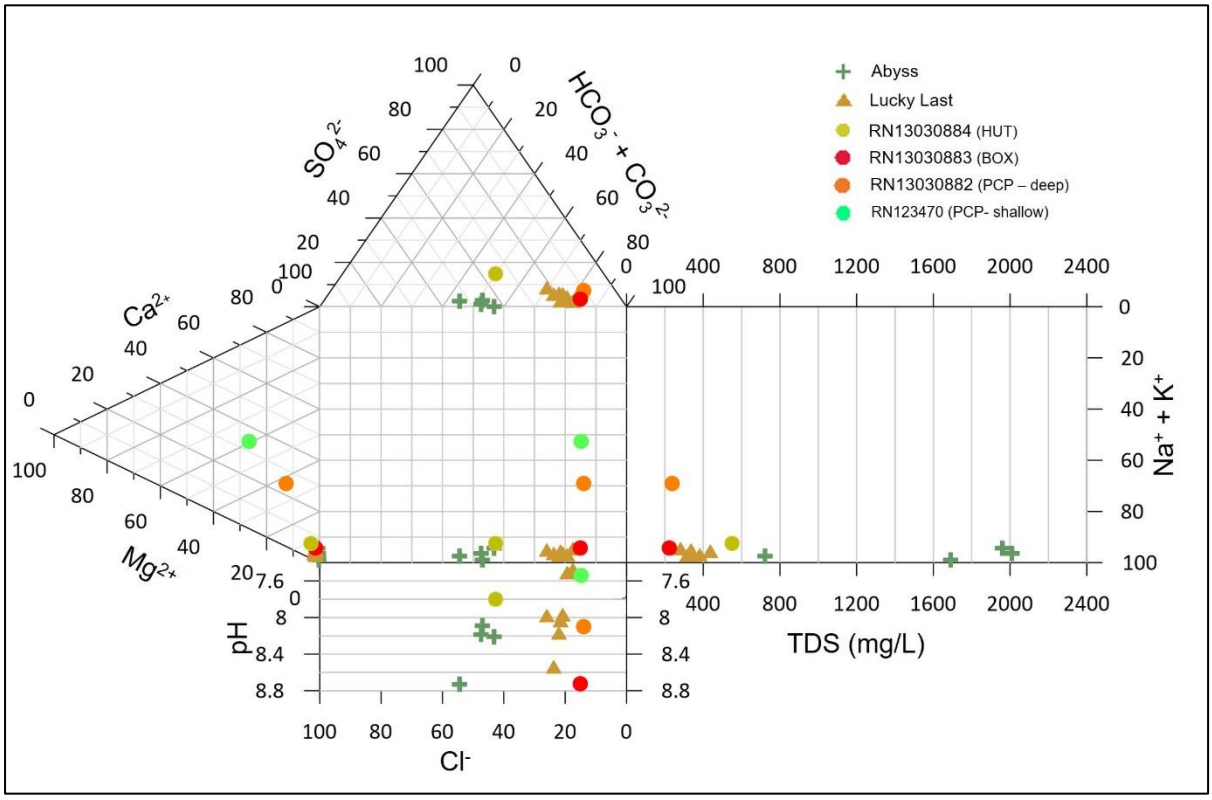

Figure 30 Extended Durov plot with water samples from springs and potential source aquifers

4.2.2.6 Key findings

Nearby seismic data and surface geology in the area of the Lucky Last and Abyss spring complexes imply likely faulting in the area of the springs. Geophysical conductivity surveys confirm the presence of a near-surface fault at this location. Seismic data confirms a complex deformation zone associated with the reactivation of the Hutton-Wallumbilla fault zone into the Surat Basin sediments.

The local geology and chemistry data suggest that the most likely source aquifer for the Lucky Last springs is the Boxvale Sandstone, while the Abyss springs are likely fed by more local groundwater flow directly from the outcropping Hutton Sandstone.

A well close to the Lucky Last springs indicates the Boxvale Sandstone occurs at approximately 30 m depth, where it is then overlain by the Evergreen Formation sediments. Even though there is

effectively 30 m aquitard material above the Boxvale Sandstone, the geophysics show a low-conductivity column extending to the near surface on the southern side of the fault. This suggests that faulting may have increased the vertical connectivity at this location to allow water from the Boxvale Sandstone to flow through a fault damage zone to the surface.

In addition to the Lucky Last springs, there are two other springs where faults provide vertical connectivity to the surface, namely the Scott's Creek and Bogomoss springs. The conceptualisation around these sites is described in more detail in technical reports (OGIA, 2015c, 2015a, 2015b).

4.2.3 Kenya East

The Kenya East fault zone is characterised by a relatively small graben structure in the centre of the Kenya East CSG production field. As shown in Figure 31, faults associated with the graben structure have a maximum observed displacement of 28 m and extend north–south with a likely length of around 2 km. Several smaller fault intersections are also present in the vicinity.

Kenya East is one the more data-rich faulted areas, with the data around this structural feature including: water level monitoring; Walloon Coal Measures and Springbok Sandstone water chemistry; and a high density of CSG wells with stratigraphic picks, lithology and associated petrophysical attributes.

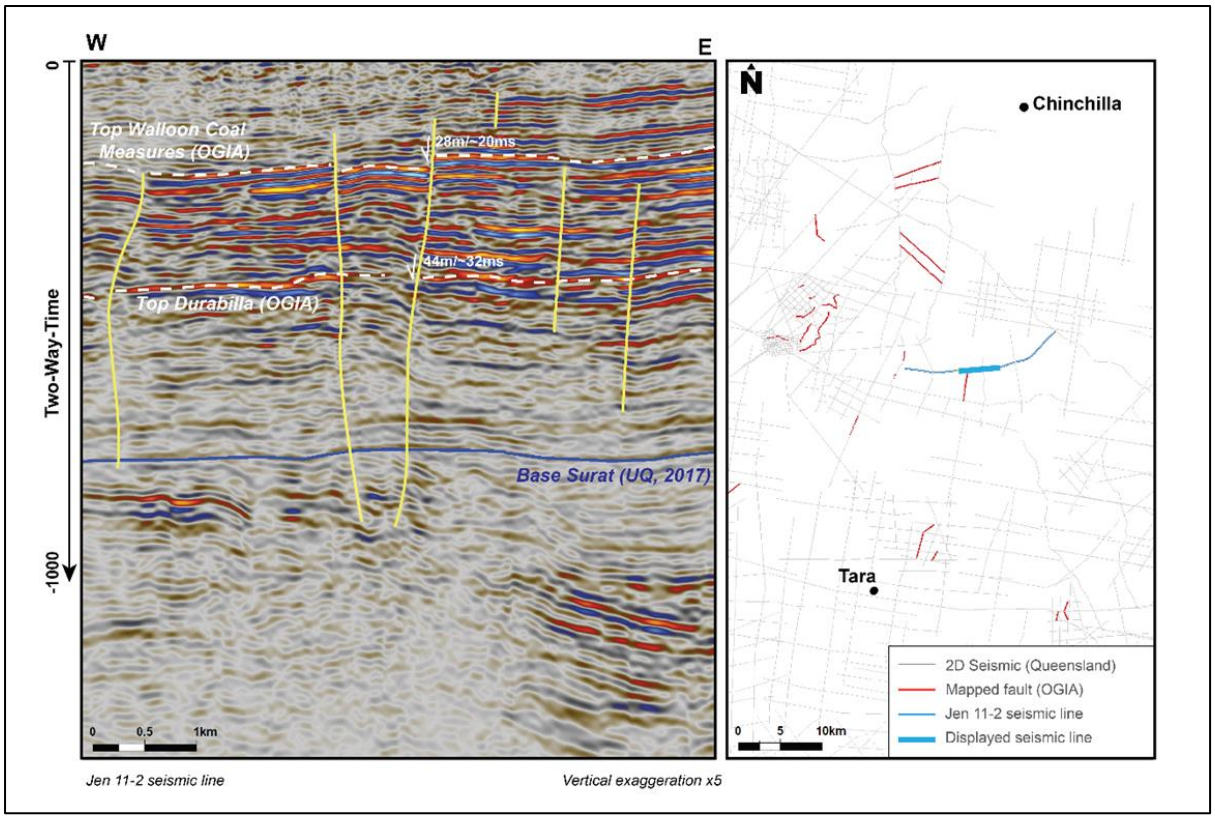

Figure 31 Seismic section showing the graben structure at Kenya East

4.2.3.1 Seismic interpretation

The fault zone exhibits characteristics of a keystone structure with a narrow, down-thrown block that is tightly folded (Copley et al., 2017). This fault style is common in the Surat Basin. It is clear from the seismic line shown in Figure 31 that the lower Springbok Sandstone is juxtaposed against the

Walloon Coal Measures. Only the fault on the western side can be correlated to a nearby seismic line. The remainder of faults have been interpreted as fault intersections.

4.2.3.2 Monitoring Data

There are two nearby Springbok Sandstone monitoring points: one (KEE_GWM004) is situated directly in the graben structure in the lower Springbok Sandstone and the other (KEE_GWM002) is 2 km to the east, in the upper Springbok Sandstone. The two monitoring points are separated by a normal fault.

Data for the lower Springbok Sandstone monitoring point (KEE_GWM004) show steadily declining pressures, from 301 mAHD in September 2014 to around 282 mAHD in January 2018, equivalent to around 19 m of total drawdown with an average rate of about 6.5 m/year. The other nearby Springbok monitoring point (KEE_GWM002), situated less than 2 km away, shows no significant drawdown (Figure 32).

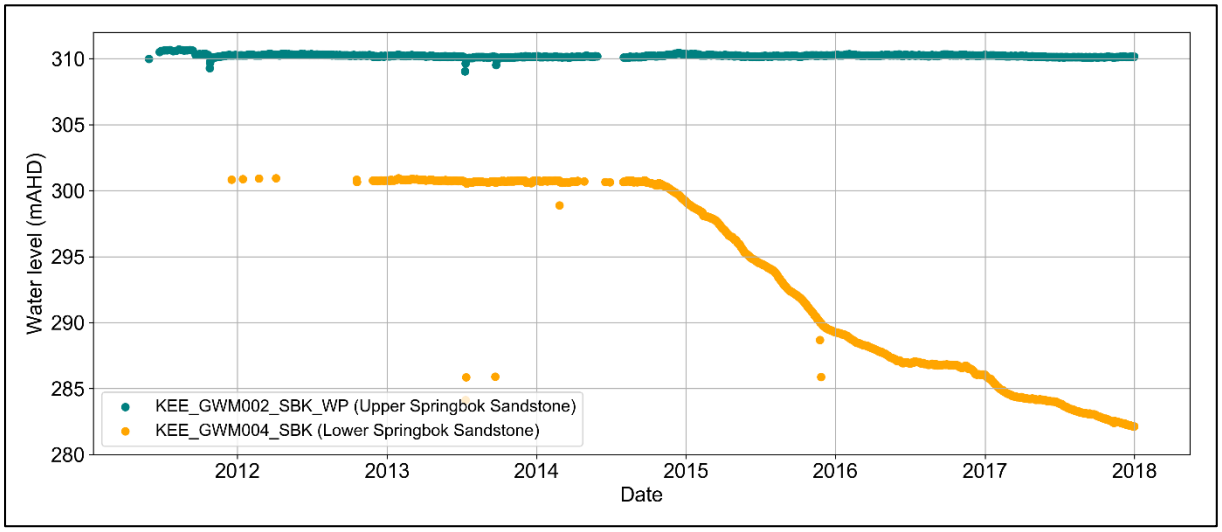

Figure 32 Water monitoring in the upper and lower Springbok Sandstone at Kenya East

As show in Figure 33, the water level decline at KEE_GWM004 coincides with the start of CSG production within 5 km. There is a short delay of approximately six months in the timing of drawdown relative to the start of nearby CSG production.

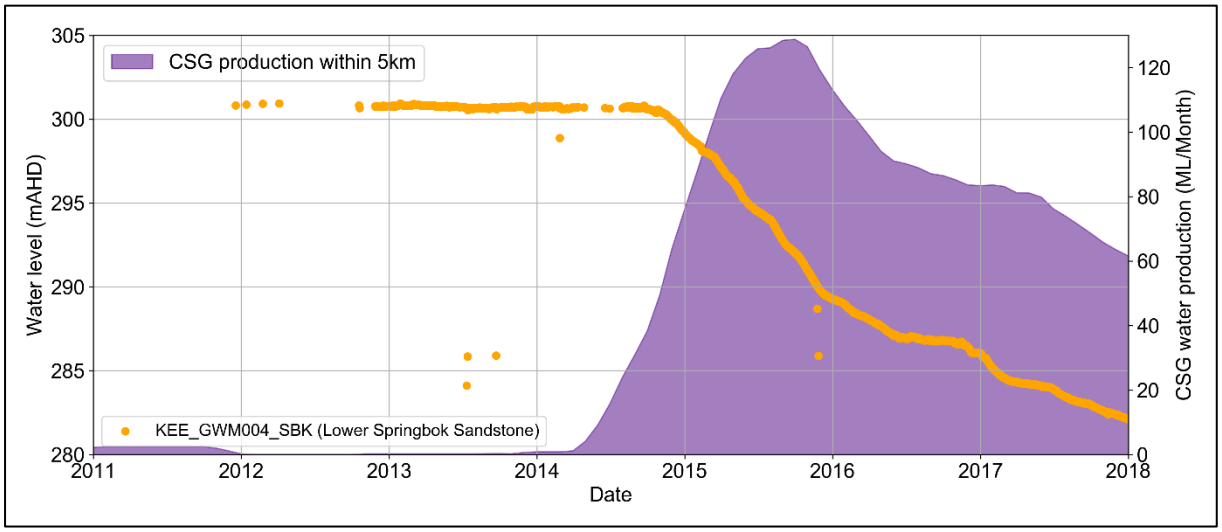

Figure 33 Water production within 5km of the Kenya East monitoring site

4.2.3.3 Hydrochemistry

As part of regular monitoring, operators routinely sample CSG wells for groundwater chemistry. Most CSG wells have some time series chemistry data available and so a Mann-Kendall analysis has been performed on chloride concentration data from CSG wells. Where a statistically significant downward or freshening trend was detected, this has been denoted as “decreasing trend”. Where no statistically significant trend was detecting but data suggested a slight decrease, this has been denoted as “potentially decreasing trend”. Inversely, the same logic has been applied to increasing trends. Conceptually, if CSG wells are drawing water from the overlying Springbok Sandstone (facilitated by faults or other connectivity features) then freshening trends in CSG well chemistry would be expected.

There are several CSG wells in the vicinity of the Kenya East fault that have either decreasing or potentially decreasing trends, as presented in Figure 34a. This suggests that CSG wells in this area may be accessing water from the overlying Springbok Sandstone, which typically exhibits a lower chloride concentration.

Furthermore, the most recent hydrochemistry data have been included in a regional compositional cluster analysis. In general, cluster classes are evolved from one another with increasing TDS, such that class 1 < class 2 < class 3 < class 4, with classes 1 and 2 being the less evolved, fresher waters.

On the eastern side of the graben, water in the Walloon Coal Measures is more saline and has been grouped into cluster class 3, while water on the western side of the fault is significantly fresher and has been grouped into cluster class 2 (Figure 34b). This is consistent with the ingress of fresher water from another aquifer, such as the Springbok Sandstone.

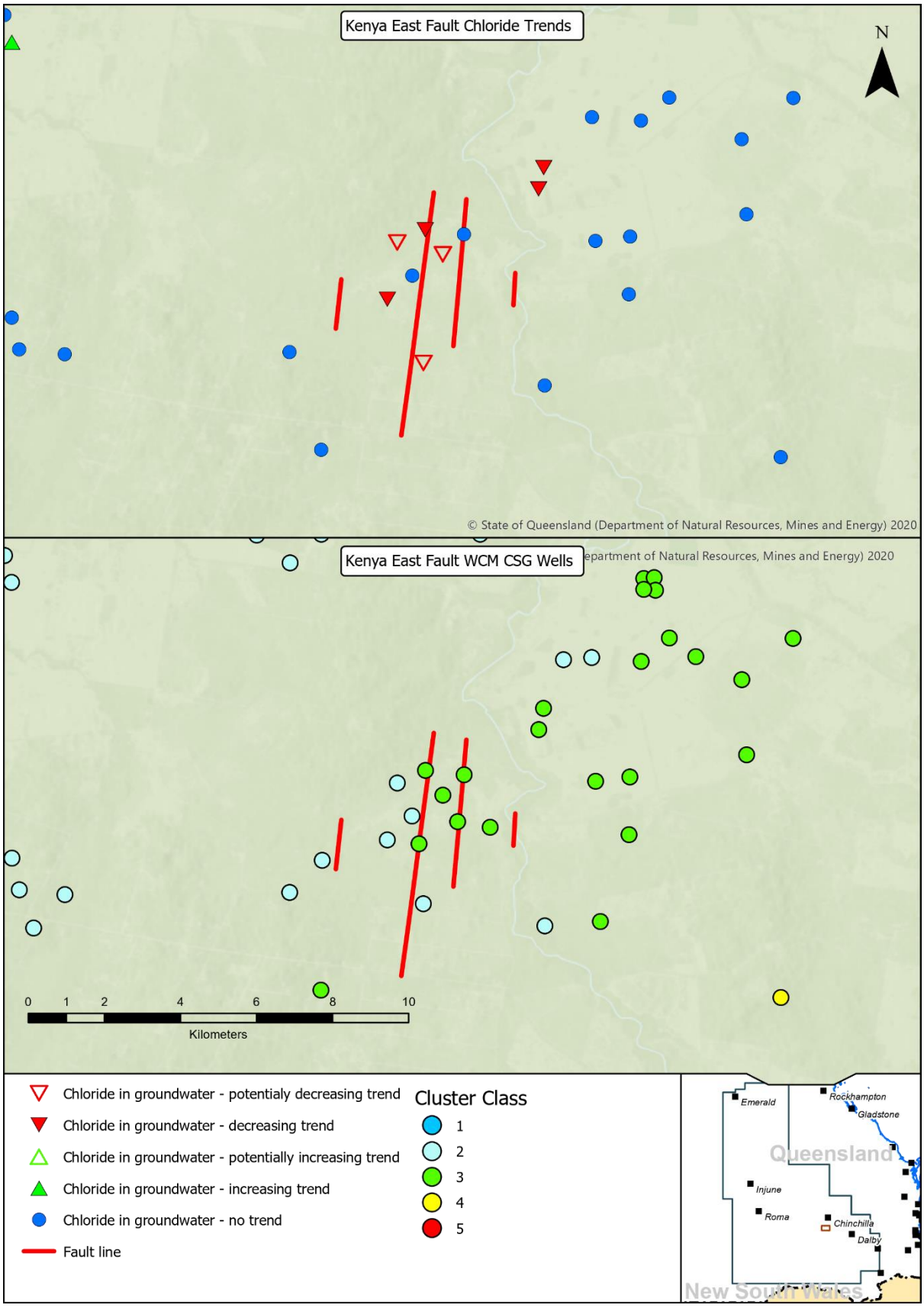

Figure 34 a) chloride concentration trends and b) cluster classes for CSG wells

4.2.3.4 Cross-fault leakage

Using the approach described in sections 3.3 and 3.4 and as per the Horrane Fault, both 1D and 2D analyses were undertaken for the Kenya East fault. The cross-fault leakage analysis was performed for the western fault of the graben structure.

The fault offset from the seismic interpretation was applied to the lithology logs from the closest well to estimate the up-thrown and down-thrown sides (Figure 35 a, b). A continuous SGR profile was calculated using Equation (1) and permeability from Equation (2) (Figure 35c). Leakage windows were then identified where sandstones and coal were found to be in contact across the fault plane (Figure 35d).

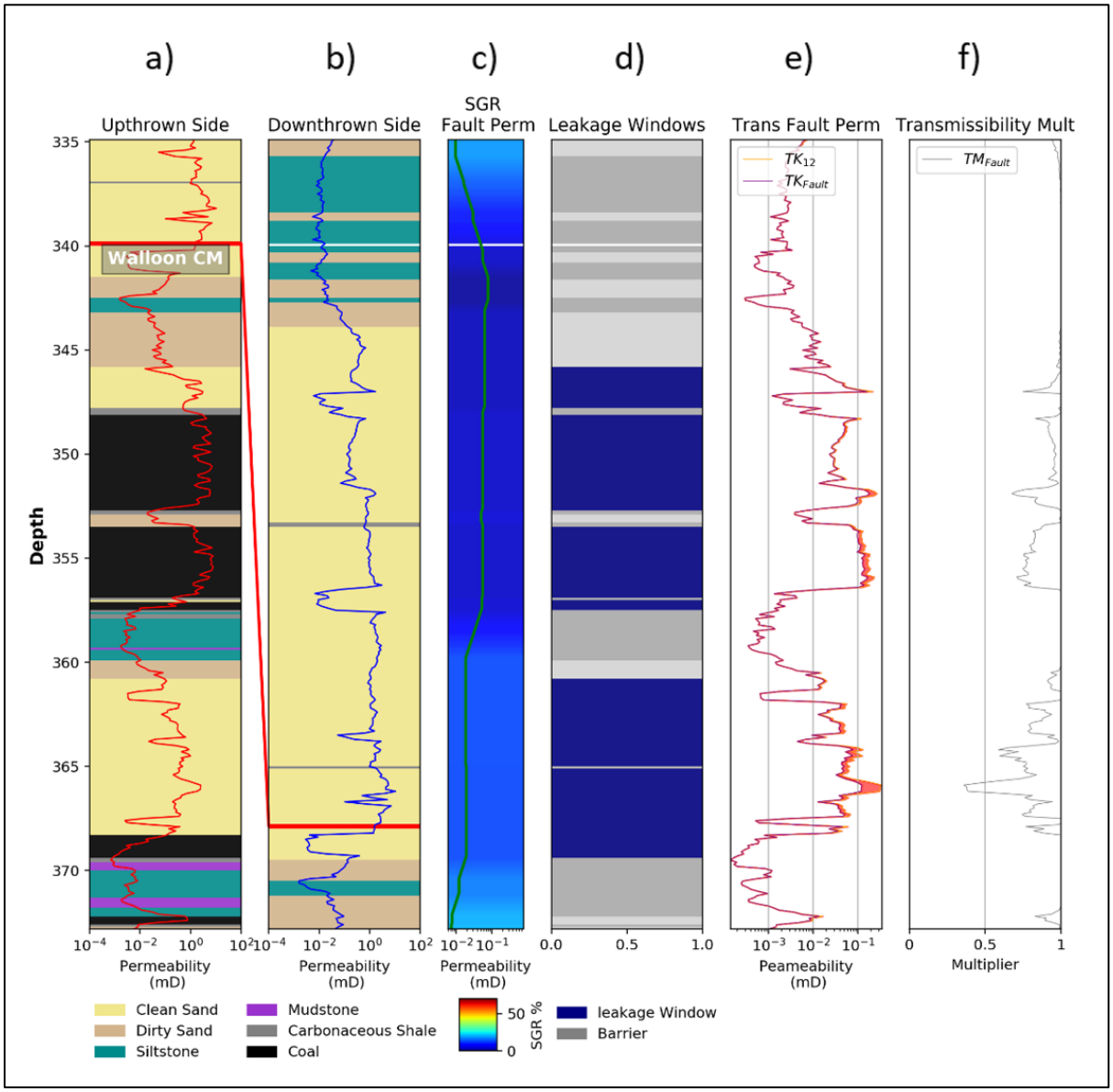

Figure 35 1D cross-fault leakage analysis at Kenya East

The lower Springbok Sandstone at this location is composed primarily of clean sand and has a permeability between 1 and 10 mD, based on petrophysical estimates at the nearest well. The Upper Juandah Coal Measures at this location is also primarily composed of sandstone, with permeability ranging between 0.1 and 1 mD.

After accounting for the estimated fault displacement of 28 m, the sandstones of the lower Springbok Sandstone are juxtaposed directly against the coal seams of the Upper Juandah Coal Measures.

Additionally, given the extremely low proportions of clay in the lower Springbok Sandstone at this location, the SGR is consistently lower than 10% at the contact between the Springbok Sandstone and Walloon Coal Measures. This translates to an estimated cross-fault permeability between 0.01 and 0.1 mD.

As shown in Figure 35f, the transmissibility multiplier is generally close to 1; as such, the fault core is unlikely to offer any significant resistance to cross-formational flow, largely since clay-smearing is estimated to be minimal.

Using the parabolic functions derived from section 3.3, a fault displacement profile was also generated for the Kenya East fault and a further 2D leakage analysis completed. The maximum displacement was initially assumed to be 28 m – the observed maximum displacement. The displacement profile was then applied to the downhole lithology log from a nearby well (Merlin Bore No 69020). This allowed the calculation of leak points along the contacted area between the Walloon Coal Measures and the Springbok Sandstone. Calculating the percentage of shale within the entrained sediment allowed the determination of SGR at each point on the fault plane.

Results for the 2D fault seal analysis are summarised in Figure 36 below. In this case, Figure 11 shows the appropriate representation of the contact area.

The analysis reveals that leakage windows comprise approximately 59% of the contact area between the Walloon Coal Measures and the Springbok Sandstone. Furthermore, the average SGR is 9.87%.

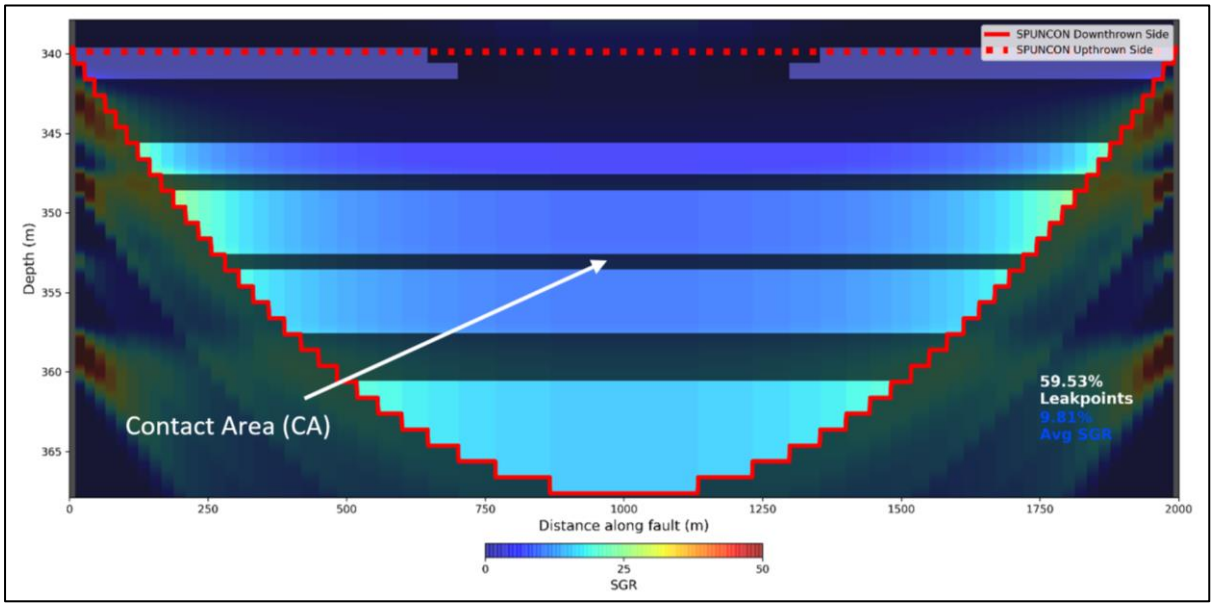

Figure 36 2D fault seal analysis for the Kenya East fault

While the maximum observed displacement on this fault is 28 m, it is possible that seismic lines have not intersected the maximum displacement of the fault; as such, the displacement profile may vary.

A sensitivity analysis subsequently evaluated the effects of under-representing the maximum displacement of this fault. The total contact area, leakage area and average SGR were evaluated for a range of maximum displacements up to 80 m. However, a normal fault with 80 m displacement would be expected to have a fault length of around 5–8 km based on a Dmax/Length ratio of 1.85–2 for normal faults (Kim & Sanderson, 2005).

The estimated contact area is consistently high for all maximum displacements on this fault and the average SGR across leakage windows between the Walloon Coal Measures–Springbok Sandstone contact is consistently <10%. Moreover, as shown in Figure 37, the proportion of the total contact area that comprises leakage windows tends to reduce with increasing displacement. This occurs as the upper Springbok Sandstone and Westbourne Formation (which are more heterogeneous than the lower Springbok Sandstone) are juxtaposed against the Walloon Coal Measures.

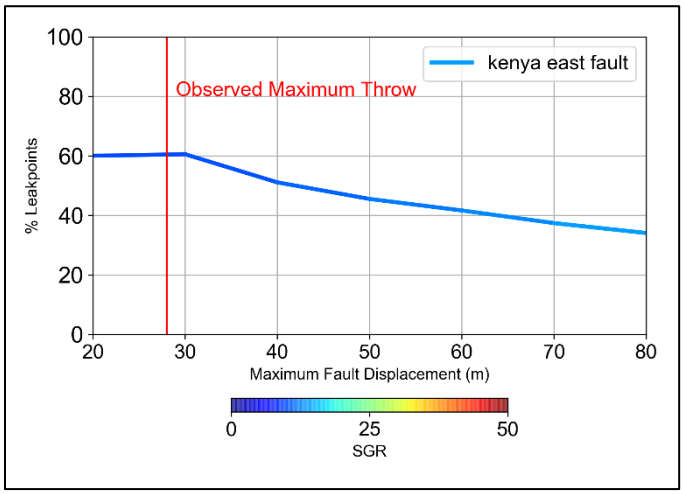

Figure 37 Sensitivity analysis, evaluating total contact area as a function of varying maximum displacement at the Kenya East fault

4.2.3.5 Groundwater modelling

A detailed groundwater model was constructed for the Kenya East area to validate the methodology for assessing cross-fault permeability described in this report (see chapter 3). This model was also constructed to explore alternative explanations for the observed drawdown in the Springbok Sandstone at this location. More information regarding the model construction is provided in Appendix C.

Parameterisation of the fault plane was undertaken using the fault parameterisation approach described in section 3.4. As shown in Figure 38, the model is able to produce drawdown similar to observed at both Springbok Sandstone monitoring points (KEE_GW004 and KEE_GW002) without any calibration. The modelled fit was then improved by calibrating to storage parameters for the Springbok Sandstone. Importantly, no calibration of the estimated cross-fault permeability was required. This suggests that the methodology for estimating cross-fault permeability, as outlined in 3.4, is appropriate for understanding the potential for horizontal connectivity around faults.

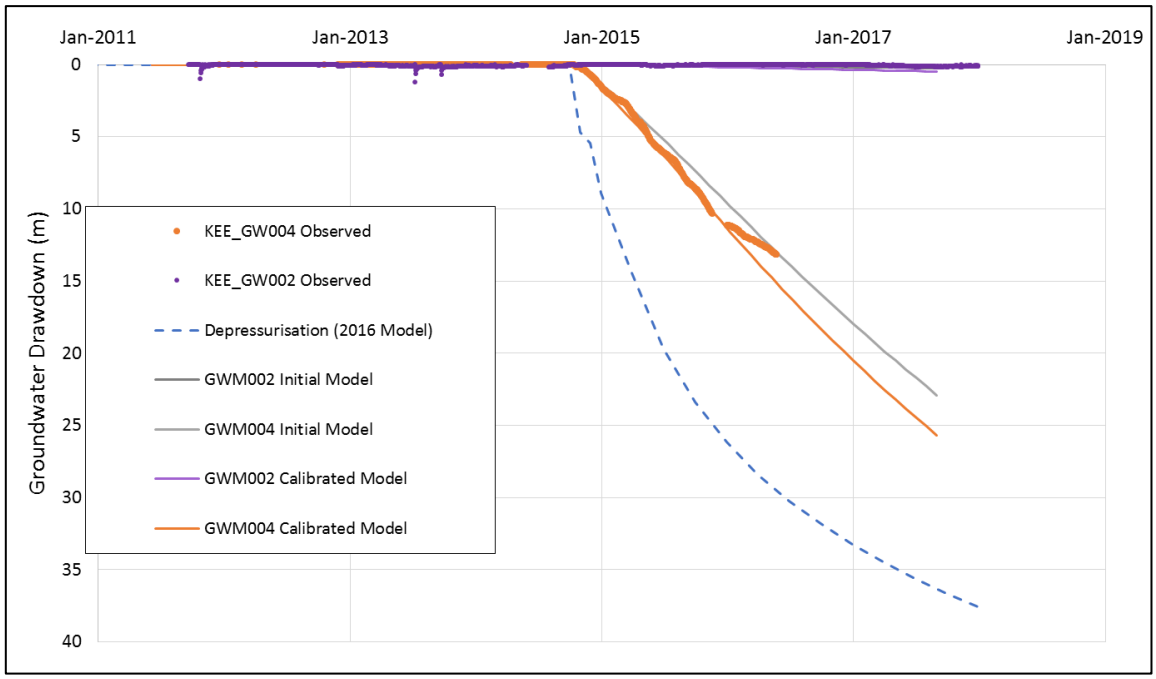

Figure 38 Modelled vs observed heads at the Kenya East site

4.2.3.6 Key findings

Decreasing water levels in the lower Springbok Sandstone coinciding with local CSG production suggest that depressurisation associated with CSG activities has affected the lower Springbok Sandstone at the Kenya East site. This drawdown has been attributed to the presence of a graben structure with 28 m of displacement, which places thick coal seams from the Upper Juandah Coal Measures in contact with blocky sandstones of the lower Springbok Sandstone. Furthermore, the similarity of Springbok Sandstone and Walloon Coal Measures water chemistry on the up-thrown side of the fault, together with freshening trends in the Walloon Coal Measures, are further evidence for increased connectivity at this location caused by faulting.

Results from numerical modelling at this site suggest that the coal juxtaposition hypothesis is able to explain both the observed drawdown in the lower Springbok Sandstone and the stable water level in the upper Springbok Sandstone.

4.3 Regional analysis

4.3.1 Connectivity between the Walloon Coal Measures and the Hutton Sandstone

4.3.1.1 Horizontal connectivity

For faults affecting the Hutton Sandstone (Figure 39) the thickness of the Durabilla Formation is the key attribute that will determine the degree of connectivity with the Walloon Coal Measures.

The vast majority of faults do not have sufficient displacement to juxtapose the Hutton Sandstone against the lower coal seams in the Walloon Coal Measures. Thus far, only two faults in the Surat Basin have maximum displacements that exceed the thickness of the Durabilla Formation (Figure 40) – the Hutton-Wallumbilla Fault zone and the Horrane Fault.

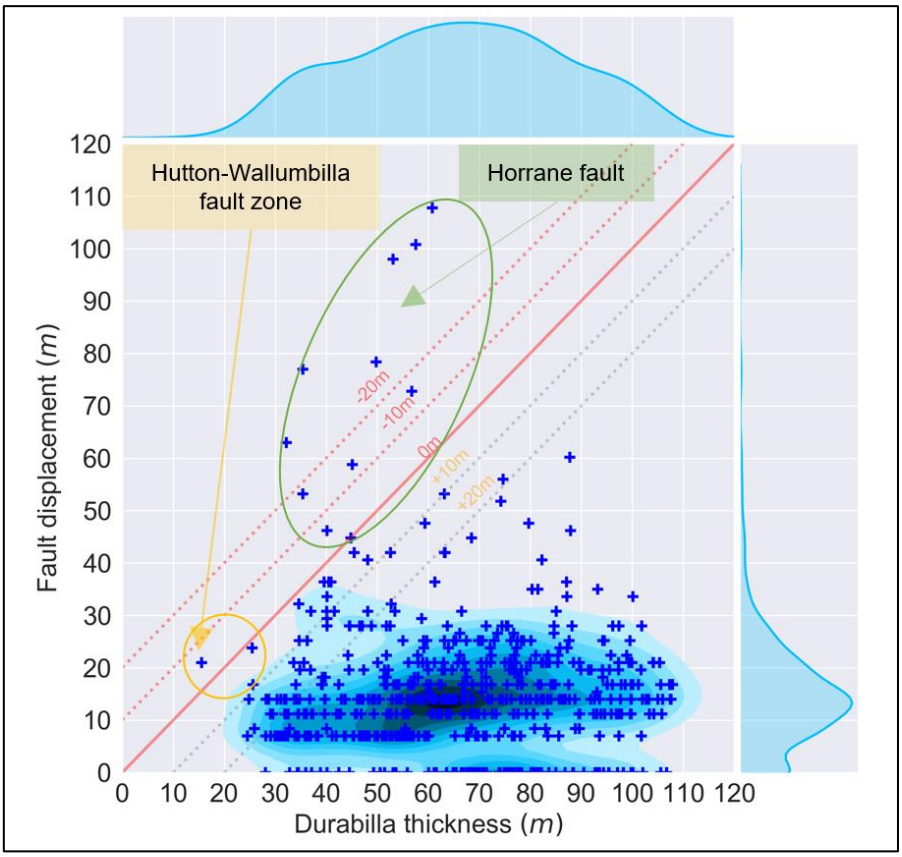

Figure 39 Fault displacement and thickness of intervening sediments on all fault intersections affecting the Hutton Sandstone

At one site near the Hutton-Wallumbilla Fault zone, the fault has a small interpreted displacement of ~20 m, whereas the modelled Durabilla Formation thickness is ~10 m. OGIA's geological model currently has few control points close to this region that can aid in constraining the Durabilla Formation thickness. Given the potential risk of connectivity at this location, OGIA has specified nested monitoring around this site as part of the 2019 Water Monitoring Strategy (UWIR 2019). These data will provide important geological controls for the Durabilla thickness but also on the hydrogeological drivers around the fault zone.

The more significant of the two features is the Horrane Fault between Cecil Plains and Dalby. Section 4.2.1 aims to determine the likelihood of cross-formational flow at this site using all the available data. Preliminary results indicate the leakage area between the Walloon Coal Measures and Hutton Sandstone across the fault is likely to be less than 5% with a relatively high degree of clay smearing since the SGR typically exceeds 35%. This high SGR may restrict flow even in areas on the fault plane where permeable units are in contact. This is primarily due to the lithological composition and structure of the upper Hutton Sandstone, which is highly heterogeneous with interbedded sandstones and siltstones.

There is currently no pressure data around the Horrane Fault in the Hutton Sandstone. As such, OGIA has specified nested monitoring sites around the Horrane Fault for ongoing groundwater level monitoring as part of its 2019 Water Monitoring Strategy (UWIR 2019). These sites will provide important information about vertical and horizontal head gradients around the fault and will be used to update the conceptualisation in the area. In the regional groundwater flow model for the UWIR 2019, flow is permitted across the fault zone in order to conservatively represent the fault. This representation will also be reviewed when the new monitoring data become available.

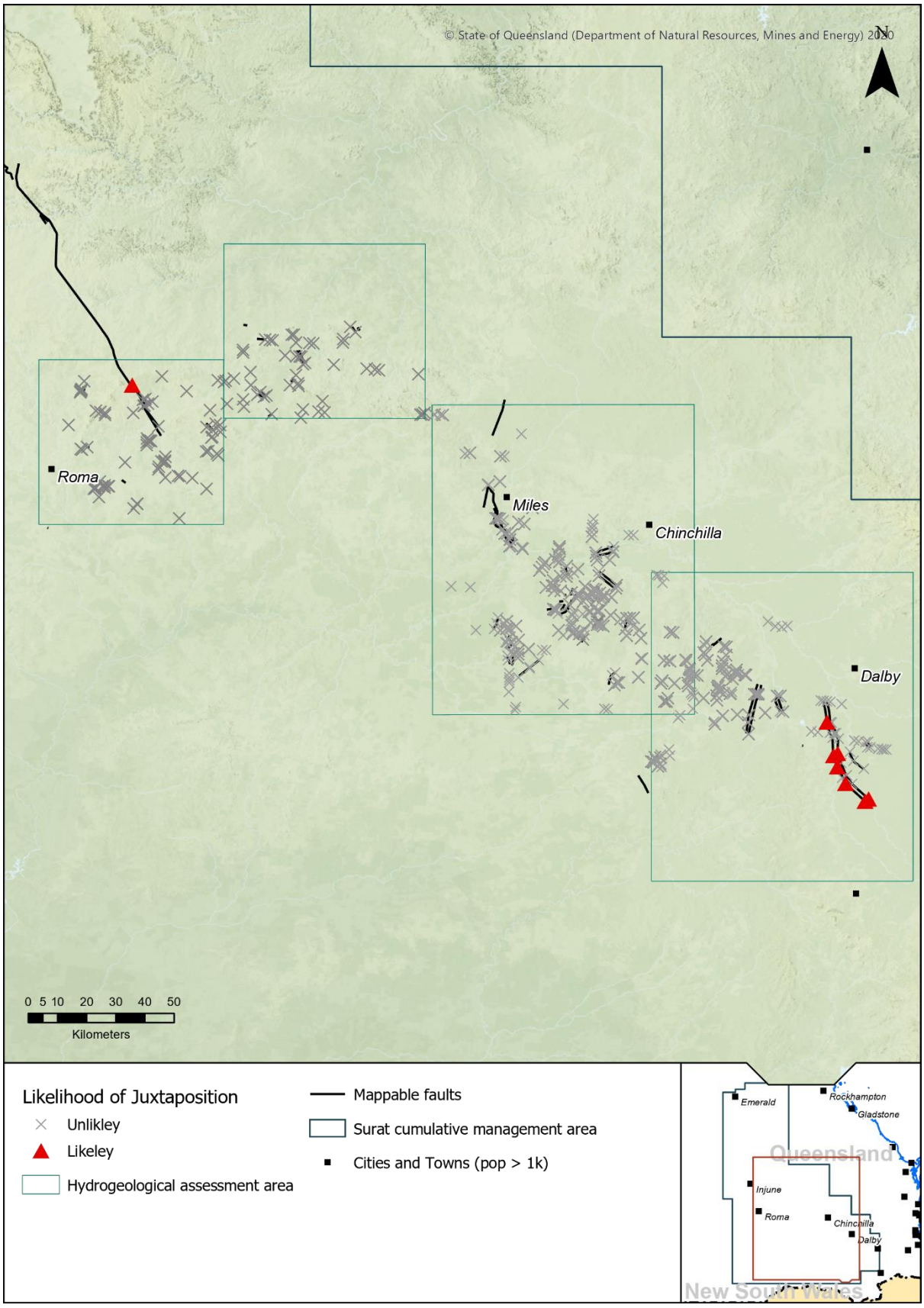

Figure 40 Faults likely to juxtapose the Walloon Coal Measures against the Hutton Sandstone

4.3.1.2 Vertical connectivity

There is little evidence to suggest vertical connectivity between the Hutton Sandstone and Walloon Coal Measures. This is likely due to the thick and ubiquitous nature of the Durabilla Formation and the high proportion of swelling clays in the Walloon Coal Measures, all of which will tend to limit the potential for open and connected fractures between the two formations and any subsequent cross-formational flow.

It is expected, however, that nested monitoring around the Horrane Fault will provide useful insight into the vertical properties around this major structure affecting the Hutton Sandstone.

4.3.2 Connectivity between the Walloon Coal Measures and the Springbok Sandstone

4.3.2.1 Horizontal connectivity

Figure 41 below shows the comparison of estimated fault displacement derived from seismic interpretation and the corresponding thickness of the material separating the uppermost coal seam of the Walloon Coal Measures from the Springbok Sandstone. The thickness of the separating material (upper non-coal zone) is critical to assessing fault-induced connectivity. Where the upper non-coal zone is absent or thin, the connectivity between the Walloon Coal Measures and Springbok Sandstone may be naturally high and a fault may not increase the degree of connectivity. Where this zone is thick, it may provide significant resistance to flow in unfaulted conditions, in which case, a fault may enhance the degree of connectivity where it displaces the upper non-coal zone.

The material separating the uppermost coal seam of the Walloon Coal Measures from the Springbok Sandstone is relatively thin; the displacement of the majority of faults therefore exceeds the thickness of this material and has the potential to juxtapose coal seams with the lower Springbok Sandstone units.

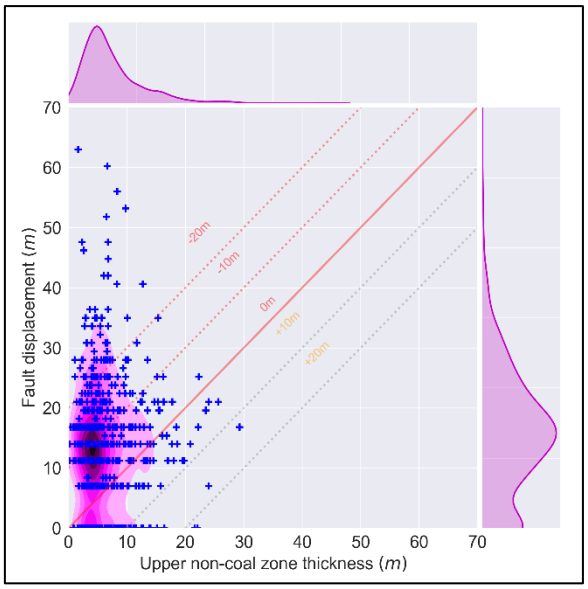

Figure 41 Fault displacement and thickness of intervening sediments on all fault intersections affecting the Springbok Sandstone

To evaluate the effect of clay-smearing on cross-fault flow, the SGR was calculated on the estimated fault contact zone between the Springbok Sandstone and Walloon Coal Measures, as well as over

potential leakage windows (sand against coal or coal against coal) for each fault as described in section 3.4.

This analysis identified fault intersections where leakage windows are present and SGR is sufficiently low to allow cross-formational flow between coal seams and the lower Springbok Sandstone.

Calculations suggest that faults affecting the Springbok Sandstone–Walloon Coal Measures boundary create 3 m of leakage windows on average, but this can vary between 0 and 23 m. The average SGR on these leakage windows is 17% and varies between 0 and 72%. The majority of faults affecting the Springbok Sandstone (65%) have sufficiently low clay-smearing (<20%), therefore offering little resistance to flow across leakage windows.

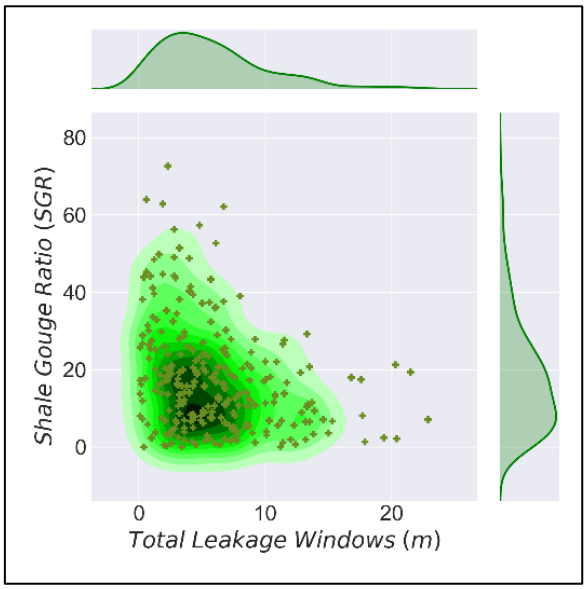

Figure 42 SGR and leakage windows between the Walloon Coal Measures and Springbok Sandstone

The horizontal hydraulic behaviour of a fault zone will be controlled not only by the properties of the fault core but also by the properties of the juxtaposed sections. Using the method described in section 3.4, the transmissibility multiplier (TM_{fault}) was calculated across the contact zone for each fault. When comparing the average TM_{fault} with the coal portion of leakage windows (where coal in the Walloon Coal Measures is in contact with sandstones in the Springbok Sandstone), it becomes apparent that the majority of faults have a TM_{fault} close to 1, which also suggests that these faults are unlikely to restrict flow across their contact zones.

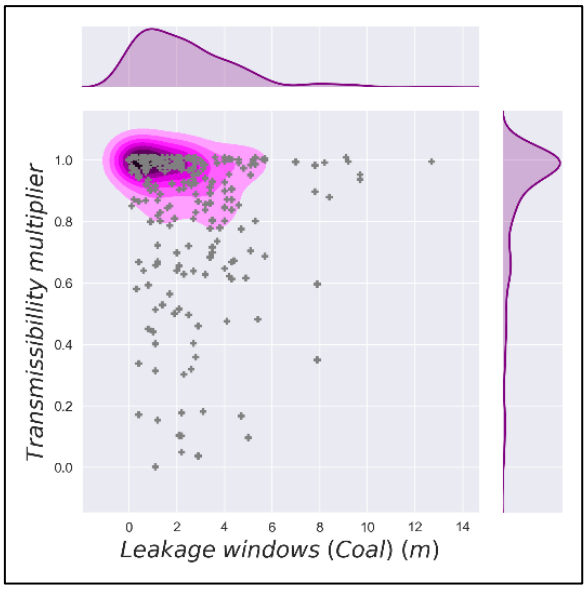

Figure 43 Transmissibility multiplier and total coal contact for each fault affecting the Springbok Sandstone

At one location in the Kenya East gas field (section 4.2.3), there are sufficient monitoring and characterisation data in the lower Springbok Sandstone to suggest that observed impact at this location is most likely caused by CSG depressurisation in the Walloon Coal Measures. This impact is likely to be propagated into the Springbok Sandstone via juxtaposition of the two units across a fault. In this case, impacts are likely caused by the juxtaposition of thick coal seams (totalling 5 m) and limited resistance on the fault plane (evidenced by average SGR of <10%). This is the only case in the Surat Basin where impact in the Springbok Sandstone can be directly attributed to a fault because of the supporting monitoring data. In total, 16 faults have been identified across the basin which have similar physical characteristics to this fault, i.e. greater than 5 m of total leakage windows and an average SGR less than 20%. A map of these faults is shown in Figure 44.

Additional monitoring in the lower Springbok Sandstone has also been specified in the 2019 Water Monitoring Strategy (UWIR 2019), strategically selected in order to validate the fault characterisation and ultimately to provide crucial hydraulic information on connectivity.

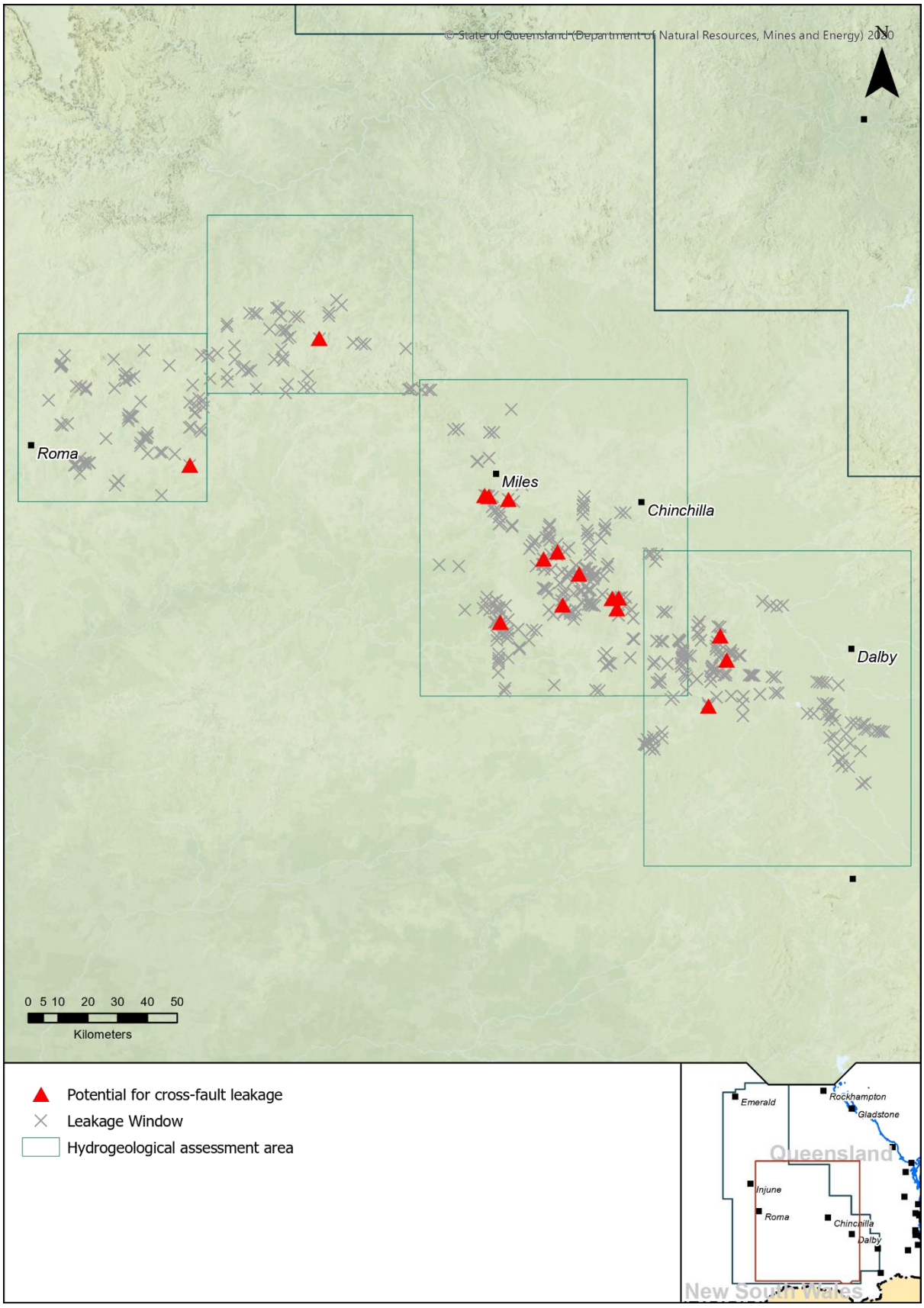

Figure 44 Potential fault-induced connectivity between the Walloon Coal Measures and Springbok Sandstone

4.3.2.2 Vertical connectivity

Using the methods outlined in 3.5, stress data were interpolated for the Surat Basin and fault orientations were estimated using methods outlined in section 3.3.

Results show that both fault orientations and stress directions vary across the Surat Basin. Consequently, as shown in Figure 45, the fault orientation relative to SH_{max} also varied across the area. In the northern Surat Basin, the majority of faults are oriented between 315 and 360 degrees relative to north and have angles of greater than 50 degrees relative to horizontal stress. At this relative angle, the resolved normal stress will be larger than the shear component, which in turn will tend to reduce fracture apertures and the fault permeability in the damage zone.

In the eastern Surat Basin, fault orientations are more variable; as such, the relative angle to SH_{max} varies significantly. In this area, fault orientations are controlled by the Undulla Nose and other bounding structural features including the Leichardt and Moonie-Goondiwindi fault systems. The mean SH_{max} in this area trends between 56 and 78 degrees, while roughly half of the mappable faults in this area are oriented less than 30 degrees relative to SH_{max}. This creates favourable conditions for fracture dilation and therefore increased permeability of fractures within fault damage zones.

Importantly, the majority of fault orientations favouring fracture dilation are found deeper in the basin, at greater than 300 m depth. The increased lithostatic pressure at these depths may reduce fracture permeability by up to three orders of magnitude and may limit the potential for vertical flow in the damage zone (see section 2.3.2). There are, however, three areas where faults with potentially dilatational characteristics are found in shallower areas (less than 100 m below ground surface).

A cluster of high-likelihood faults are found in the Orana gas field, nearby to the Condamine River gas seeps. Investigations by APLNG have identified near-surface faulting to be the most likely mechanism creating preferential pathways for gas migration at this site (Baldwin & Thomson, 2014).

Based on the depth and orientation criteria assessed, two other sites have also been identified with potential of vertical connectivity – the north-eastern Surat Basin area between Roma and Wandoan; and the south-eastern Surat Basin area between Chinchilla and Dalby – however, there are no known surface features in these areas to evidence vertical connectivity.

Some additional evidence of faults affecting vertical flow are noted at spring sites such as the Lucky Last Spring, Scott's Creek and Bogomoss spring complexes (OGIA, 2015c, 2015a, 2015b).

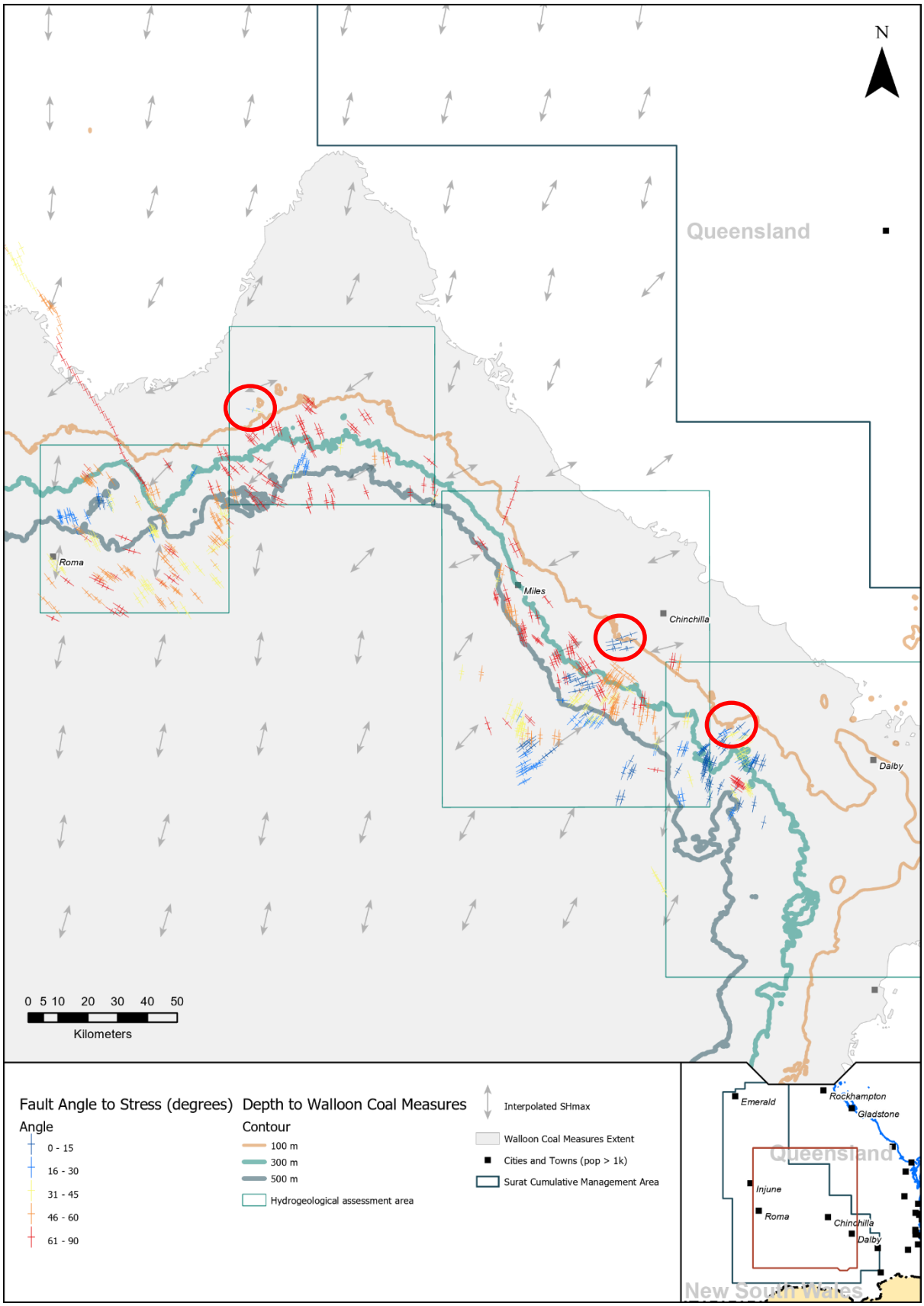

Figure 45 Fault orientations relative to the principal stress direction (SHmax) and depth to Walloon Coal Measures contours

4.3.3 Faults in the near surface

As mentioned previously, faults are difficult to identify in near-surface sediments in seismic data, due to poor resolution of seismic data at shallow depths. As such, it is not known whether faulting in the Surat Basin extends into shallower Cenozoic units such as the Condamine Alluvium. This will largely depend on the time of the most recent fault reactivation and whether this occurred pre-depositionally or post-depositionally. As mentioned previously, if faulting occurred syn-depositionally or post depositionally, it may be possible for coal seams in the upper portion of the Walloon Coal Measures to be juxtaposed against these sediments and/or for fault-related fractures to connect both aquifers. However, if deposition of the alluvium followed the last fault reactivation event, connectivity may be less likely.

Although in a different hydrogeological setting, studies in Broken Hill in far western New South Wales have revealed significant expression of near-surface faulting in Quaternary sediments affecting the recharge mechanisms (Lawrie et al., 2012).

While the extent of neo-tectonics in the Surat Basin is not well understood, further assessment in this area may be beneficial to hydrogeological conceptualisation.

5. Conclusion

This assessment involved multi-disciplinary case studies to validate the conceptual understanding of fault hydrogeology. This was accompanied by a regional analysis including: fault mapping and interpretation of displacement; estimation of leakage windows and fault seal analysis; assessment of principal stress direction in relation to fault orientation; and identification of faults with characteristics consistent with observed fault-induced connectivity.

The following conclusions are drawn from the synthesis of those investigations:

Faults affecting the contact between the Springbok Sandstone and Walloon Coal Measures

1. These are likely to juxtapose coals in the Walloon Coal Measures and sandstones in the lower Springbok Sandstone at some locations.
2. For most of these faults, the contact area is likely to be small and may not facilitate significant cross-formational flow.
3. A smaller proportion of such faults (5%) are identified with physical characteristics that are similar to a fault where observed data has confirmed propagation of CSG impact from the Walloon Coal Measures to the Springbok Sandstone.

Faults affecting the Hutton Sandstone and Walloon Coal Measures

4. These generally do not have sufficient displacement to juxtapose the two units and as such, the risk of cross-formational flow is low.
5. Two identified faults in the Surat Basin – the Hutton-Wallumbilla Fault zone and the Horrane Fault – have the sufficient displacement to cause cross-formational flow, although the degree of clay-smearing is sufficiently high and may limit such flow.

General

6. A small number of faults have been identified that may facilitate vertical connectivity between near-surface features and the Walloon Coal Measures.

OGIA is continuing to build on the findings in this report through the acquisition and interpretation of new monitoring and multidisciplinary data sets. These technical assessments will continue to inform the development of numerical modelling approaches to explore fault facilitated groundwater impacts in the Surat CMA.

6. References

Adiotomre, E. (2014). Structure and Displacement Characteristics of the Brage Fault, Northern North Sea Sedimentary Basin. *The International Journal of Engineering And Science (IJES)*, *3*(6), 2319–1805.

Allan, U. S. (1989). Model for hydrocarbon migration and entrapment within faulted structures. *American Association of Petroleum Geologists Bulletin*, *73*(7), 803–811. https://doi.org/10.1306/44b4a271-170a-11d7-8645000102c1865d

APLNG. (n.d.). *Condamine River seeps*. APLNG. https://www.aplng.com.au/topics/coal-seam-gas/condamine-river-seeps.html

Babaahmadi, A., Sliwa, R., & Esterle, J. (2015). Understanding faults in the Surat Basin from interpretation of seismic lines, aeromagnetic and gravity data. In *University of Queensland*. The University of Queensland.

Babaahmadi, A., Sliwa, R., & Esterle, J. (2016). Mapping fault lineaments in the basement of the Surat Basin from potential field data. *School of Earth Sciences, University of Queensland*.

Baldwin, D., & Thomson, J. (2014). *Condamine River Gas Seep Investigation: Technical Report*. www.norwestcorp.com

Bense, V. F., & Person, M. A. (2006). Faults as conduit-barrier systems to fluid flow in siliciclastic sedimentary aquifers. *Water Resources Research*, *42*(5). https://doi.org/10.1029/2005WR004480

Bense, V. F., Van den Berg, E. H., & Van Balen, R. T. (2003). Deformation mechanisms and hydraulic properties of fault zones in unconsolidated sediments; the Roer Valley Rift System, The Netherlands. *Hydrogeology Journal*, *11*(3), 319–332. https://doi.org/10.1007/s10040-003-0262-8

Bouvier, J. D., Kaars-Sijpesteijn, C. H., Kluesner, D. F., Onyejekwe, C. C., & Van Der Pal, R. C. (1989). Three-dimensional seismic interpretation and fault sealing investigations, Nun River Field, Nigeria. *American Association of Petroleum Geologists Bulletin*, *73*(11), 1397–1414. https://doi.org/10.1306/44b4aa5a-170a-11d7-8645000102c1865d

Bradley Thomas Grosser. (2012). *Fault and fracture reactivation in the penola trough, Otway Basin*. https://digital.library.adelaide.edu.au/dspace/bitstream/2440/92254/1/02wholeGeoHon.pdf

Caine, J. S., Evans, J. P., & Forster, C. B. (1996). Fault zone architecture and permeability structure. *Geology*, *24*(11), 1025–1028.

Chester, F. M., & Logan, J. M. (1987). Composite planar fabric of gouge from the Punchbowl Fault, California. *Journal of Structural Geology*, *9*(5–6), 621-IN6. https://doi.org/10.1016/0191-8141(87)90147-7

Coote, S. (1984). *GSQ Taroom 17 – Preliminary lithologic log and composite log*. Queensland Department of Natural Resources and Mines, Record 1984/66 cr_41845.

Copley, J., Mukherjee, S., Babaahmadi, A., Zhou, F., Barboas, K., Hurter, S., & Tyson, S. (2017). *Faults and fractures in the Surat Basin: Relationships with permeability*. The University of Queensland. https://ccsg.centre.uq.edu.au/files/5331/UQ-CCSG Final Report Faults and Fractures.pdf

DNRM. (2005). *Hydrogeological Framework Report for the Great Artesian Basin Water Resource Plan Area*. Department of Natural Resource Management, Queensland Government.

Dolson, J. (2016). *Understanding oil and gas shows and seals in the search for hydrocarbons*. https://books.google.com.au/books?id=0uV6DAAAQBAJ&pg=PA229&lpg=PA229&dq=AAPG+Bulletin+thematic+issue+on+fault+seals&source=bl&ots=QRskFp6cIZ&sig=ACfU3U19c3NxE0_SI_Gc4I9qvpTXf8Gv4g&hl=en&sa=X&ved=2ahUKEwjf5dXU2ojiAhWCYisKHcVSDbYQ6AEwC3oECAcQAQ#v=onepage&q=

Egholm, D. L., Clausen, O. R., Sandiford, M., Kristensen, M. B., & Korstgård, J. A. (2008). The mechanics of clay smearing along faults. *Geology*, *36*(10), 787–790. https://doi.org/10.1130/G24975A.1

Engelder, T. (1974). Cataclasis and the Generation of Fault Gouge. In *Geological Society of America Bulletin* (Vol. 85). https://doi.org/10.1130/0016-7606(1974)85<1515:CATGOF>2.0.CO;2

Esteban, L., Pervukhina, M., Mallants, D., Clennell, M. B., Verrall, M., Raven, M., & Nguyen, D. (2015). *Experimental Study of Background Permeability of Formations in the Walloon Sub Group (Surat Basin)*. CSIRO.

Exon, N. F. (1976). *Geology of the Surat Basin in Queensland* (Vol. 166). Australian Government Publishing Service.

Faulkner, D. R., Jackson, C. A. L., Lunn, R. J., Schlische, R. W., Shipton, Z. K., Wibberley, C. A. J., & Withjack, M. O. (2010). A review of recent developments concerning the structure, mechanics and fluid flow properties of fault zones. *Journal of Structural Geology*, *32*(11), 1557–1575. https://doi.org/10.1016/j.jsg.2010.06.009

Ferrill, D. A., & Morris, A. P. (2001). *Dilational normal faults*. https://www.nrc.gov/docs/ML0129/ML012950377.pdf

Fisher, Q., & Knipe, R. (2001). The permeability of faults within siliclastic petroleum reservoirs of the North Sea and Norwegian Continental Shelf. In *Marine and Petroleum Geology* (Vol. 18). https://doi.org/10.1016/S0264-8172(01)00042-3

Gale, J., Laubach, S., Marrett, R., Olson, J., Holder, J., & Reed, R. (2004). Predicting and characterizing fractures in dolostone reservoirs: Using the link between diagenesis and fracturing. In *Geological Society, London, Special Publications* (Vol. 235). https://doi.org/10.1144/GSL.SP.2004.235.01.08

Gong, J., & Rossen, W. R. (2017). Modeling flow in naturally fractured reservoirs: effect of fracture aperture distribution on dominant sub-network for flow. *Petroleum Science*, *14*(1), 138–154. https://doi.org/10.1007/s12182-016-0132-3

Grasemann, B., Exner, U., & Tschegg, C. (2011). Displacement-length scaling of brittle faults in ductile shear. *Journal of Structural Geology*, *33*(11), 1650–1661. https://doi.org/10.1016/j.jsg.2011.08.008

Green, P. M. (1997). *The Surat and Bowen Basins, south-east Queensland* (Queensland, Issue Queensland Minerals and Energy Review Series). Queensland Department of Mines and Energy.

Hamilton, S. K., Esterle, J. S., & Sliwa, R. (2014). Stratigraphic and depositional framework of the Walloon Subgroup, eastern Surat Basin, Queensland. *Australian Journal of Earth Sciences*, *61*(8), 1061–1080.

Hensen, E. J. M., & Smit, B. (2002). Why Clays Swell. *Journal of Physical Chemistry B*, *106*(94), 12664–12667. https://doi.org/10.1021/jp0264883

Himes, R. E., Vinson, E. F., & Simon, D. E. (1991). Clay Stabilization in Low-Permeability Formations. *SPE Production Engineering*, 252–258.

Hippler. (1993). *Deformation Microstructures and Diagenesis in Sandstone Adjacent to an Extensional Fault: Implications for the Flow and Entrapment of Hydrocarbons*. *77*(4), 625–637. https://doi.org/10.1306/BDFF8CB8-1718-11D7-8645000102C1865D

Holland, M., Urai, J. L., Van Der Zee, W., Stanjek, H., & Konstanty, J. (2005). *Fault gouge evolution in highly overconsolidated claystones*. https://doi.org/10.1016/j.jsg.2005.10.005

Ingraham, M. D., Bauer, S. J., Quintana, E. C., Bolintineau, D., Rao, R. R., & Lechman, J. B. (2015). Proppant and host rock deformation in fractured shale flow through experiments. *American Rock Mechanics Association Symposium*. https://www.scopus.com/inward/record.uri?eid=2-s2.0-84964928596&partnerID=40&md5=5487aff89305979f0861b5332455f00f

Jensen, A. R., Gregory, C. M., & Forbes, V. R. (1964). *The Geology of the Taroom 1:250 000 Sheet Area and of the Western part of the Mundubbera 1:250 000 Sheet Area*.

Jing, L., & Stephansson, O. (2007). 10 - Discrete Fracture Network (DFN) Method. In L. Jing & O. B. T.-D. in G. E. Stephansson (Eds.), *Fundamentals of Discrete Element Methods for Rock*

Engineering (Vol. 85, pp. 365–398). Elsevier. https://doi.org/https://doi.org/10.1016/S0165-1250(07)85010-3

Jones, J., & Veevers, J. J. (1983). Mesozoic origins and antecedents of Australia's Eastern Highlands. *Journal of the Geological Society of Australia*, *30*(3–4), 305–322.

Kim, Y.-S., & Sanderson, D. J. (2005). The relationship between displacement and length of faults: a review. *Earth-Science Reviews*, *68*(3), 317–334. https://doi.org/10.1016/J.EARSCIREV.2004.06.003

Korsch, R. J., & Totterdell, J. M. (2009). Evolution of the Bowen, Gunnedah and Surat basins, eastern Australia. *Australian Journal of Earth Sciences*, *56*(3), 271–272.

Korsch, R. J., Totterdell, J. M., Fomin, T., & Nicoll, M. G. (2009). Contractional structures and deformational events in the Bowen, Gunnedah and Surat Basins, eastern Australia. *Australian Journal of Earth Sciences*, *54*, 477–499.

Krantz, R. W. (1991). Normal fault geometry and fault reactivation in tectonic inversion experiments. *The Geometry of Normal Faults*, *56*, 219–229. http://sp.lyellcollection.org/

Laubach, S. E., Eichhubl, P., Hargrove, P., Ellis, M. A., & Hooker, J. N. (2014). Fault core and damage zone fracture attributes vary along strike owing to interaction of fracture growth, quartz accumulation, and differing sandstone composition. *Journal of Structural Geology*, *68*, 207–226. https://doi.org/10.1016/J.JSG.2014.08.007

Lawrie, K. C., Brodie, R. S., Gibson, D., Tan, K. P., Magee, J., Clarke, J. D. A., Halas, L., Gow, L., Somerville, P., Apps, H. E., Smith, M., Christensen, N. B., Abraham, J., Hostetler, S., & Brodie, R. C. (2012). *Securing Broken Hill's Water Supply: Assessment of Conjunctive Water Supply Options Involving Managed Aquifer Recharge and/or Groundwater Extraction at Menindee Lakes*. Geoscience Australia.

Lin, L., Jia, H., & Yu, Y. (2007). Fracture network characteristics of a deep borehole in the Table Mountain Group (TMG), South Africa. *Hydrogeology Journal*, *15*, 1419–1432. file:///C:/Users/SchoningG/Downloads/fulltext_paper.pdf

Mahdi, H., Sanaei, A., & Sepehrnoori, K. (2017). Hydraulic Fracturing Fluid Effect on Clay Swelling in Stimulated Naturally Fractured Reservoirs. *, Unconventional Resources Technology Conference*.

Mal'kovskii, V. I., & Pek, A. (2001). Evaluation of the Influence of a Highly Permeable Fault on Transport of Pollutants by the Local Groundwater Flow. *Geology of Ore Deposits*, *43*, 216–223.

Manzocchi, T., Walsh, J. J., Nell, P., & Yielding, G. (1999). Fault transmissibility multipliers for flow simulation models. *Petroleum Geoscience*, *5*(1), 53–63.

Moretti, I. (1998). The role of faults in hydrocarbon migration. *Petroleum Geoscience*, *4*, 81–94. https://doi.org/10.1144/petgeo.4.1.81

Mozley, P. S., & Goodwin, L. B. (1995). Patterns of cementation along a Cenozoic normal fault: A record of paleoflow orientations. *Geology*, *23*(6), 539. https://doi.org/10.1130/0091-7613(1995)023<0539:POCAAC>2.3.CO;2

OGIA. (2015a). *Wetland Conceptualisation, Sub-report 4, Scott's Creek Complex*. OGIA, Department of Natural Resources and Mines.

OGIA. (2015b). *Wetland Conceptualisation; Sub-report 1, Lucky Last and Abyss complexes, Version 1.2, 30/04/2015*. Department of Natural Resources and Mines.

OGIA. (2015c). *Wetland Conceptualisation; Sub-report 7, Boggomoss, Dawson River 2 and 6, Version 1.3, 21/04/2015*. Department of Natural Resources and Mines.

OGIA. (2015d). *Wetland Conceptualisation: A summary report on the conceptualisation of springs in the Surat Cumulative Management Area. Version 2.0*. OGIA, Department of Natural Resources and Mines.

OGIA. (2016a). *Groundwater Connectivity Between the Condamine Alluvium and the Walloon Coal Measures*. OGIA, Department of Natural Resources and Mines.

OGIA. (2016b). *Groundwater modelling report for the Surat Cumulative Management Area*.

OGIA. (2016c). *Hydrogeological Conceptualisation Report for the Surat Cumulative Management Area*. OGIA, Department of Natural Resources and Mines. https://drive.google.com/file/d/0B5u2TKAmnh_iaWsydHlfZVR0VVk/view

OGIA. (2016d). *Springs in the Surat Cumulative Management Area: A report on spring research, knowledge and management approaches in the Surat CMA*. Department of Natural Resources and Mines.

OGIA. (2016e). *Underground Water Impact Report for the Surat Cumulative Management Area*. Department of Natural Resources and Mines, State of Queensland. https://www.dnrm.qld.gov.au/__data/assets/pdf_file/0003/409359/uwir-submission-summary.pdf

OGIA. (2017). *Identification of gaining streams in the Surat Cumulative Management Area. Hydrogeology investigation report*. Department of Natural Resources and Mines. https://www.dnrm.qld.gov.au/__data/assets/pdf_file/0008/1241747/gaining-streams-surat-cumulative-report.pdf

OGIA. (2019a). *Hydrogeological Assessment Report - South-eastern Surat Basin gas fields*.

OGIA. (2019b). *Hydrogeological Assessment Report – Eastern Surat Basin gas fields*.

OGIA. (2019c). *Hydrogeological Assessment Report – Northern Surat Basin gas fields*.

OGIA. (2019d). *Summary of Hydrogeological Conceptualisation – Surat Cumulative Management Area*.

OGIA. (2019e). *Underground Water Impact Report for the Surat Cumulative Management Area*. https://www.dnrme.qld.gov.au/__data/assets/pdf_file/0020/1461242/uwir-main-report.pdf

OGIA. (2019f). *Updated Geology and Geological Model for the Surat Cumulative Management Area*.

OGIA. (2019g). *Water extraction in the Surat Cumulative Management Area; Technical method and results*.

Park, R. G. (R. G. (2000). *Foundations of structural geology*. Stanley Thornes (Publishers). https://books.google.com.au/books?id=ycASqdxSG3YC&pg=PA11&redir_esc=y

Peacock, D. C. P., & Sanderson, D. J. (1994). Geometry and Development of Relay Ramps in Normal Fault Systems. *AAPG Bulletin*, *78*(2), 147–165. file:///C:/Users/SchoningG/Downloads/Geometry_and_Development_of_Relay_Ramps_in_Normal_.pdf

Peacock, D. C. P., & Sanderson, D. J. (1997). Geometry and development of normal faults. In *Evolution of Geological Structures in Micro- to Macro-scales* (pp. 27–46). Springer Netherlands. https://doi.org/10.1007/978-94-011-5870-1_3

QGC. (2014). *Surat Basin Geology*. QGC.

Rawling, G. C., Goodwin, L. B., & Wilson, J. L. (2001). Internal architecture, permeability structure, and hydrologic significance of contrasting fault-zone types. *Geology*, *29*(1), 43–46. https://doi.org/10.1130/0091-7613(2001)029<0043:IAPSAH>2.0.CO;2

Raza, A., Hill, K. C., & Korsch, R. J. (2009). Mid-Cretaceous uplift and denudation of the Bowen and Surat Basins, eastern Australia: Relationship to Tasman Sea rifting from apatite fission-track and vitrinite-reflectance data. *Australian Journal of Earth Sciences*, *56*(3), 501–531. https://doi.org/10.1080/08120090802698752

Robertson, J. O., & Chilingar, G. V. (2000). Faulting, fault sealing and fluid flow in hydrocarbon reservoirs.: Editors: G. Jones, Q.J. Fisher and R.J. Knipe. 1998, 318 pages; Publisher: Geological Society London; {ISBN} 1-86239-022-3. In *Journal of Petroleum Science and Engineering* (Vol. 25, Issues 1–2). https://doi.org/http://dx.doi.org/10.1016/S0920-4105(00)00002-4

Ryan, D., Hall, A., Erriah, L., & Wilson, P. (2012). The Walloon coal seam gas play, Surat Basin, Queensland. *The APPEA Journal*, *52*(1), 273. https://doi.org/10.1071/aj11020

Schlische, R., Young, S., Ackermann, R., & Gupta, A. (1996). Geometry and scaling relations of a population of very small rift-related normal faults. *Geology*, *24*(8), 683–686. https://doi.org/10.1130/0091-7613(1996)024<0683:GASROA>2.3.CO;2

Schwenck Galvão, M., Barroso, E., & Leão, M. (2018). *Fault Zones Control on Permeability of Poorly Lithified Sandstone*.

Shakoor, A., & Sarman, R. (1992). Swelling potential classification of mudrocks based on geotechnical properties. *Proc ISRM Symposimn: Eurock'92*, *14–17*, P75-80. https://doi.org/10.1016/0148-9062(93)92889-X

Sliwa, R. (2013). Eastern Surat Basin structural framework from 2D seismic interpretation. In *Arrow Energy Limited*.

Smith, D. A. (1966). Theoretical Considerations of Sealing and Non-Sealing Faults. *AAPG Bulletin*, *50*, 363–374. https://doi.org/10.1306/5d25b48f-16c1-11d7-8645000102c1865d

Underschultz, J., Esterle, J., Strand, J., & Hayes, S. (2018). *Conceptual representation of fluid flow conditions associated with faults in sedimentary basins*. Prepared for the Department of the Environment and Energy by The University of Queensland Centre for Coal Seam Gas, Queensland.

van der Zee, W., & Urai, J. L. (2005). Processes of normal fault evolution in a siliciclastic sequence: A case study from Miri, Sarawak, Malaysia. *Journal of Structural Geology*, *27*(12), 2281–2300. https://doi.org/10.1016/j.jsg.2005.07.006

Van Olphen, H. (1964). An introduction to clay colloid chemistry. *Journal of Pharmaceutical Sciences*, *53*(2), 230. https://doi.org/10.1002/jps.2600530238

Viljoen, R., Pinder, B., Mukherjee, S., & Herbert, S. J. (2020). Hydrogeological implications of fault behaviour from in situ pressure measurements of the Horrane Fault in the Surat Basin (Great Artesian Basin, Australia). *Hydrogeology Journal*, *28*(1), 161–174. https://doi.org/10.1007/s10040-019-02093-x

Vrolijk, P. J., Urai, J. L., & Kettermann, M. (2016). Clay smear: Review of mechanisms and applications. *Journal of Structural Geology*, *86*, 95–152. https://www.sciencedirect.com/science/article/pii/S0191814115300390

WaterMark Numerical Computing. (2012). *Predictive Uncertainty of the Regional-Scale Groundwater Flow Model for the Surat Cumulative Management Area*. QWC.

Wibberley, C. A. J., Yielding, G., & Di Toro, G. (2008). Recent advances in the understanding of fault zone internal structure: A review. In *Geological Society Special Publication* (Vol. 299, pp. 5–33). https://doi.org/10.1144/SP299.2

Yielding, G., Bretan, P., & Freeman, B. (2010). Fault seal calibration: A brief review. *Geological Society Special Publication*, *347*, 243–255. https://doi.org/10.1144/SP347.14

Yielding, G., Freeman, B., & Needham, D. T. (1997). Quantitative fault seal prediction. *AAPG Bulletin*, *81*(6), 897–917. https://doi.org/10.1306/522b498d-1727-11d7-8645000102c1865d

7. Glossary

Antithetic fault: a minor or secondary fault with opposite displacement to the major fault.

Aquifer: a saturated underground geological formation or group of formations, that can store water and yield it to a bore or spring. A saturated formation that will not yield water in usable quantities is not considered an aquifer.

Aquitard: a geological formation that prevents significant flow of water due to its low permeability (e.g., clay layers or tight deposits of shale).

Cataclasis: the fracturing and breaking of rocks that occurs during faulting.

Cataclasites: rocks formed during cataclasis.

Damage zone: the volume of deformed and fractured rock around a fault plane.

En echelon faulting: Parallel or sub-parallel, overlapping and closely spaced faults oblique to the major faulting orientation.

Fracture closure: the closing of fracture apertures, decreasing potential for fluid flow.

Fracture dilation: the opening of fracture apertures, increasing the potential for fluid flow.

Fault (geological): a break in a geological formation along which some measurable movement, or displacement.

Graben: a down-thrown block between two normal faults.

Lithology: the physical characteristics of rock, with reference to qualities such as colour, composition and texture.

Leakage window: area on the fault plane where permeable units are juxtaposed against one another.

Litharenites: rocks containing greater than 5% lithic fragments.

Protolith: the un-faulted host rock.

Quartzarenites: rocks containing greater than 90% detrital quartz.

Relay ramps: Areas between of reoriented bedding between overlapping faults.

Synthetic faults: A minor or secondary fault with displacement on the same side as the major fault.

Appendix A Previous assessments

- ***Water level trends in the Hutton Sandstone, Springbok Sandstone and Condamine Alluvium*** (OGIA,2019h). This report presents the hydrogeological characteristics of the Springbok and Hutton sandstone formations and the Condamine Alluvium, the groundwater level trends in each formation, and outlines the possible factors and mechanisms which may be influencing these trends.
- ***Non-CSG Water Use estimates for the Surat Cumulative Management Area*** (OGIA, 2019g)***.*** This report provides a summary of OGIA's estimates for non-CSG water use for each major hydrostratigraphic unit with the Surat CMA.
- ***Updated Geology and Geological Model for the Surat Cumulative Management Area*** (OGIA, 2019f)***.*** This report provides a revised geological framework and geological model for the Surat CMA for use in the UWIR 2019.
- ***Summary of Hydrogeological Conceptualisation – Surat Cumulative Management Area*** (OGIA, 2019d)***.*** OGIA provided a comprehensive review of hydrogeological conceptualisation as part of the UWIR 2016. This new report provides details on specific aspects of conceptualisation that have been revised since that original publication and reflects the direction of OGIA's technical investigations undertaken to support UWIR 2019.
- ***Hydrogeological conceptualisation report for the Surat Cumulative Management Area*** (OGIA, 2016c). This report summarises key groundwater processes operating in the Surat, Clarence-Moreton and Bowen basins within the Surat CMA.
- ***Condamine groundwater connectivity report*** (OGIA, 2016a). This report provides a summary of investigations into the potential for groundwater flow between two major geological formations in the Surat Basin: the Condamine Alluvium and the Walloon Coal Measures.
- ***Springs in the Surat Cumulative Management Area – A summary report on spring research and knowledge*** (OGIA, 2016d).This report summarises our current understanding of springs in the Surat CMA
- ***Identification of gaining streams in the Surat Cumulative Management Area*** (OGIA, 2017). This report provides a remapping of gaining streams in the Surat CMA based on contemporary data sets and a field-validation of this mapping at selected priority sites.
- ***Groundwater modelling report for the Surat Cumulative Management Area*** (OGIA, 2016b)This report describes the construction and calibration of the regional groundwater flow model used by OGIA to predict water pressure impacts on aquifers in the Surat CMA.
- ***Predictive Uncertainty of the Regional-Scale Groundwater Flow Model for the Surat Cumulative Management Area*** (WaterMark Numerical Computing, 2012). This report summarises the results of a numerical analysis undertaken to assess the uncertainty associated with predictions reported in the UWIR 2012.

Appendix B Curvature map

Formation curvature maps were generated for the top of Walloon Coal Measures, as there is significant well control on this surface due to the high density of CSG wells in the areas of interest.

Mean curvature was initially calculated in Schlumberger's Petrel platform. These data were then exported to Python where a series of transformations were undertaken to scale the data for visualisation. The data were standardised between 0 and 1, and the colour scale was applied to two standard deviations either side of the mean. This scale has no units and it is not possible to infer positive or negative curvature; rather, this was done in order to visualise the contrast around linear features. The resulting curvature map is presented below.

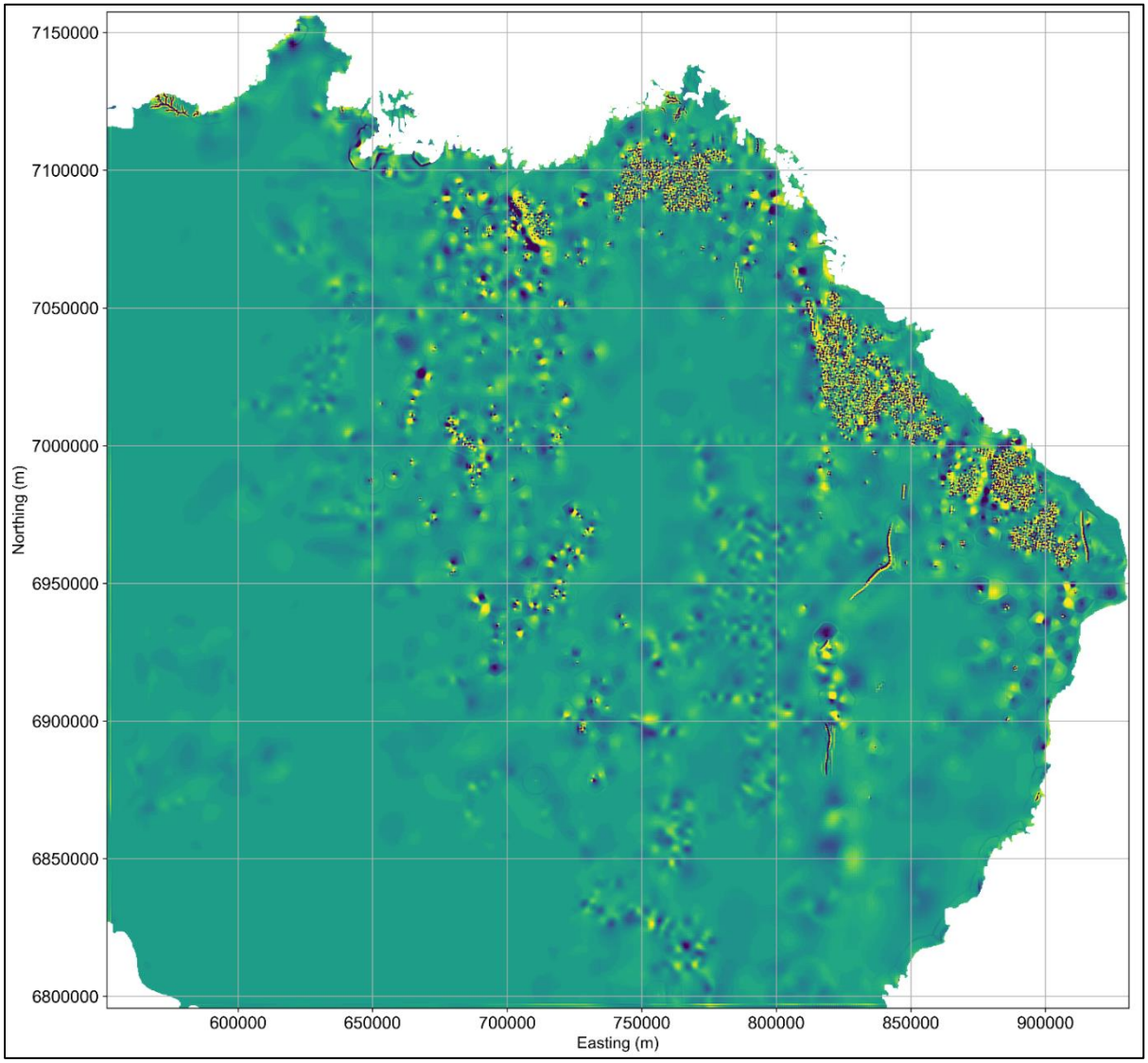

Figure 1 Curvature index map for the Walloon Coal Measures

Appendix C Numerical groundwater modelling of the Kenya East graben structure

C.1 Objectives

The objectives of this work are as follows:

- Develop a simple numerical groundwater flow models to investigate the potential impact of faults affecting the Springbok Sandstone – Walloon Coal Measures interface on pressures in the overlying Springbok Sandstone (SBK). Structures of the models are based on field locations where groundwater observations are available in the upper or lower SBK formations. Calibration is focused primarily on the permeability or conductance of the elements of the model representing the faults (and also on storage parameters of the upper and lower SBK formations).
- Improve understanding of possible head distributions in the SBK in response to depressurisation at greater depths. For example, how much drawdown is expected in the lower SBK at locations where minor drawdown is observed in the upper SBK. This information may inform groundwater monitoring network design.
- Confirm if observed drawdown in the lower SBK at Kenya East (KEE_GW004) is anomalous and quantify conductance for as many faults as possible. This may then inform how to incorporate small faults into the regional model. For example, if the groundwater behaviour at Kenya East is an anomaly then it may not be necessary/appropriate to do this as it is not a regional impact. Conversely if the groundwater behaviour at Kenya East is not an anomaly and all faults return relatively high conductance values and may potentially be causing significant drawdown in the lower SBK across most of the area, then some representation in the regional model may be required.

C.2 Background

Kenya East is located approximately 30 km southwest of Chinchilla (Figure 1). A fault with a 28-m displacement lies between two groundwater monitoring bores, KEE_GW002 and KEE_GW004 (Figure 2). A second fault lies to the east of KEE_GW004.

Bore KEE_GW002 is screened in the upper SBK (approximately 55m above the base of the upper SBK) and is located approximately 1,000 m west of the fault alignment. Bore KEE_GW004 is screened in the lower SBK (approximately 13 m above the base of the lower SBK) and is located approximately 400 m east of the fault alignment.

Pre-development (1947) groundwater levels in the SBK have been estimated to be in the range of 305 to 312 mAHD, as shown in Figure 3. As of December 2017, no change in groundwater level is observed at KEE_GW002, whereas at KEE_GW004, approximately 15 m of drawdown is observed (Figure 4).

KEE_GW002 and KEE_GW004 are separated by approximately 1,700 m horizontally and 100 m vertically.

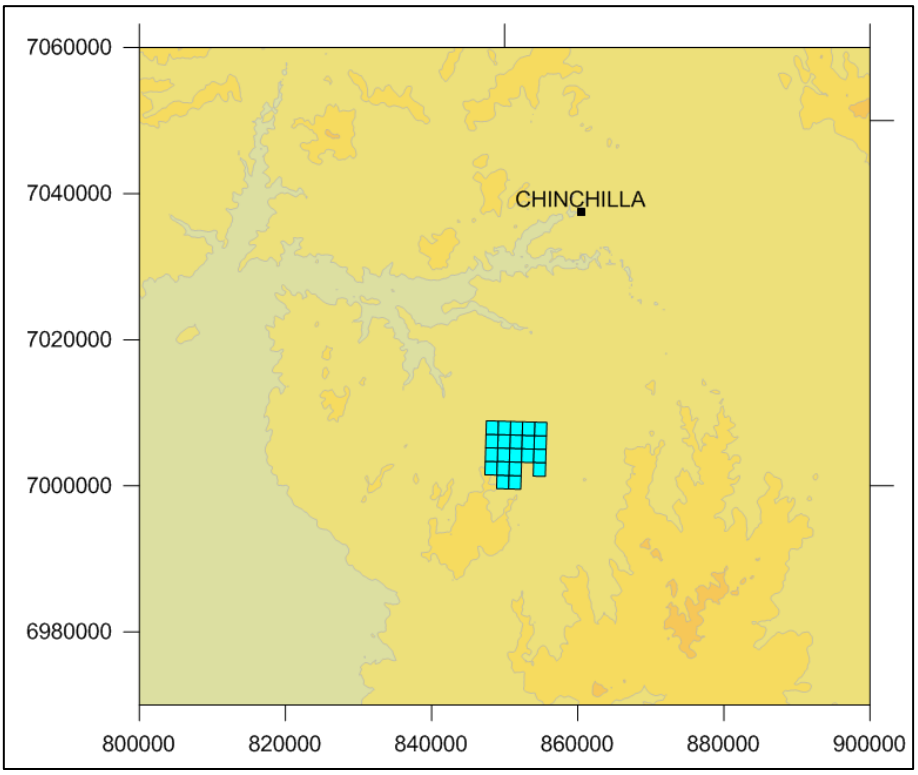

Figure 1 Kenya East (blue) location

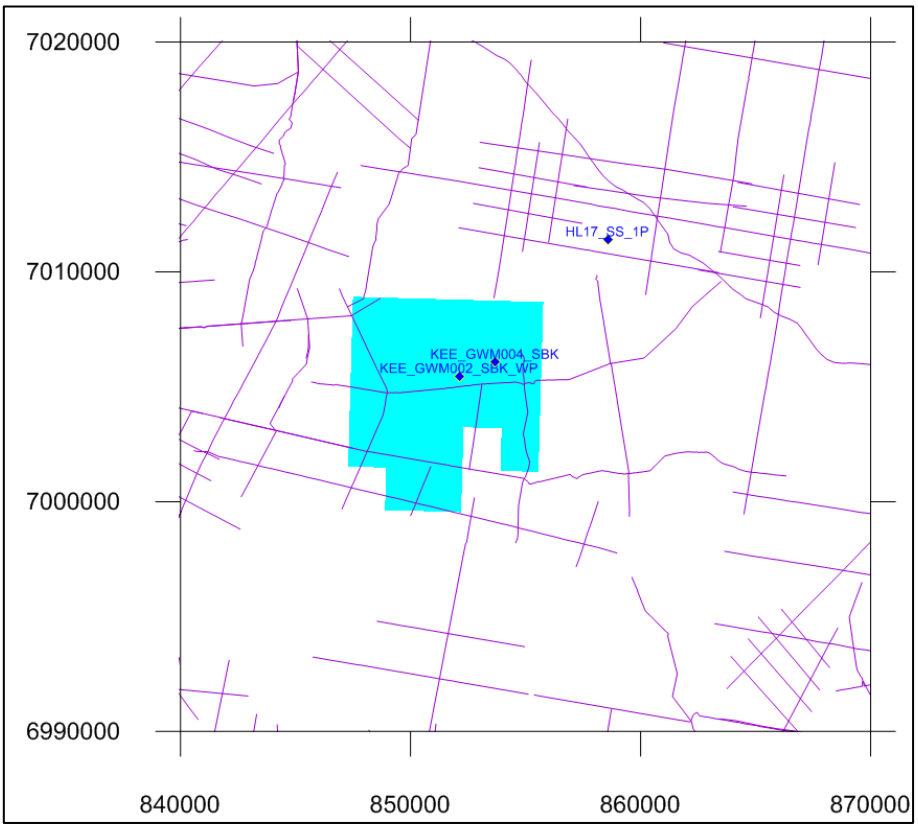

Figure 2 Faults and groundwater monitoring bores

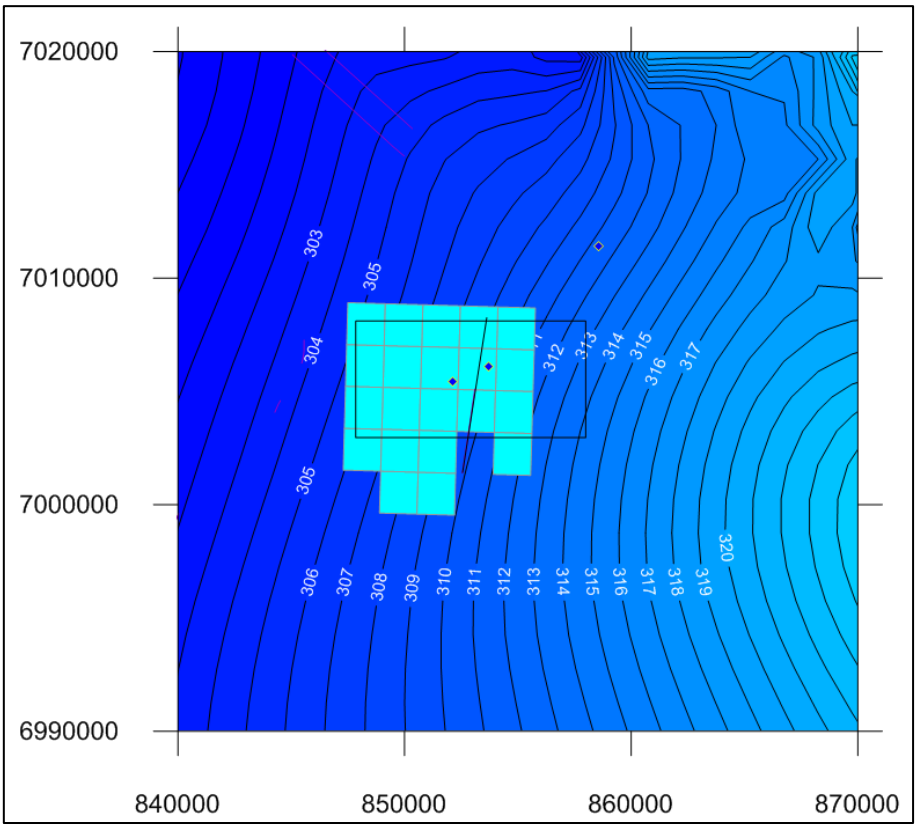

Figure 3 Upper SBK pre-development groundwater levels (mAHD) from UWIR 2016 regional model

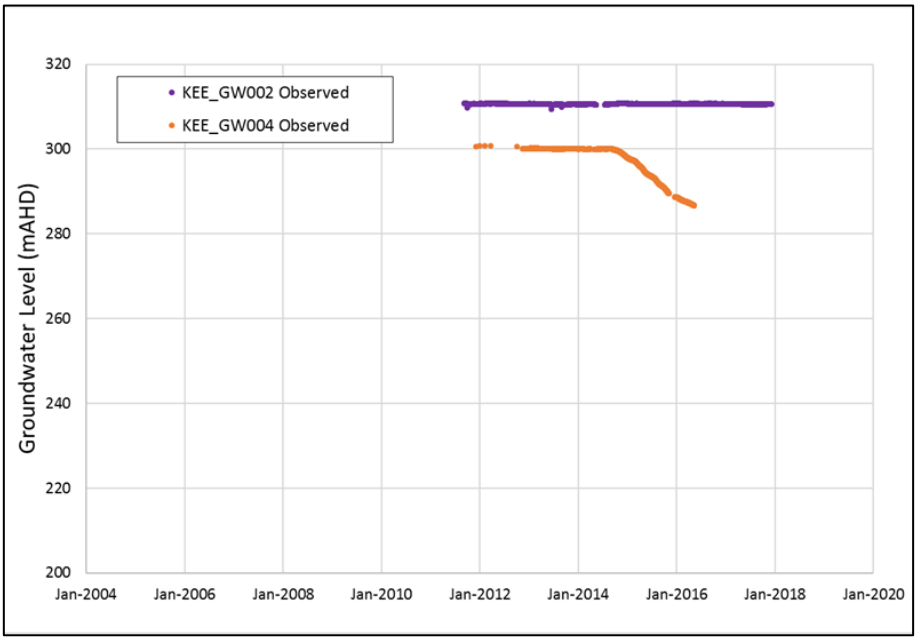

Figure 4 Observed groundwater levels (mAHD) at KEE_GW002 and KEE_GW004

C.3 Model design

Several model designs have been considered in the course of this work. During their development, some model designs were deemed unsuitable or insufficient to accomplish the modelling objectives.

C.3.1 Model domain

To better incorporate fault orientation, groundwater flow direction and both horizontal and vertical separation of the two observation bores, a 3D model domain (oriented as shown as the black rectangle in Figure 3) comprising 50×50×1-m cells has been constructed as shown in Table 1.

Table 1 3D model domain

	Discretisation	Length of cell side	Total length
x-Direction (Horizontal)	100 columns	50 m	5,000 m
y-Direction (Horizontal)	200 rows	50 m	10,000 m
z-Direction (vertical)	111 layers	1 m	111 m
Total Number of cells	**2,220,000**		

C.3.2 Layering

Elevations of the upper and lower SBK have been provided by the 250-m resolution groundwater flow model surfaces. On the up-throw sides of the fault, the lowest 28 layers (corresponding to the 28-m throw of the fault) are used to define the sub-units of the Walloon Coal Measures (WCM) immediately underlying the lower SBK. The remaining model layers define the lower SBK and lower portion of the upper SBK. Model layering is described in Table 2 and shown in Figure 5.

Table 2 Model layers

Formation	Layers	Thickness (m)	Top elevation (mAHD)
Upper SBK (partial)	1–55	55	68
Lower SBK	56–83	28	14
Clean sand	84–85	2	-15
Dirty sand	86	1	-17
Clean sand	87	1	-18
Dirty sand	88	1	-19
Clean sand	89–91	3	-20
Coal	92–95	4	-23
Dirty sand	96	1	-27
Coal	97–99	3	-28
Shale	100	1	-31
Sandstone/siltstone	101	1	-32
Mudstone	102	1	-33
Sandstone/siltstone	103–105	3	-34
Clean sand	106	1	-37
Sandstone/siltstone	107	1	-38
Dirty sand	108–110	3	-39
Clean sand	111	1	-42

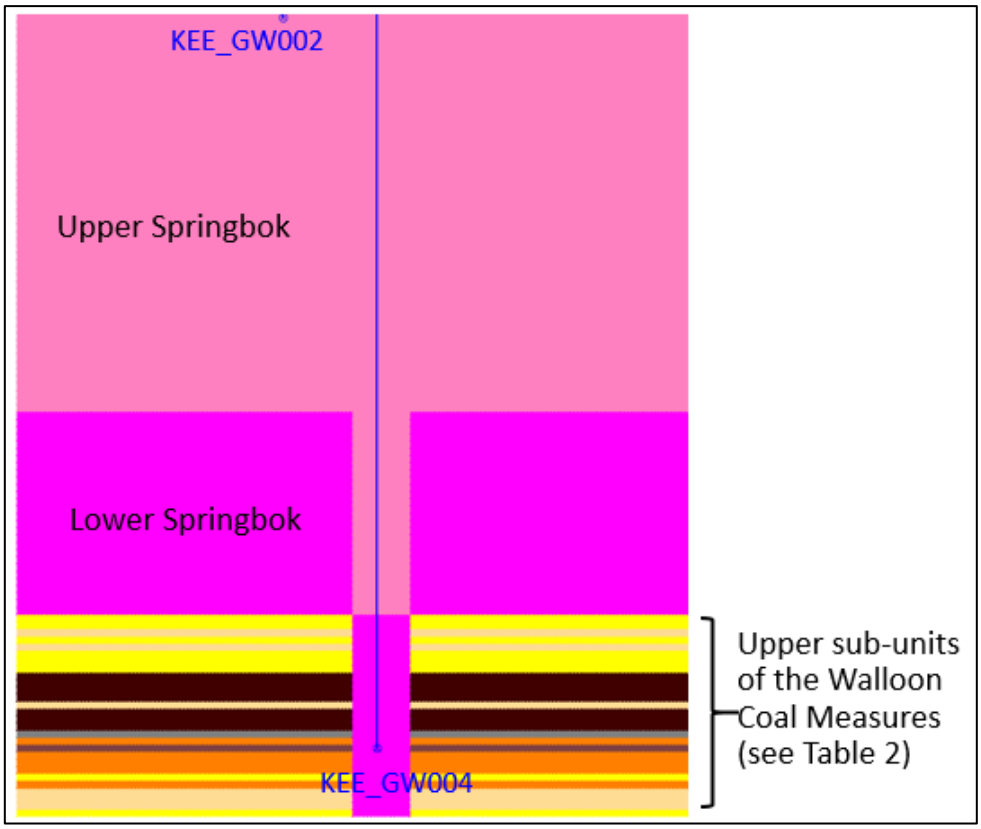

Figure 5 Vertical cross-section (west to east) showing model layers, formations and groundwater observation bores

C.4 Initial and boundary conditions and simulation period

Initial groundwater levels are set to a uniform 310 mAHD across the model domain, based on pre-development (1947) groundwater levels provided by the UWIR 2016 regional groundwater model.

A depressurisation signal (representing the depressurisation of the coal seams) has been provided by the UWIR 2016 regional groundwater model at the location of the observation bore KEE_GWM032, which is screened in the upper WCM and shows a depressurisation of approximately 75 m occurring from 2008 onwards (Figure 6). In early versions of the model, the depressurisation signal was applied as a general head boundary (GHB) condition on the coal layers, with the conductance parameter of the GHB representing signal transmission across the fault interface. However, with data pertaining to fault properties being available, the depressurisation signal is currently applied as a time-varying specified head condition on the model cells comprising the coal seam layers (layers 92–95 and 97–99, shown in Figure 7). The signal transmission across the fault interface will be governed by the hydraulic conductivity of horizontal flow barriers (HFB) applied along the fault throw

The model conducts a transient simulation from 1995 to 2017 using monthly stress periods. No recharge is applied.

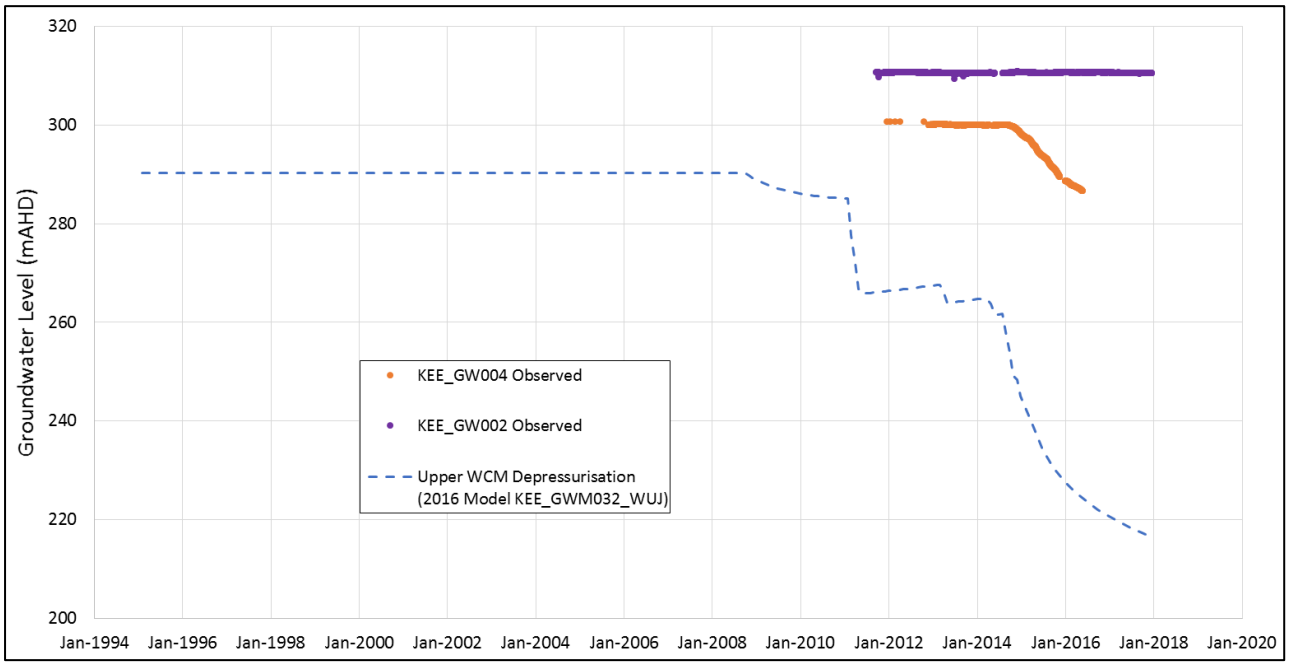

Figure 6 Upper WCM depressurisation from the UWIR 2016 regional groundwater model

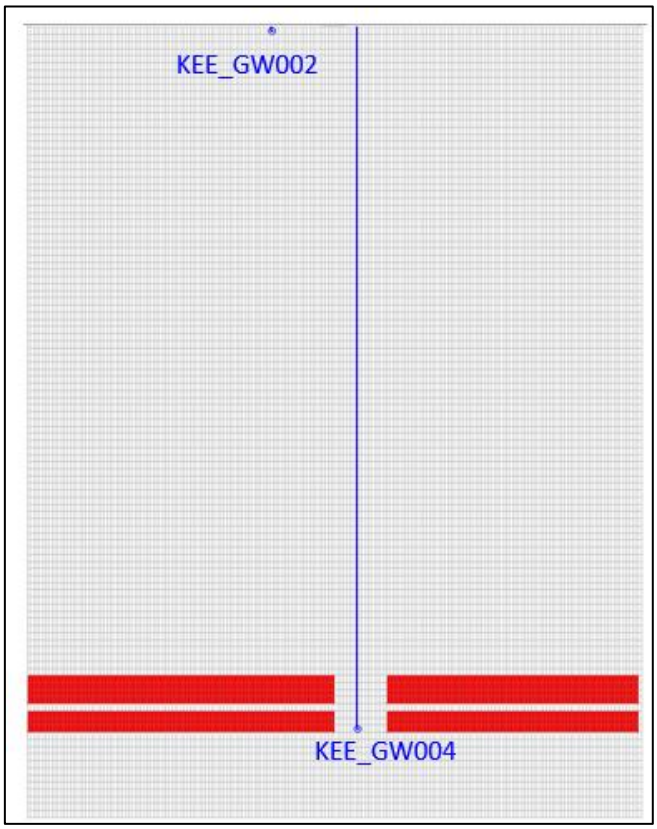

Figure 7 Coal cells (red) on which time-varying head boundary conditions are applied

C.5 Initial parameterisation

Initial values for hydraulic parameters (K_h: horizontal hydraulic conductivity; K_v: vertical hydraulic conductivity; and Ss: specific storage) have been provided by the UWIR 2016 regional groundwater model for the upper and lower SBK. For the upper WCM units, high-resolution petrophysical estimates of permeability were utilised. A summary of initial parameter values are presented in Table 3.

The fault zone is defined where the sub-units of the WCM are in contact with the lower SBK (Figure 8). Fault zone properties (modelled as HVB) are composed of thickness (set to 1 m) and horizontal hydraulic conductivity (K_h). The K_h for each layer within the fault zone is calculated from the permeability of the sub-unit and the Shale Gauge Ratio (SGR).

Table 3 Initial model parameter values

	K_h (m/day)	K_v (m/day)	Ss	Fault K_h (m/day)
Upper SBK	9.80E-03	2.22E-06	4.76E-05	-
Lower SBK	7.35E-03	2.37E-05	2.86E-05	-
Clean Sand	3.32E-05	3.32E-06	3.84E-06	6.86E-05
Dirty Sand	2.43E-04	2.43E-05	4.73E-06	4.84E-05
Sandstone/siltstone	5.32E-06	5.32E-07	5.88E-06	2.96E-05
Mudstone	2.78E-06	2.78E-07	7.31E-06	4.77E-05
Shale	2.00E-03	2.00E-04	2.00E-09	8.53E-05
Coal	5.36E-03	5.36E-05	5.07E-06	8.75E-05

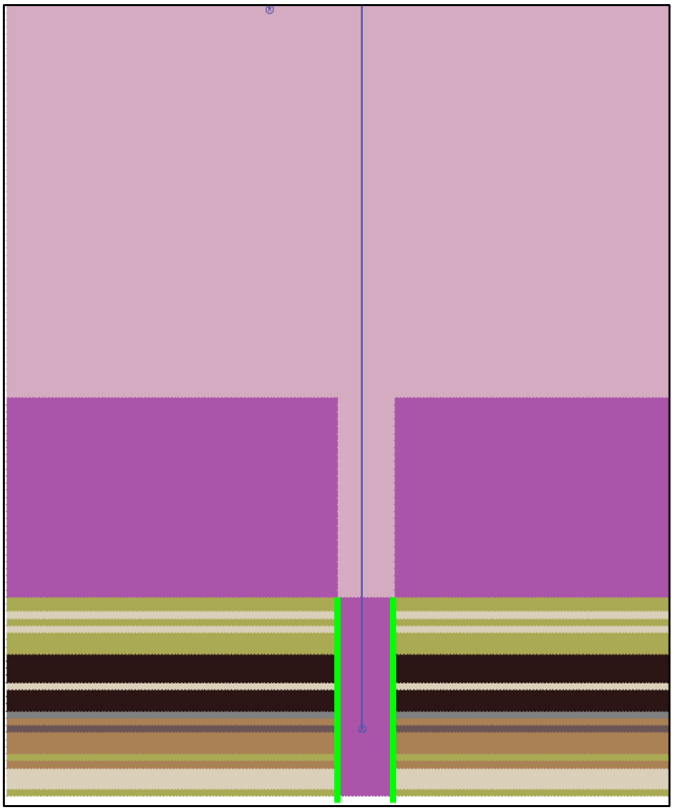

Figure 8 Location of horizontal flow barriers (green)

C.6 Calibration and simulation results

Calibration has been to monthly average (i.e. smoothed) observed groundwater drawdown in nearby SBK observation bores, KEE_GW002 and KEE_GW004. The calibration parameters are the specific storage of the upper and lower SBK, and the conductivity of the fault.

Figure 6 shows that the groundwater levels observed at KEE_GW004 do not appear to respond to any depressurisation signal prior to late 2014. This indicates that the drawdown observed may only be in response to local depressurisation activities. As such, the drawdown used for calibration will be calculated from groundwater levels observed in October 2014.

Table 4 shows the calibrated values for specific storage of the upper and lower SBK. The hydraulic conductivity of the fault remains unchanged from the initial values presented in Table 3.

Table 4 Calibrated Springbok Sandstone storage values

	Initial Ss	Calibrated Ss
Upper SBK	4.76E-05	3.57E-05
Lower SBK	2.86E-05	2.15E-05

Figure 9 shows the groundwater drawdown (calculated post-October 2014) for the observation bores and simulation results from the model for initial parameter values and calibrated parameter values. Figure 10 shows the groundwater levels for the observation bores and simulation results from the model for initial parameter values and calibrated parameter values.

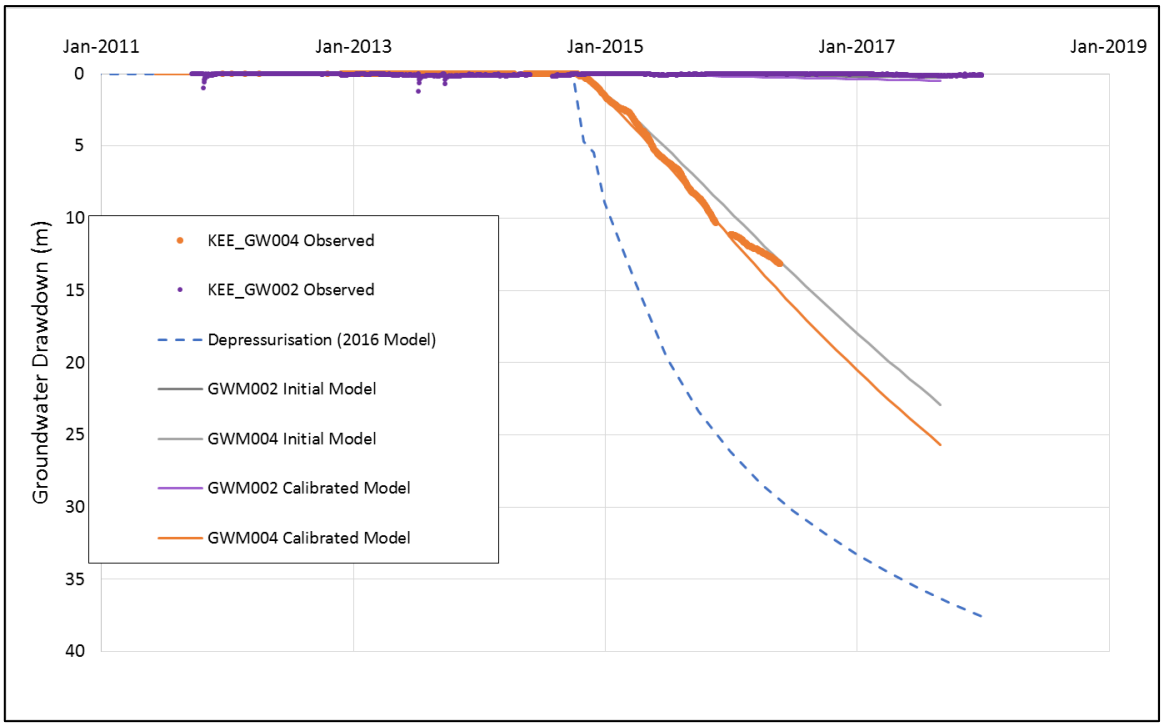

Figure 9 Observed and modelled (initial model and calibrated model) drawdown (from October 2014) at observation bores

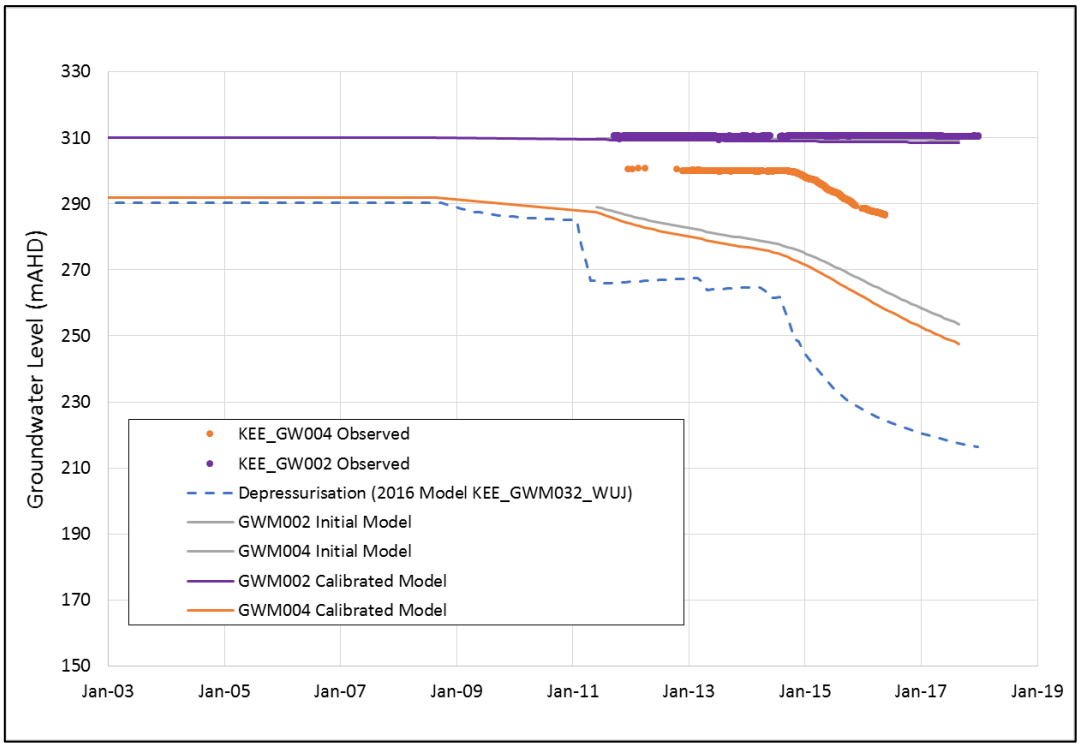

Figure 10 Observed and modelled (initial model and calibrated model) groundwater levels at observation bores

Figure 11 presents a vertical cross-section of the groundwater level distribution for December 2017. It shows that groundwater drawdown can propagate vertically from the coal seams, through the sub-units of the upper WCM (mostly sands at this location) and into the lower SBK. These results indicate that drawdown induced by depressurisation in the coal seams may be greater directly above the coal seams than in the region of the fault, depending on the properties of the units above the coal seams.

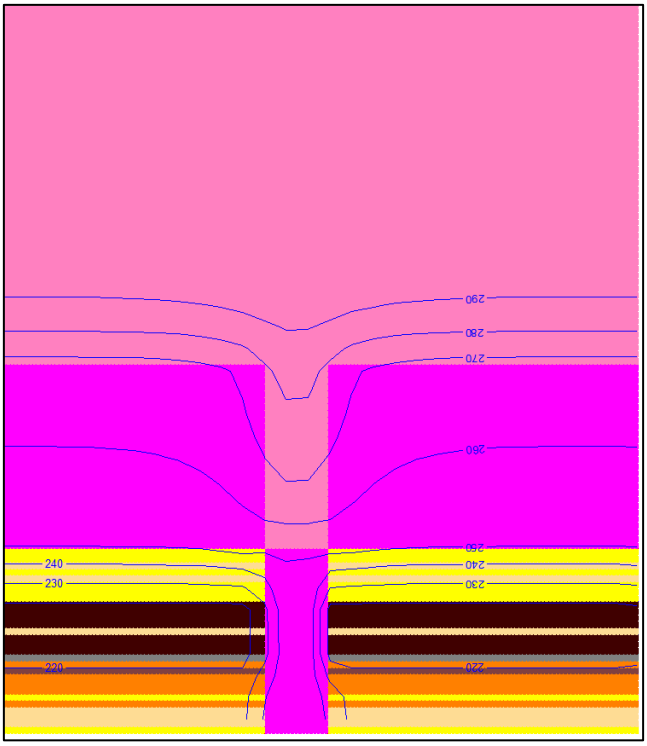

Figure 11 Vertical cross-section showing modelled groundwater levels (mAHD) for December 2017


Queensland
Government